FOOT MOTION-BASED FALLING RISK EVALUATION FOR PATIENTS WITH PARKINSON'S DISEASE

A Dissertation

by

RUI HUA

Submitted to the Graduate and Professional School of
Texas A&M University
in partial fulfillment of the requirements for the degree of

DOCTOR OF PHILOSOPHY

Chair of Committee,	Ya Wang
Committee Members,	James E. Hubbard Jr.
	Deanna M. Kennedy
	Bobak Jack Mortazavi
Head of Department,	Guillermo Aguilar

May 2022

Major Subject: Mechanical Engineering

ABSTRACT

Parkinson's disease (PD) affects motor functionalities, which are closely associated with increased risks of falling and decreased quality of life. However, there is no easy-to-use definitive tools for PD patients to quantify their falling risks at home. To address this, in this dissertation, we develop Monitoring Insoles (MONI) with advanced data processing techniques to score falling risks of PD patients following Falling Risk Questionnaire (FRQ) developed by the U.S. Centers for Disease Control and Prevention (CDC). To achieve this, we extract motion tasks from daily activities and select the most representative features associated with PD that facilitate accurate falling risk scoring.

To address the challenge in uncontrolled daily life environments and to identify the most representative features associated with PD and falling risks, the proposed data processing method firstly recognizes foot motions such as walking and toe tapping from continuous movements with stride detection and fast labeling framework, and then extracts time-axis and acceleration-axis features from the motion tasks, at the end provides a score of falling risks using regression. The data processing method can be integrated into a mobile game to be used at home with MONI.

The main contributions of this dissertation includes: (i) developing MONI as a low power solution for daily life use; (ii) utilizing stride detection and developing fast labeling framework for motion recognition that improves recognition accuracy for daily life applications; (iii) analyzing two walking and two toe tapping tasks that are close to real life scenarios and identifying important features associated with PD and falling

risks; (iv) providing falling scores as quantitative evaluation to PD patients in daily life through simple foot motion tasks and setups.

DEDICATION

To my beloved parents, who teach me about life, support my studies and encourage me all the time.

ACKNOWLEDGEMENTS

During my studies, I am very grateful that I met great people who helped, encouraged, and inspired me to learn to be a researcher and an engineer.

Many thanks go to my advisor and committee chair Dr. Ya Wang who recognized my potentials, gave me opportunities to try different roles, provided me endless support and patience, guided me during my studies and taught me to be a researcher. I am very grateful to have Dr. Ya Wang as my advisor and I enjoyed working with Dr. Ya Wang in the past few years.

I would like to thank my committee members Dr. James E. Hubbard Jr., Dr. Deanna M. Kennedy, and Dr. Bobak Jack Mortazavi for spending time guiding me and providing constructive advice to my research topics and skills.

I also would like to thank Dr. Krystal Kazmierski and Dr. Benjamin White for their support and suggestion to my experiment with patients with Parkinson's disease, Ms. Nancy Knutson, Ms. Stacy Lambert, Ms. Cindy Conte, the senior residents from Arbor Oaks at Crestview in Bryan Texas, the fighters (patients) and their caregivers from our local Parkinson's disease community in College Station and Bryan Texas and for their long-term support to my research.

I would like to thank Mr. Scott Tierno and Dr. Kenneth Short for their huge influence on me of teaching and applying engineering skills to solve problems.

I am thankful to students who helped, inspired, and worked with me along my studies: Mr. Ahmad Jawad, Mr. Yiyu Wang, Mr. Ibrahim Almuteb, Mr. Nguyen

Nguyen, Ms. Rachel Williams, and the senior students from two COMSOLE capstone teams from Mechanical Engineering at Texas A&M University. I also would like to thank J. Mike Walker '66 Department of Mechanical Engineering and Texas A&M University for the countless resources they provided to me during my studies.

Thanks also go to Dr. Haili Liu who helped me get started research during my first semester, my lab mates and friends: Dr. Libo Wu, Dr. Zhangjie Chen and Ms. Jingfan Chen for their support in the past few years, my close friends Dr. Yuan Gao and Ms. Dongxue Jia for their consistent encouragement and company during the time I was far away from family.

Finally, thanks to my parents and grandparents for their all-time support and love.

CONTRIBUTORS AND FUNDING SOURCES

Contributors

This work was supervised by a thesis (or) dissertation committee consisting of Dr. Ya Wang as the advisor, Dr. James E. Hubbard Jr. of the Department of Mechanical Engineering, Dr. Deanna M. Kennedy of the Department of Health and Kinesiology and Dr. Bobak Jack Mortazavi of the Department of Computer Science and Engineering.

The Figure 1.5 3D Model of MONI prototype in Chapter 1 was prepared by Ms. Rachel Williams of the Department of Civil Engineering at New York State University at Buffalo. The data analyzed in Chapter 3 was partially collected by Mr. Ahmad Jawad of the Department of Mechanical Engineering at Texas A&M University.

All other work conducted for the dissertation was completed by the student independently.

Funding Sources

The research was partially supported by DOE ARPAE DE-AR0000945 (2018-2022), MEEN Research Priming Seed Grant Program (2020) and MEEN Graduate Summer Research Grant (GSRG) (2020).

TABLE OF CONTENTS

Page

LIST OF FIGURES

Page

LIST OF TABLES

Page

1. INTRODUCTION [*†]

1.1. Parkinson's Disease and Falling Risks

Parkinson's disease (PD) affects motor functionalities. Disordered motor functionalities are closely associated with increased risks of falling and decreased quality of life. As shown in Figure **1.1**, the prevalence of PD increases with age, so does the falling risks. Over 45% of PD patients experience falling every year and over 50% of them have experienced multiple falls [1]. Medication and treatments associated with falling expense for PD patients are close to double of healthy elderlies [2]. Thus, early identification of patients with high falling risks is important [3].

However, falling risk evaluation normally requires frequent clinical visits [4], where doctors can assess the risk of falling through questionnaires and observations. However, the moment-to-moment assessments in such a supervised and controlled environment may not reflect the actual conditions in daily life. Recently, the U.S. Centers for Disease Control and Prevention (CDC) developed a Falling Risk Questionnaire (FRQ) [5], which can be used as a pre-screening tool. Multiple studies [6, 7] have validated that the FRQ has high correlations to clinical examinations [8].

---

[*] Part of this chapter is reprinted from "Monitoring insole (MONI): A low power solution toward daily gait monitoring and analysis." by Hua, R. and Wang, Y., *IEEE Sensors Journal* 19.15 (2019): 6410-6420.

[†] Part of this chapter is reprinted from "Robust Foot Motion Recognition Using Stride Detection and Weak Supervision-based Fast Labelling." by Hua, R. and Wang, Y., *IEEE Sensors Journal* 21.14 (2021): 16245 – 16255.

However, to fill out the questionnaire with subjective answers, patients may need caregivers' help [9] as PD patients tend to overestimate their ability [10].

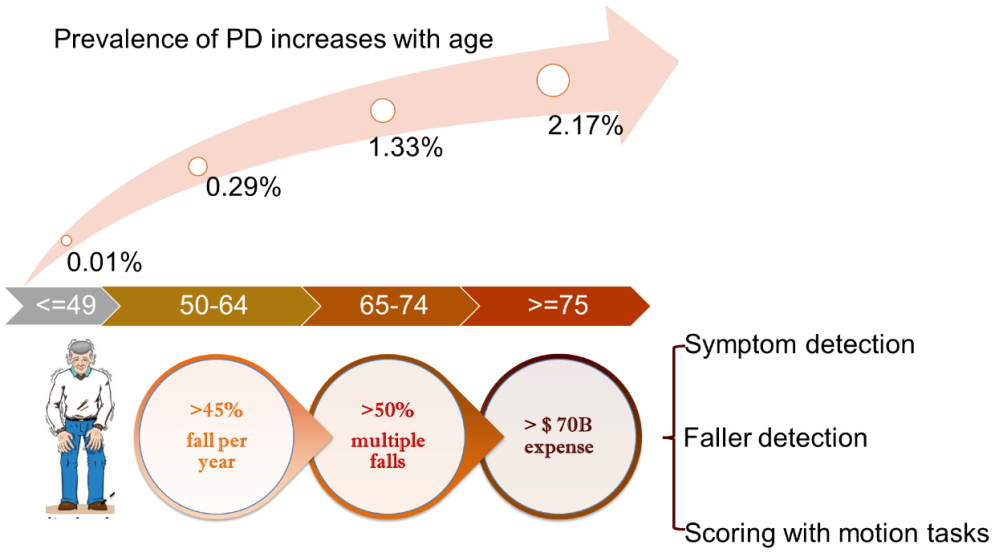

Figure 1.1 **Statistics of age distribution, falling events and falling risk evaluation approaches of PD patients.**

As shown in Figure **1.1**, besides FRQ and doctor's assessments, falling risks can also be evaluated through three different approaches as detailed below. Symptom detection, such as detection of freezing of gait, is a popular approach to evaluate falling risks of PD patients. However, freezing of gait may happen randomly and thus it is difficult to prevent falling during sudden episodes. It only applies to patients who are at mid- or late-stage and it is with a low symptom detection accuracy of 70% [11]. Another approach is to differentiate faller from non-faller using machine learning [12]. Even though it can be applied to all PD patients with an accuracy over 90% [13], it does not provide quantitative evaluation on falling risks. Thus, there is an increasing demand for scoring falling risks. This can be done through evaluation of multiple motion tasks [14],

and it can be applied to all PD patients; and thus with the quantitative scores, it can be more effective to prevent falling as patients and their caregivers can have a better understanding of the balance and falling conditions. However, it lacks ground truths for the scores and thereby difficult to validate if the score is accurate for each PD patient.

Besides the challenges stated above, providing an at-home quantitative evaluation of falling risks for PD patients still faces other challenges, such as easy setups and processes for daily use. Once these challenges are addressed, PD patients can better understand their falling risks and thus better prevent falling.

1.2. Smart Wearable Devices and Falling Risk Evaluation

For daily life uses, wearable devices need to be light-weighted, unobtrusive, wireless communicated, portable, easy to don and doff, user friendly, cost-effective, and low power consumed [15]. Inertial sensors (accelerometers, gyroscopes, and measurement units (IMU)) are the mostly used devices for detecting falling and evaluating falling risks [16, 17]. The device can be placed at chest, waist, wrist, shin, thigh, in-shoe, and a combination of all these positions when using multiple devices [18]. Figure 1.2 summarizes the typical steps of using smart wearable devices/sensors for falling risk evaluation. Most studies [19] collect data in fully controlled environments where subjects follow specific instructions and perform one type of motion at a time. Then, various kinds of features are extracted from motion data and analyzed with machine learning methods to either classify falling or non-falling or assessing PD symptoms. The collected data is usually split into train, test and validation set to develop the learning algorithms. There is always a challenge of data limitation lying in small

amount of available data or data lack of diversity. Moreover, daily life is fully uncontrolled environments and thus the application of the machine learning algorithms developed by fully controlled data is not suitable. Another type of data collection is to continuously collect data in uncontrolled or semi-controlled environments [14]. Machine learning algorithms automatically detect PD symptoms relying on patients' self-labeling to adjust the pretrained algorithms. Such method has a high requirement of low power device and large amounts of resources for data storage. Additionally, unexpected motions during the data collection and mistakes made by self-labeling may confuse the algorithm and thus the results won't be accurate.

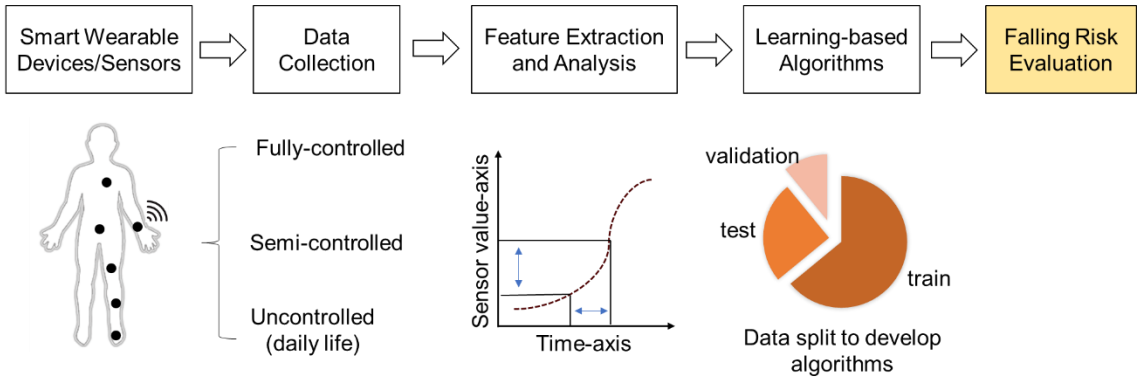

Figure 1.2 Summary of steps of using smart wearables for falling risk evaluation.

Thus, to develop a robust data processing method, the data must be collected in semi-controlled or uncontrolled environments and unexpected or mistakenly performed motions needs to be removed before any feature extraction.

1.3. Smart Wearable Devices and Foot Motion Recognition

Among all kinds of motors and commonly used motions, such as voice and pronounce [20], and hand movement and writing [21], for the use of PD detection and

falling risk evaluation (as shown in Figure 1.3), foot motions [22], including continuous motions resulted from continuous full body movements (named as sequential motions) and repetitive foot motions that are often produced repetitively (named as repetitive motions), are commonly used in clinical tests [23, 24] for characterizing motor functionality in supporting early-stage detection of neurodegenerative diseases, such as PD.

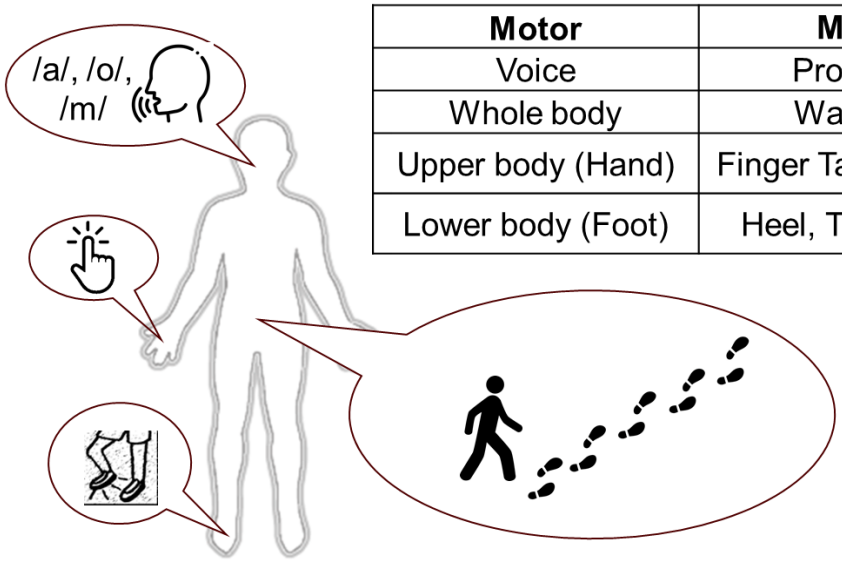

Motor	Motion
Voice	Pronounce
Whole body	Walk, Turn
Upper body (Hand)	Finger Tapping, Write
Lower body (Foot)	Heel, Toe Tapping

Figure 1.3 Falling risk evaluation through different types of motors and motions.

Reliable smart devices facilitating daily foot motion recognition and monitoring are in high demand to avoid frequent doctor visits. However, most existing devices, designed for activity tracking, cannot be directly used for foot motion recognition. Some wearable devices have the capacity, such as smart phones [25] and smart watches [26], but their accuracy for recognizing foot motions from continuous movements under uncontrolled environments are limited by their positions; while non-wearable devices, such as cameras [27] and radar [28, 29], may produce higher accuracies but their

application is limited by their field of view [30]. It requires high resolutions and/or multiple devices to identify continuous fine-grained foot motions, such as toe tapping. Smart insoles [31, 32] are portable, low-cost, easy to use, and can provide enough information needed for foot motion recognition.

Recognizing foot motions from continuous movements in uncontrolled environments faces two major challenges. The first is how to recognize the foot motions of interest from the movements with high robustness. Not like fully controlled experiments, where designed motions are always carried out individually and can be recognized by traditional machine learning frameworks in high accuracies [33], in uncontrolled environments, foot motions often have continuous and complex forms [34]. Thus, traditional machine learning methods underperform in such settings. Complex and computation-hungry machine learning methods [35-38], such as Recurrent Neural Network and Long Short-term Memory, can improve the accuracy but will need a very large amount of training data. As motion data collection is quite expensive, these models do not work well in leave-one-subject-out cross-validation due to a lack of training data. Another limitation of existing studies on continuous movement recognition lies on data preprocessing: how to fast and accurate segment continuous movement data. Most studies [39-43] use sliding windows for segmentation, and the window size is often a fixed threshold value determined by features analysis [44] or sensor sampling frequency [45]. The resulted segment using this approach may contain multiple motions, leading to inaccurate labeling. This can be improved by using an adaptive sliding window, such as

through greedy algorithms [46] or the regression models [47]. However, this requires high computing complexity.

The second challenge is to extract ground truths from uncontrolled continuous movements in an accurate, simple, and less-costly way. Existing ground truths are typically manually extracted and labeled from video/camera recordings. This is very time-consuming, and its application for uncontrolled settings is impossible due to privacy concerns. Some studies [48] utilizes user self-reporting as ground truths, which often has unavoidable mistakes. To address this, weak supervision, such as multiple instance learning [49] or stratified labeling with weak classifiers [48], has shown improved performance when recognizing a specific motion from a period of continuous movements in uncontrolled environments. Another study trains classifiers [50] with inaccurate labels (noises) and then use multilabel learning methods to further improve recognition accuracy. These weak supervision methods can provide fast labeling options for applications that do not require high quality labels [51], such as image and text classification, but are not well explored in continuous movement recognition.

1.4. Design and Development of Monitoring Insoles (MONI)

Foot-worn wearable devices, satisfying all the requirements for daily life use, become the next favorite for daily uses besides smart watches. Moreover, foot-worn wearable devices can effectively measure lower limb movements, including local and full body movements. Compared to the smart shoes [52-54], smart insoles [55] are invisible, portable, compact, easily embedded with small-size electronics in a low

fabrication cost. Smart insoles are the best form of wearable devices for falling risk evaluation in daily life through foot motions.

1.4.1. Review of Smart Insole-like Devices

Smart insole-like devices include smart shoes and smart insoles. Smart insoles refer to designs in an insole shape, invisible from outside of the shoes, portable to be fitted to any shoes, compact, easily integrating small-size electronics in a low fabrication cost. Thus, smart insoles are very likely to be one of the top essential wearables in our life soon, which is the focus in our review. Our review also includes some smart shoes refer to designs with some parts attached to the shoe and some parts embedded in the insole.

Daily life uses of smart-insole like devices would be desirable for applications of gait studies in foot pressure measurement [56-77], gait spatiotemporal parameter extraction [44, 55, 58, 78-97], and gait pattern analysis [82, 98-107], activity recognition [31, 32, 44, 84, 88, 93, 95, 97, 108-116] for health monitoring, support to disease diagnosis, rehabilitation, fitness training, foot gesture recognition for human machine interaction [117-121] and so many more [122-127], rather than only being used in labs or clinics as medical devices [15, 107, 128]. The key factors for daily life uses are data, power, wearable factor, connectivity, cost, and robustness. During the past decade, the proposed insole-like devices have transformed from bulky to light-weighted or even "invisible" designs and the corresponding sensory signal processing algorithms have achieved good performance in in-lab tests and been making progress in real-time computations [40, 129-131]. Most recent studies [32, 80, 85, 86, 90, 92, 93, 95, 114,

117, 132, 133] are being aggressive of taking daily life uses into considerations. However, it is generally agreed that most of the current designs are not ready for daily life uses mainly due to the reasons that uncontrolled factors in real life settings are not well considered when validating the functionalities in lab settings. Even though various types of wearable devices in diverse applications and their corresponding signal processing and sensor information analysis focusing on big data technologies have been making great progress in recent years, well reviewed by a great number of papers [128, 134-138], the machine learning frameworks and data analysis for smart insole-like devices are still lack of robustness when exposed to new environments and new users due to limited data from limited number and diversity of subjects in experiments.

Besides research studies, there are some emerging commercial products [139-150] in the past years. Due to the relative high prices, specific functionalities and complex setups, these products are not well-accepted for daily life uses, but only used within small groups such as patients, clinics, and researchers [116, 123, 151-158].

Figure 1.4 is a technology-centered evolution map of smart insole-like devices with a focus on the representative designs among the 79 prototypes from the past decade. Technologies with significant impacts to the field in the past decade are microelectromechanical systems (MEMS), flexible/textile electronics, machine learning, sensor system integration and footstep energy harvesting within an insole shape. The development is summarized into three periods: the primary exploration prior to year 2008, the fast development period from year 2008 to 2013 and the booming period from year 2014 to 2019.

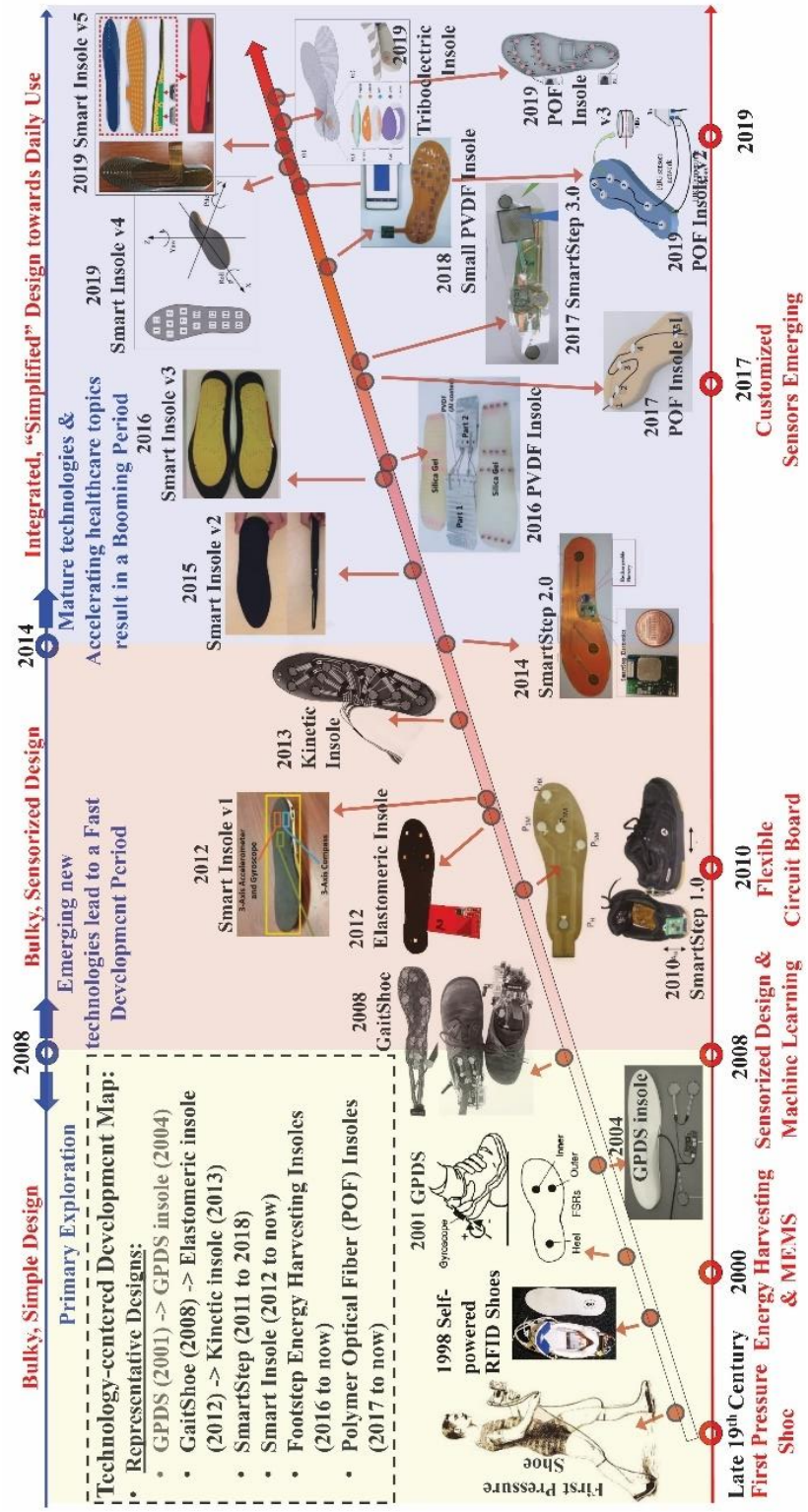

Figure 1.4 A technology map of smart insole-like devices.

1.4.2. MONI Design

After reviewing smart wearable devices for falling risk evaluation and foot motion recognition, and the existing smart-insole like devices, MONI is designed and developed specially for PD patients for the use of falling risk evaluation through simple foot motions.

1.4.2.1. MONI Prototype

MONI (Figure 1.5), a smart insole designed with comfort, has a microcontroller (MCU) (MSP430F149), two accelerometers (ACC) (ADXL362) and a Bluetooth (BLE) Low Energy Module (CC2540). These modules are integrated into two Printed Circuit Boards (PCB) with associated peripheral circuits: one under the heel, and the other one under the first metatarsal of the right foot.

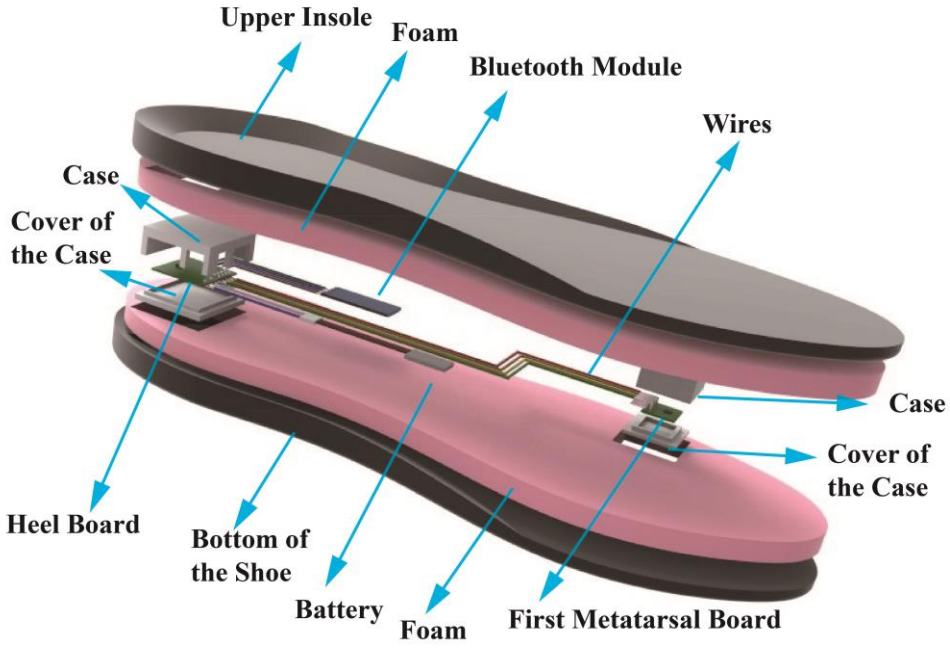

Figure 1.5 3D model of the prototype of the proposed MONI. Layers of the design are clearly shown. © 2021 IEEE. Reprinted with permission from [95].

MSP430F149, ADXL362 and CC2540 are chosen particularly due to their ultralow power consumption. MSP430F149 has six working modes (active mode and low power modes of LPM0 – LPM4) and a large internal storage (60 KB). ADXL362 has three low-power operating modes (standby, wake-up and measure mode) and an on-chip first in, fist out (FIFO) buffer (512 word-large). These modes can be smartly managed by the proposed WMM algorithm. In addition, ADXL362 has on-chip comparators to differentiate "activity" from "inactivity" with preset thresholds.

1.4.2.1.1. Sensor Position

It is reported that the most reliable sensor positions for characterizing typical gait patterns, such as heel strike, flat foot contact, toe-off and swing, would be the heel and metatarsals [159]. For early-stage PD assessments, gait characteristics extracted from the heel, lateral and medial arch, and first metatarsal play more critical roles compared to these extracted from other positions [89]. Many existing smart insoles use force sensors to measure temporal gait parameters and inertial sensors to extract spatial parameters, which is redundant for sensors. It has been proved by a variety of research that the temporal gait parameters can be accurately extract from inertial sensors attached to the shoe [160].

Therefore, MONI only has two accelerometers, one under the heel and one under the first metatarsal, as shown in Figure 1.6(a). Data collected from the first metatarsal and the heel, as shown in Figure 1.6(b), represent the movement of the front and the back of the foot, and contain the most typical gait characteristics, which favors the activity recognition as well.

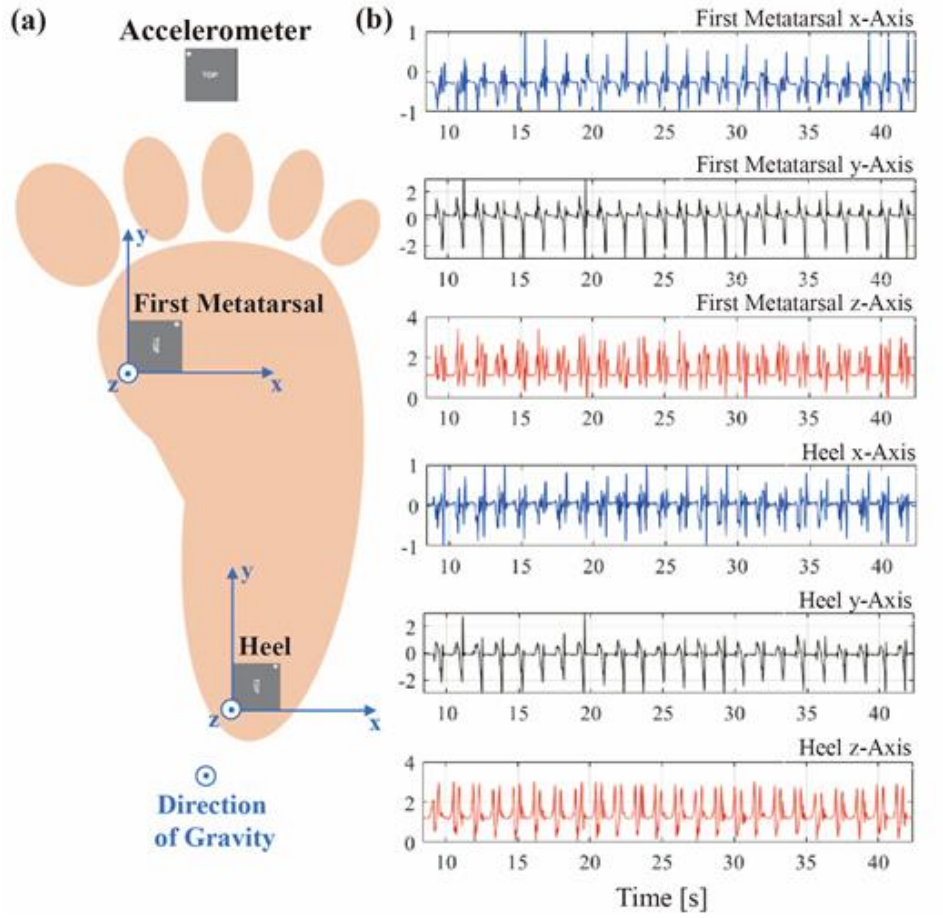

Figure 1.6 (a) Axis Directions of Accelerometer and Sensor Position; (b) The raw data collected by MONI beneath the right foot, with 25 seconds' regular walking in a straight routine; the y-axis of (b) is acceleration in gravity g = 9.81 m/s^2. Note that, the x, y and z-axis of the accelerometer align with the lateral-medial, anterior-posterior, and superior-inferior directions of the user. © 2021 IEEE. Reprinted with permission from [95].

1.4.2.2. Early Version of MONI

Built from the lab prototype, the early version of MONI still has two accelerometers with the sampling frequency of 150 Hz, positioned at the heel and the first metatarsal area, respectively (Figure 1.7). The rigid printed circuit boards are connected via flat flexible cables and all the electronics are sandwiched between black

high-density tape foams. The Bluetooth Low Energy (BLE) module is connected to the inner side of the shoe. To be fit for different shoe sizes, flexible cables can be switched so that the accelerometers are ensured to be at the same position. In our experiment, we install MONI in the same kind of shoes with different sizes for all the subjects to collect foot motion data, for further evaluation of the user's motor functionality.

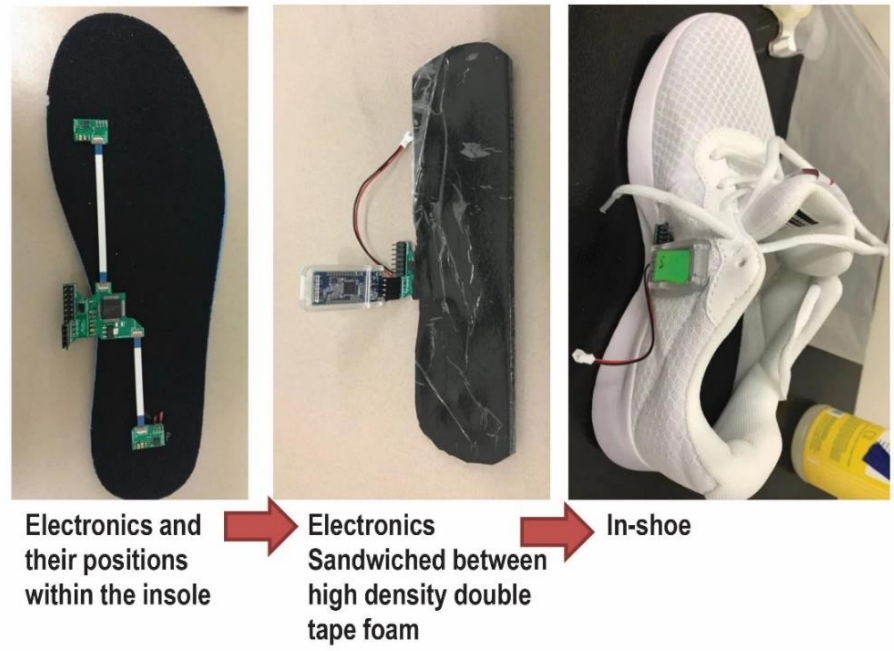

Figure 1.7 The prototype and in-shoe installation of the early version of MONI. © 2021 IEEE. Reprinted with permission from [161].

1.4.2.3. Upgraded Version of MONI

The MONI, upgraded from our previous versions [161], contains two accelerometers positioned at the heel and the first metatarsal, a microcontroller (MCU) and a Bluetooth Low Energy (BLE) module. This upgraded MONI has all electronics are sandwiched between two high-density textile foam layers, and then buried into epoxy resin for protection. As shown in Figure 1.8(a), the battery is connected via jumpers

through two holes at the inner side of the insole for the ease of power-on and off. In the future, the battery can be directly connected to the electronics layer. For different shoe sizes, the electronic components are the same, but the length of flexible cables and the size of high-density textile foams are different. We prepare 6 pairs of upgraded MONI inserted in shoes with size 8 to 13. As shown in Figure 1.8, being unobtrusive, portable, and comfortable, the upgraded MONI can collect comprehensive foot motion information from PD patients in daily life.

Figure 1.8 The prototype of upgraded MONI (size 8): (a) the bottom layer (the foam with electronics), and the top layer (the high-density textile foam); (b) the top view and (c) the side view inside a pair of MONI inserted in shoes.

1.4.3. A Low-power Solution for Daily Life Use

A Working-mode Management (WMM) algorithm is designed to be implemented in MONI in real time, which minimizes the power consumption of MONI. The WMM algorithm features six working modes, namely Deep Sleep Mode, Check Mode, Idle Mode, Data Acquire Mode, BLE-ON Mode and Sleep Timer Mode. It is developed to ensure that MONI can sample the right amount of effective data from foot motions such as walking throughout a day, while remaining at Deep Sleep Mode if possible. It can be disenabled if continuous data collection is needed.

The WMM algorithm, a finite state machine implementation, smartly evaluates, classifies, and judges the output acceleration signals, while taking full advantage of low-power features of the MCU and accelerometers to achieve mode alternation. Moreover, to ensure an accurate and efficient assessment, the data will be sampled during continuous walking (or other foot motions) without stopping. The following subsection introduces the classification and detailed alternations of the six working modes of MONI, as shown in Figure 1.9(a).

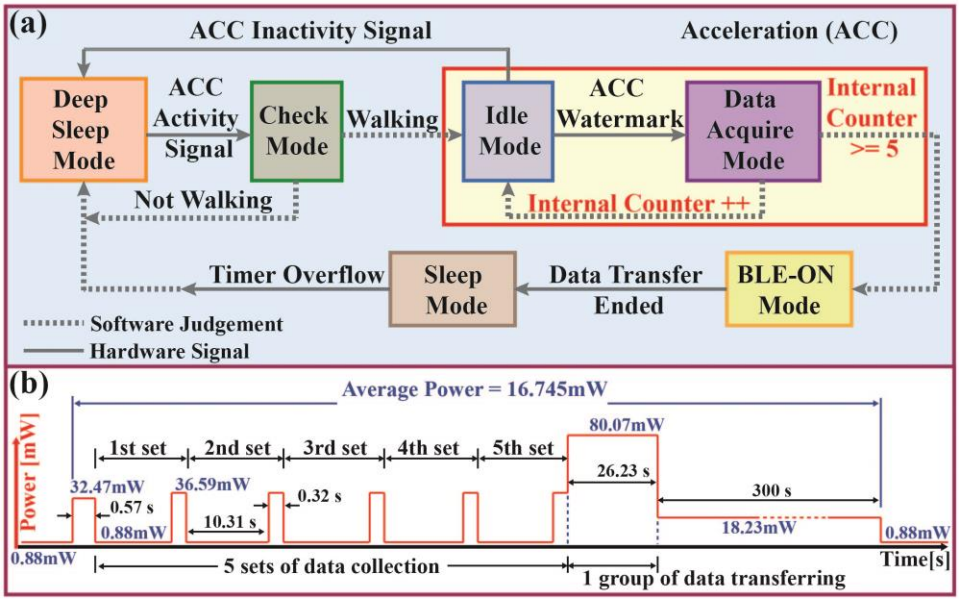

Figure 1.9 Working flow of Mode Management in the proposed WMM algorithm; (b) The Power Trace of an example mode alternation: each mode is tested separately with a supply voltage of 3.3V as shown in TABLE I. The example alternation follows: *Deep Sleep Mode-> Check Mode -> Idle Mode -> Data Acquire Mode -> Idle Mode -> Data Acquire Mode -> Idle Mode -> Data Acquire Mode -> Idle Mode -> Data Acquire Mode -> Idle Mode -> Data Acquire Mode -> BLE-ON Mode -> Sleep Timer Mode (5 minutes) -> Deep Sleep Mode*. © 2021 IEEE. Reprinted with permission from [95].

Deep Sleep Mode: both accelerometers sample data at a low frequency (12.5 Hz). If acceleration variation reaches the preset threshold value of 0.2 g, MONI will be switched to the *Check Mode*.

Check Mode: MONI receives an ACC Activity signal, suggesting the possibility of walking or other foot motions. The AAR algorithm will further identify whether it is a motion, MONI will be switched to the *Idle Mode*. Otherwise, MONI will be switched back to the *Deep Sleep Mode*.

Idle Mode: accelerometers sample data at 25 Hz, which has been proven enough for gait parameter extraction [19-20], and the on-chip FIFO is activated for data

recording. The FIFO will be full in 6.8s with a storage of 170 sub-datasets (three axis acceleration data (x, y, z) as a sub-dataset). Once the FIFO is full, a signal (ACC Watermark) generated by the accelerometer will trigger MONI to the *Data Acquire Mode*. If the FIFO is not full and the sampling data is smaller than a preset threshold for a period (1 s), a signal (ACC inactivity) from the accelerometer will bring MONI back to the *Deep Sleep Mode*, and all data recorded in FIFO will be cleared. Such a design ensures that a series of acceleration data of continuous walking will be recorded, eliminating any "inactivity" data for efficient gait analysis.

Data Acquire Mode: MCU reads the datasets from accelerometers and stores them into its internal storage. The internal counter automatically adds by one when reading ends. MONI goes back to the *Idle Mode* to continuously record acceleration data. If the internal counter reaches five, suggesting that five sets of data (as a group of data) from each accelerometer are stored, MONI will be switched to the *BLE-ON Mode*.

BLE-ON Mode: a controlled MOSFET switch is turned on. A group of data (five sets) of each accelerometer will be sent through the BLE module to a smart phone, and then MONI will enter the *Sleep Timer Mode*.

Sleep Timer Mode: an internal timer runs. Length is adjustable depending on how active the user is. If the user is highly active, it is suggested to use a longer timer so that data will be better scattered throughout the day. When the timer overflows, the system will go back to the *Deep Sleep Mode* to start a new round of alternation. By setting up the *Sleep Timer Mode*, MONI ensures that data is sampled throughout the whole day instead of in a continuous time period.

Table 1.1 details the breakdown of power consumption, execution time and status of each component in each mode. The execution time of the *Deep Sleep Mode* will be determined based on how active the user is. A simple mode alternation example with the power trace of WMM is shown in Figure 1.9(b). The average power is 16.745 mW without the *Deep Sleep Mode*. When the *Deep Sleep Mode* is applied, the daily power can be further minimized.

Table 1.1 Power consumption, execution time, and status of each component (MCU, ACC and BLE). © 2021 IEEE. Reprinted with permission from [95].

Working Mode	**Power Consumption**	**Execution Time**	**MCU**	**ACC**	**BLE**
Deep Sleep	0.88 mW	/	LPM4	Measure	OFF
Check	32.47 mW	0.57 s	Active	Measure	OFF
Idle	0.88 mW	10.31 s	LPM4	Measure	OFF
Data Acquire	36.59 mW	0.32 s	Active	Standby	OFF
BLE-ON	80.07 mW	26.23 s	Active	Standby	ON
Sleep Timer	18.23 mW	300 s	LPM3	Standby	OFF

1.5. Scopes and Objectives of the Dissertation

The dissertation aims to provide quantitative analysis of falling risks for PD patients in daily life to help prevent falling at home through foot motions in easy setups and simple processes using MONI as shown in Figure 1.10. To achieve the goal, the

dissertation mainly focuses on the data processing method for MONI, which incorporates foot motion recognition, feature extraction and analysis, and falling risk scoring through foot motion tasks to provide compatible results to the FRQ.

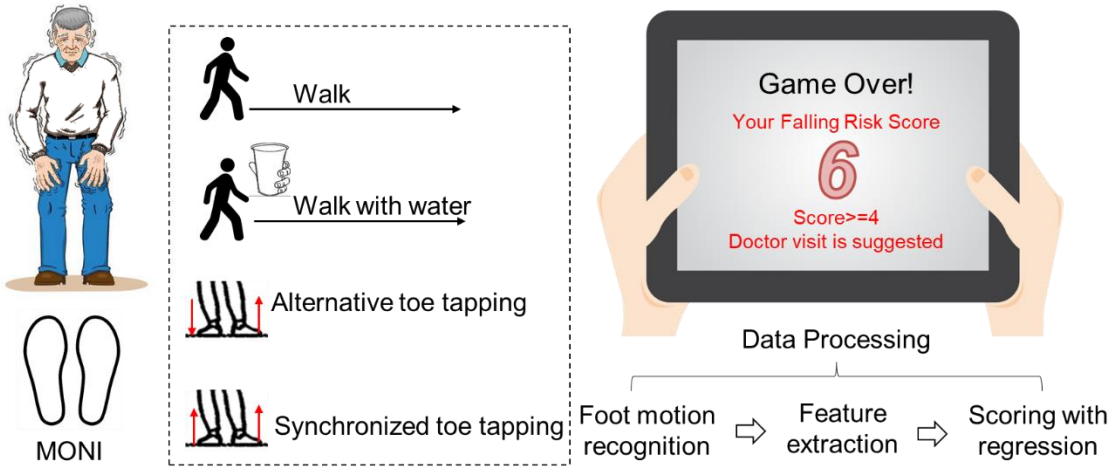

Figure 1.10 Proposed quantitative falling risk scoring with built-in data processing using MONI.

The main contributions of this dissertation includes: (i) designing and developing versions of MONI to be used in daily life (introduced in Chapter 1); (ii) utilizing stride detection and developing fast labeling framework for motion recognition that improves recognition accuracy for daily life uses; (iii) analyzing two walking and two toe tapping tasks and identifying important features associated with PD and falling risks; (iv) providing falling scores as quantitative results to PD patients in daily life through the simple foot motion tasks.

Chapter 2 presents our proposed method of fast labeling framework for robust foot motion recognition in daily life. The Chapter first introduces experiment done using early version of MONI and subjects who participate. Datasets are built and stated. Then,

the proposed motion recognition methods are detailed, and the validation of the proposed motion recognition method used for gait feature analysis is presented. Finally, based on the literature review, foot motions are selected to be used for falling risk analysis for PD.

Chapter 3 focuses on walking-based falling risk evaluation. Through literature review, two tasks (walking and walking with a cup full of water) are analyzed. Gait and acceleration-axis features are extracted. Features associated with PD are identified and falling risks are evaluated through regression models which provide a falling risk score compatible to the clinically verified falling risk questionnaire.

Compared to walking-based falling risk evaluation, Chapter 4 investigates toe tapping-based falling risk evaluation. Using coordination dynamics, two toe tapping tasks are designed (anti-phase and in-phase tapping). Time-axis and acceleration-axis features are extracted and analyzed. Features to distinguish PD from HC are identified and falling risks are evaluated through the same regression methods in Chapter 3.

In the end, Chapter 5 compares our method to other similar methods and summarizes the dissertation in the contributions and future work to make the proposed data processing method for MONI be used in real life.

2. FOOT MOTION RECOGNITION[*†‡§]

Foot motion recognition in daily life faces two challenges imposed by traditional machine learning frameworks: how to robustly recognize various foot motions from continuous movements in uncontrolled environments, and how to accurately extract ground truths. To address these challenges, we propose a stride detection method to robustly identify each stride (over 99% accuracy). We then investigate two weak supervision-based fast labeling frameworks to automatically label the stride segmentations. Finally, we use these two frameworks to identify foot motions from continuous movements integrated on a route map. The route map can be replaced by a virtual-reality video game to play in daily life so that the user's long-term foot functionality can be profiled and evaluated. We test our proposed approaches using the early version of MONI with twenty-two subjects whose movement data are collected through the route map setting while video camera recordings serve as the ground truth. The route map integrates seven foot motions in one complete play, which includes three continuous motions resulted from continuous full-body movements (named as sequential

---

[*] Part of this chapter is reprinted from "Monitoring insole (MONI): A low power solution toward daily gait monitoring and analysis." by Hua, R. and Wang, Y., *IEEE Sensors Journal* 19.15 (2019): 6410-6420. Copyright © 2019 IEEE

[†] Part of this chapter is reprinted from "A Customized Convolutional Neural Network Model Integrated with Acceleration-Based Smart Insole Toward Personalized Foot Gesture Recognition." by Hua, R., and Wang, Y., *IEEE Sensors Letters* 4.4 (2020): 1-4. Copyright © 2020 IEEE

[‡] Part of this chapter is reprinted from "Age-Dependent Mobility Decline Analysis Through Sequential Foot Motion Reproduction." by Hua, R. and Wang, Y., *IEEE Sensors Letters* 5.11 (2021): 1-4. Copyright © 2021 IEEE

[§] Part of this chapter is reprinted from "Daily locomotor movement recognition with a smart insole and a pre-defined route map: Towards early motor dysfunction detection." By Hua, R., and Wang, Y., 2019 IEEE Healthcare Innovations and Point of Care Technologies (HI-POCT): pp 87-90.

motions) and four repetitive foot motions that are produced repetitively (named as repetitive motions). Compared to the best traditional machine learning methods, our proposed approach improves the leave-one-subject-out cross-validation accuracy of all subjects by 6.12% for the three sequential motions, 2.71% for the four repetitive motions and 4.90% for the total of seven foot motions. In addition, our proposed method saves 25% to 50% time in data labeling. Figure 2.1 is the abstract of this chapter.

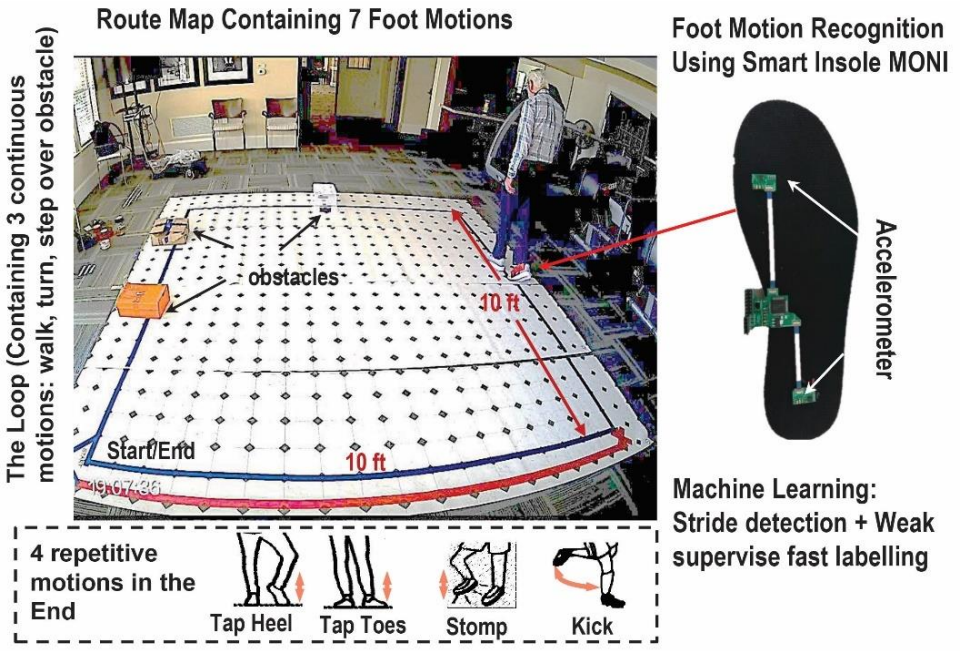

Figure 2.1 Graphical abstract of Chapter 2. © 2021 IEEE. Reprinted with permission from [161].

2.1. Experiment

The route map (Figure 2.2) has one loop containing three sequential motions: walking, half turning and stepping over obstacles. Four repetitive motions are performed in the end of the loop, including tapping heel, tapping toes, stomping, and kicking independently from the loop. These seven foot motions are selected from the standard

clinical tests of Balancing Test [23] and Unified Parkinson Disease Rating Scale (UPDRS) [24] for the purpose of evaluating foot motor functionality. The route map (10 ft * 10 ft) can be easily replaced by a virtual game setting.

A complete play includes one loop of the route map from the start to the end point (following blue arrows) for continuous motion data collection, followed by a collection of four repetitive motions.

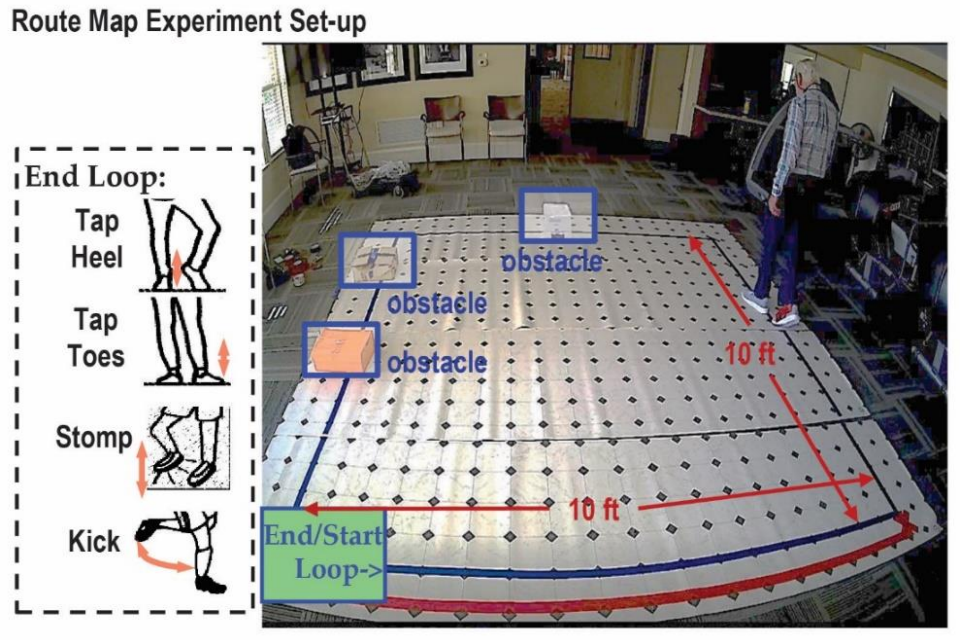

Figure 2.2 Photographic representation of the pre-designed route map experiment set-up. © 2021 IEEE. Reprinted with permission from [161].

2.2. Subjects and Datasets

We collect three types of foot motion datasets (Table 2.1) with two experiments using the route map shown in Figure 2.2. *Sequential Motion Dataset* is collected when subjects looping the route map from the start to the end, and data is segmented with stride detection method presented in Chapter 2.4. *Repetitive Motion Dataset* is collected

separately after the looping when subjects are in the standing posture and performing repetitive foot motions of Tap Heel, Tap Toe, Stomp and Kick. Subjects perform each repetitive motion continuously following instructions to start and end typically within 10 - 15s. Repetitive motion data is segmented with a 1.5s sliding window. We add walking data (collected separately by asking subjects to walk at their own pace and segmented with a 1.5s sliding window) as the noise data set to *Repetitive Motion Dataset*. Each experiment is repeated five times by each subject, indexed as experiment process 1 to 5. Ground truth is collected by manually labelling the video camera recording. *Route Map Dataset* is the combination of *Sequential Motion Dataset* and *Repetitive Motion Dataset* without the noise data set (walking).

There are a total of twenty-two subjects (Max Age: 89, Min Age: 20; Max Height: 188cm, Min Height: 155cm; Max Weight: 95.25kg, Min Weight: 47.63 kg; Max Shoe Size (U.S.): 12, Min Shoe Size (U.S.): 6) participated in the route map experiment, while the sequential motion data of two subjects are lost during the experiment.

Table 2.1 Three types of foot motion datasets by subjects.

	No. of Motions	Motions	No. of Subjects	Height (cm)	Weight (kg)	Age
Sequential	3	Walk Half Turn Step Over Obstacles	20	172.8	74.3	41.4
Repetitive	4	Kick Stomp Tap Heels Tap Toes	22	173.7	74.2	38.8
Route Map	7	Walk Half-Turn Step Over Obstacles Kick Stomp Tap Heels Tap Toes	20	172.8	74.3	41.4

2.3. Data Preprocessing

Figure 2.3 shows the flowchart of data preprocessing, and the feature set is used to develop the recognition algorithm. As stated in the previous Section 2.2, raw data is first filtered with a 4th order low-pass filter with the cut-off frequency of 10 Hz and offset errors are removed by normalization on all axes. Stride detection is applied to sequential motions and continuous data is segmented into strides as the segments. Sliding window with a fixed size of 1.5s is used for repetitive motions and continuous data is segmented into short windows as the segments. Acceleration features are then extracted from the segments. A label to the segment is added which is from the ground truth (camera recordings) or from our proposed fast labeling framework.

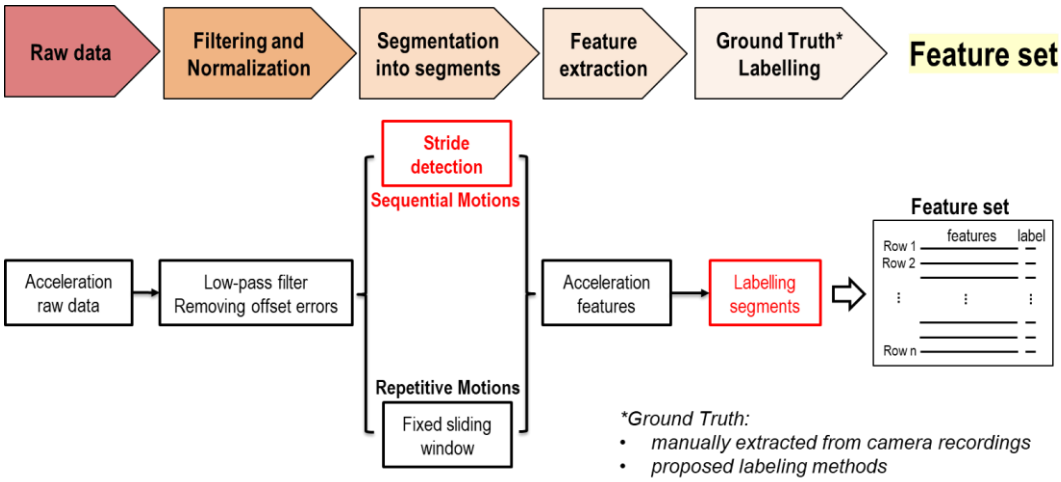

Figure 2.3 Flowchart of data preprocessing.

2.4. Stride Detection

Figure 2.4 shows the flowchart of our stride detection method. The raw data from each accelerometer are $(x_t, y_t, z_t)_p$, where t is the index of N sampling points: $t \in [1, N]$ for each axis, and $p \in [heel, first\ metatarsal]$ is the position of each accelerometer. A 4th order low-pass filter with the cut-off frequency of 10 Hz is applied. The standard deviation std_t of $(x_t, y_t, z_t)_p$ is calculated for all the sampling points as the 4th axis. The discrete differential transform of all the 4-axis data is $(\Delta x_t, \Delta y_t, \Delta z_t, \Delta std_t)_p$ for each accelerometer.

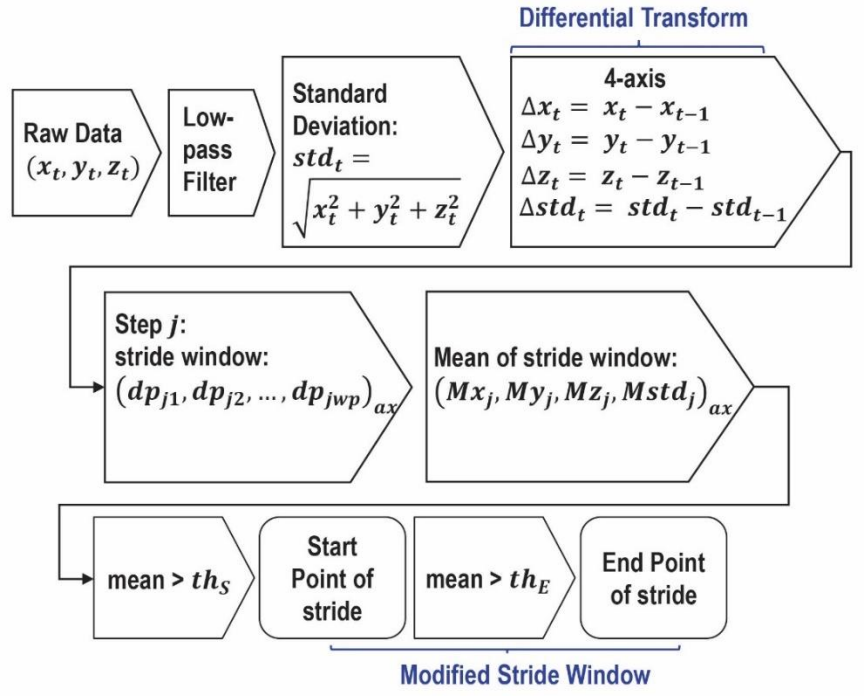

Figure 2.4 Flowchart of the proposed stride detection method. © 2021 IEEE. Reprinted with permission from [161].

Next, we define the stride window containing *wp* data points (window size) of 4-axis as $(\Delta x_t, \Delta y_t, \Delta z_t, \Delta std_t)_p$. The stride window moves one point forward each step for a total of *Ws* steps, where $Ws=N-wp+1$. The data points within the stride window for step $j \in [1, W_s]$ is $(dp_{j1}, dp_{j2}, \ldots, dp_{jwp})_{ax}$, where *ax* is one of the axes in *(x, y, z, std)*. The mean values $(Mx_j, My_j, Mz_j, Mstd_j)_{ax}$ of the stride window are calculated, and then compared to the start point threshold values $(th_S)_{ax}$ and the end point threshold values $(th_E)_{ax}$ to determine the start and the end point of each stride.

After the start and the end point of the stride are identified, we move the start point of each stride *(2*wp)* data points ahead and move the end point *(2*wp)* data points behind to make sure that a complete stride is detected. This is defined as the modified

stride window to identify each stride with high accuracies for further use in continuous movement segmentation. There is an additional judgement to remove some incomplete or partial strides: If the size of the modified stride window is larger than *(40%*150)*, where 150 is the number of datapoints collected per second), it is a full stride.

We find that the key parameter to identify the start point of the stride is the threshold value $(th_S)_z$ from both accelerometers, while the critical parameters to detect the end point of the stride are the threshold values $(th_E)_x$, $(th_E)_y$ and $(th_E)_{std}$ of both accelerometers. The stride window size *wp* is also crucial to the detection accuracy.

The stride detection only applies to sequential motions including walking, half-turning and stepping over obstacles (Table 2.1) from twenty subjects. The threshold value $(th_S)_z$ to detect the start point of a stride is set as 0.002 for both accelerometers.

We perform nested grid search for the threshold values th_E for axes of *(x, y, std)*, where the best combination values are 0.003, 0.0015 and 0.002 as shown in Figure 2.5(a-c), and best value of *wp* is 7 in Figure 2.5(d). These best threshold values, red dots in Fig. 7(a-d), work well for all twenty subjects despite different subject characteristics of age, height, weight, and shoe size. Figure 2.5(e) shows the stride detection for each subject under the best combination of the threshold values. There are a total of 1145 strides, where our stride detection method detects 1143 strides correctly. That is, our method has a detection accuracy of 99.83%.

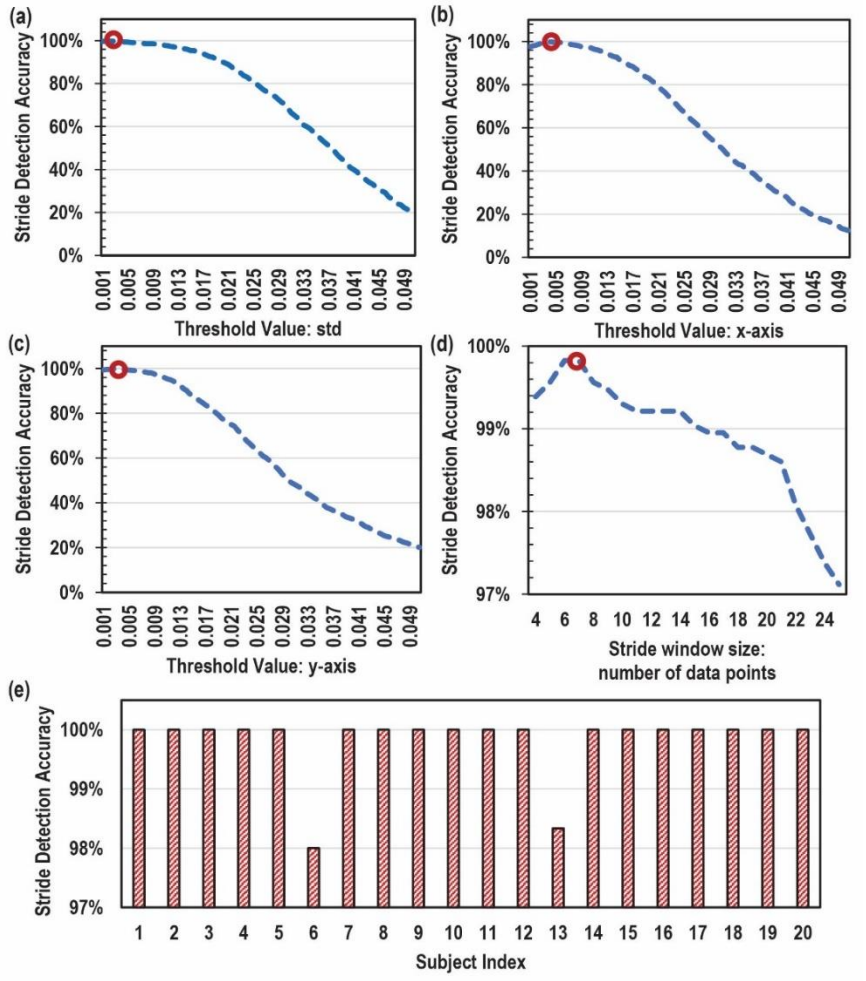

Figure 2.5 Threshold value th_E search; (d) threshold value *wp* search; (e) detection accuracy for each subject. © 2021 IEEE. Reprinted with permission from [161].

Our stride detection method reaches an average accuracy of 99.83% for twenty subjects with a wide variety of characteristics in age, height, weight and shoe size. The discrete differential transform on acceleration data minimizes the influence of the threshold values $(th_E)_{ax}$ on individuals with wide varieties. In such way, a slight change of $(th_E)_{ax}$ won't affect the accuracy much as shown in Figure 2.5(a-c). Fine-tuning these threshold values would work well for new subjects. Thus, our proposed stride detection

method is robust and effective for foot motions of walking, half-tuning and stepping over obstacles.

Compared to the existing studies [162-169] using different methods as shown in Table 2.2, our methods show the best accuracy and applied to stride detection in different kinds of sequential motions (besides walking).

Table 2.2 Comparison to the existing studies using different methods.

Method	**Motion**	**Accuracy**	**Pros**	**Cons**
Peak-detection	Walk	93%-99%	Low computation Low accuracy	Only effective to specific motion
Dynamic time wrapping		99%	High accuracy/robustness	Large amount of training data high computation demand
Hidden Markov		91%		
Residual neural networks		96%		
Our method	**Walk, Turn and Step over obstacle**	**99%**	**Low computation + high accuracy**	**Effective to motions in experiment**

2.5. Feature Extraction

After the segmentation of sequential and repetitive motions, using the stride detection and sliding window, respectively, we will move forward for feature extraction. After reviewing the most representative features from acceleration data [170] for activity recognition, we manually craft 19 features to be extracted from the 4-axis segmented

data of both accelerometers in time-domain. Table 2.3 lists the math description of the selected features used in this study, where *(d_1, d_2, …, d_n)* represents a total of *n* segmented datapoints of each stride in time series. We then sort these datapoints in the order of smallest to largest and denote as data array *D* to be used in the training and test datasets.

Table 2.3 Math description of features of interest. © 2021 IEEE. Reprinted with permission from [161].

Feature Name	Math Description	Feature Name	Math Description
Mean	$\mu = \frac{1}{n}\sum_{i=1}^{n} d_i$	Skewness	$\frac{1}{n\sigma^3}\sum_{i=1}^{n}(d_i-\mu)^3$
Minimum	$min(d_1, d_2, \cdots d_n)$	Kurtosis	$\frac{1}{n\sigma^4}\sum_{i=1}^{n}(d_i-\mu)^4$
Maximum	$max(d_1, d_2, \cdots d_n)$	Signal Power	$\sum_{i=1}^{n} d_i^2$
Median	$median(d_1, d_2, \cdots d_n)$	Root Mean Square	$\sqrt{\frac{1}{n}\sum_{i=1}^{n} d_i^2}$
Standard Deviation	$\sigma = \sqrt{\frac{1}{n}\sum_{i=1}^{n}(d_i-\mu)^2}$	Number of Positive Peaks	N/A
Coefficients of Variation	$\frac{\sigma}{\mu}$	Number of Negative Peaks	N/A
Peak-to-Peak Amplitude	$max - min$		
Percentiles	$Percentile(D, n_k) = (n_k/100) \times D$, where $n_k =$ 10, 25, 50,75,90 and D is $(d_1, d_2, \cdots d_n)$ sorted from smallest to largest	Interquartile Range	$Percentile\ (D,\ 75) - Percentile(D,\ 25)$

2.6. Fast Labeling Framework

For the benchmark framework in Figure 2.6(a), we use KNN, RF and SVM as the end classifier as they are commonly used and have low computational costs compared to deep learning models. The benchmark framework needs all the available training data labelled with ground truths, and then uses this training dataset to train and test each classifier. The trained classifier generates a recognition result *y* for new dataset.

We investigate two types of fast labeling frameworks: Label Model Framework (LMF), which uses the label model to label training datasets and then provides recognition results as shown in Figure 2.6(b), and Combined Framework (CF) integrating the benchmark and the LMF framework as shown in Figure 2.6(c). The weak supervision is applied to these two fast labeling frameworks by using weak classifiers as the label functions.

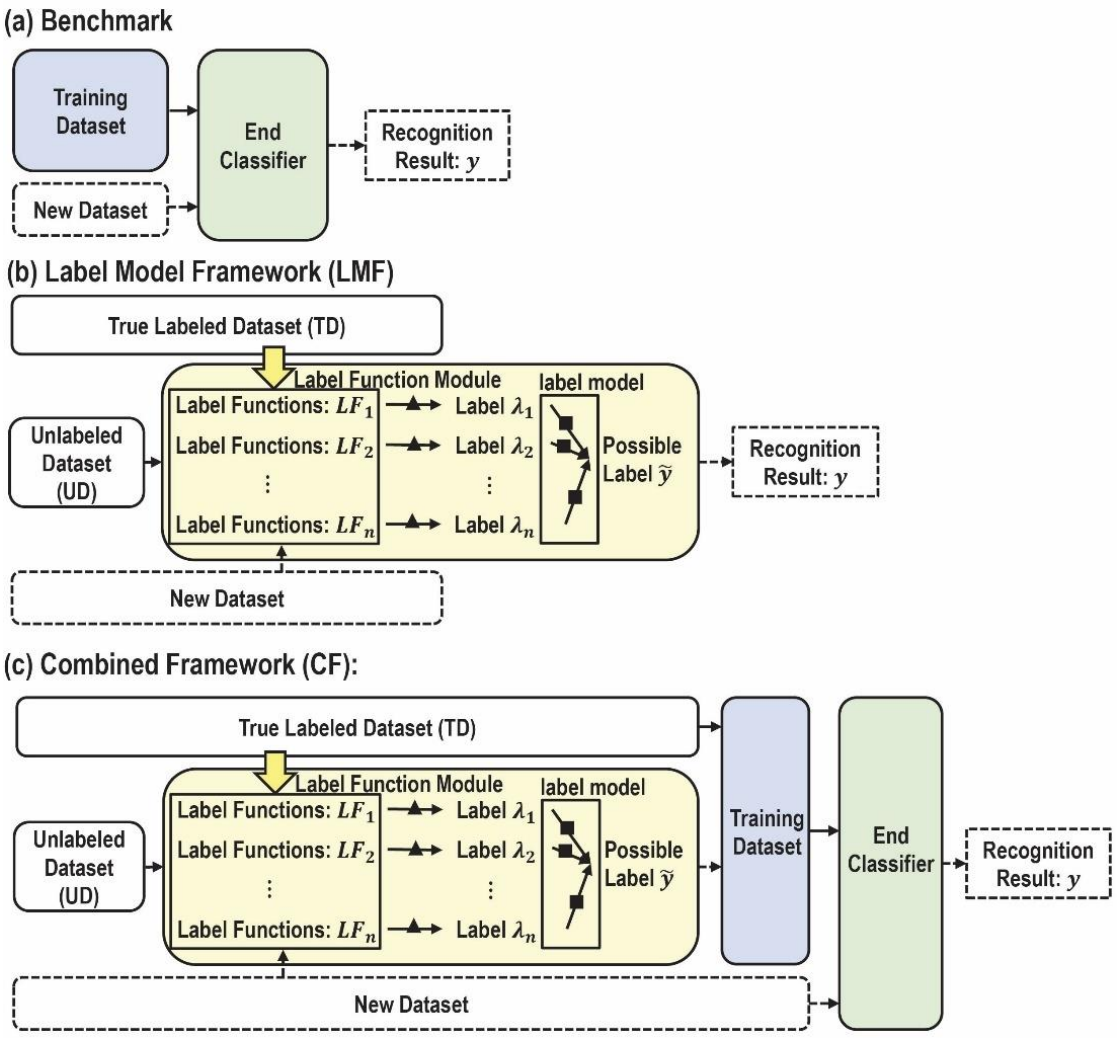

Figure 2.6 Fast labeling framework (a) Benchmark: traditional machine learning framework; (b) LMF; (c) CF. © 2021 IEEE. Reprinted with permission from [161].

2.6.1. Label Model Framework (LMF)

We first split the total available training data into two groups: True-labelled Dataset (TD) and Unlabeled Dataset (UD). TD contains data labeled with ground truths, and UD contains unlabeled data. Next, we produce a set of labels from the label function module containing different label functions. Finally, a label model is applied to generate a final label from the set of labels as the final recognition result. All the label functions

are weak classifiers (SVM, RF or KNN), which are first trained with TD without fine-tuning hyperparameters and then the hyperparameters are tuned with UD with labels provided by the label model as shown in Figure 2.6(b). After these processes, LMF is ready to provide recognition results for the new dataset.

2.6.1.1. Data Splitting

We define two strategies to split training data into TD and UD. One strategy is to split data based on subject characteristics including age, height, weight, and shoe size. This ensures that the TD and UD both have data from different subjects with similar characteristics. The other strategy is to split data using experiment process index. This ensures that the TD and UD both have data from the same subjects. Here, we set the splitting ratio between TD and UD as 1:1 or 3:1. The ratio of 1:1 saves 50% of manually labeling time, while 3:1 saves 25%. Thus, in total, there are four different data preparation of TD and UD based on the splitting.

2.6.1.2. Label Functions

Each label function represents a weak classifier (SVM, RF or KNN) trained with TD without fine tuning all the hyperparameters. Each label function module provides a set of labels for the UD or the new dataset.

2.6.1.2.1. Label Function Module

Two label function modules are defined: MODULE1 has three label functions, while MODULE2 has five label functions. Each label function in the module provides a label as shown in Figure 2.7, MODULE2 uses possibility check to determine the labels produced by each label function (Figure 2.7(b)). The possibility is computed by

classifiers, which is the confidence of the classification result. If the confident possibility pt_i of the label λ_i from LF_i, where $i<=4$, is larger than the threshold value P_{th}, the label is recorded as λ_i; if not, the label from LF_i is set as *ABSTAIN* (can't decide). The 5th label function provides a label λ_5 without the possibility check, which ensures that there is at least one label available for the situation where all the first four label functions provide *ABSTAIN*.

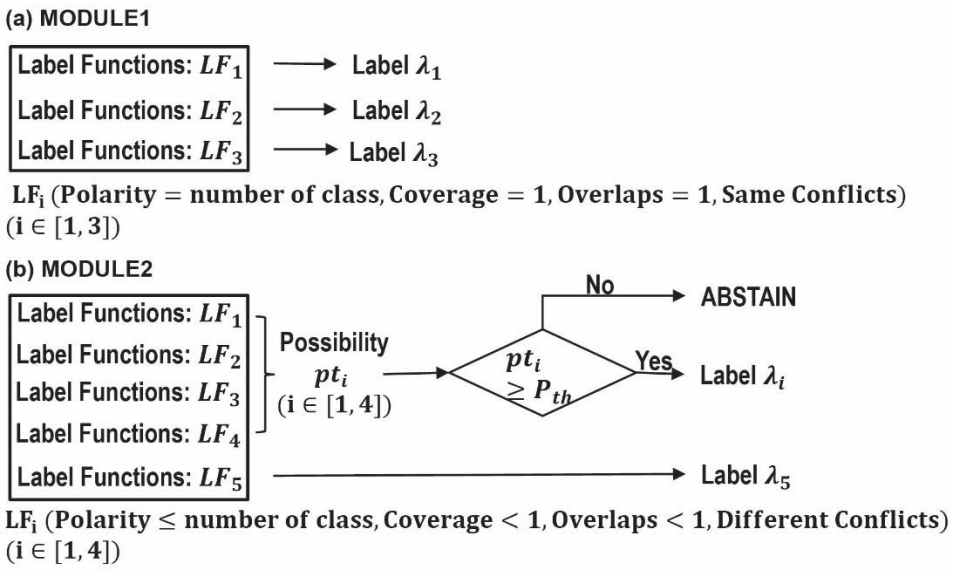

Figure 2.7 Label function module (a) MODULE1; (b) MODULE2. © 2021 IEEE. Reprinted with permission from [161].

2.6.1.2.2. Label Function Properties

We use the properties of polarity, coverage, overlaps and conflicts to determine which label function is used. Polarity is the set of valid labels the label function provides (excluding *ABSTAIN*). Coverage shows the fraction of the dataset a label function covers. Overlaps mean the fraction of the dataset where this label function and at least one other label function provides a valid label (not *ABSTAIN*). Conflicts represent the

fraction of the dataset where this label function disagrees with at least one other label function.

For MODULE1, the polarity of each label function includes all classes in the dataset; the coverage for each label function is one; overlaps are one and every label function has the same conflicts, as every label function provides a valid label (not *ABSTAIN*) for every data segment, as summarized in Figure 2.7(a).

For MODULE2, the label functions checked with possibility pt_i do not cover the whole dataset due to the reason that such label function may provide *ABSTAIN* when the possibility of the label is lower than the threshold value P_{th}. Thus, except LF_5 has polarity of all classes in the dataset, coverage of one and overlap of one, other label functions are with coverage, overlaps and conflicts smaller than one, as shown in Figure 2.7(b).

2.6.1.2.3. Label Function Selection

Label functions are selected based on their properties. The general selection rule is that the label functions in the module should be diverse. That is, label function module should include different kinds of classifiers, imbalanced accuracies on different classes, and with limited coverage, less overlaps, and less conflicts. By checking the properties of each label function and the accuracy for each class of the training dataset TD, we can decide which label function to be used in the label function module.

2.6.1.3. Label Model

Two kinds of label models are explored to combine the set of labels to a final label for an unlabeled dataset, named as the unweighted majority vote model and the

Snorkel label model [171]. The unweighted majority vote model treats all the labels $(\lambda_1, \lambda_2, \ldots, \lambda_v)$ equally, where v is the number of label functions in the label function module. That is, the final label is the label appears maximum number of times within the set of labels. If there are two or more labels (tied options) are with the same maximum number of times, the label model selects the final label randomly from the tied options.

Different from direct voting, the Snorkel label model [51] is a generative model that learns from the correlations and dependencies between label functions by estimating the conditional label function probabilities. If the Snorkel label model can't decide the final label due to the situation of tied options, it randomly selects one label among the tied options.

2.6.2. Combined Framework (CF)

Modified from the LMF, an end classifier (either KNN, SVM or RF) is added at the end of the LMF as shown in Figure 2.6. The LMF in the CF is only used to label the UD with the majority vote model as the label model. These labels provided by LMF with data in UD are combined with TD as the training dataset to train the end classifier. Different from the LMF, label functions are not fine-tuned.

2.6.3. Weak Supervision

There are multiple noise sources in the label functions where the weak supervision is employed. We identify three major noise sources: (i) the label functions, which are weak classifiers trained by a limited amount of data with true labels, and thus are insufficient for our tasks of foot motion detection when applied to new dataset; (ii) the UD, which is labeled by the label model, not 100% accurate compared to ground

truths, and thus these labels with the data in UD are used to fine-tune the weak classifiers in the LMF; and (iii) both the unweighted majority vote model and Snorkel label model, which randomly choose a label among tied options.

2.6.4. Evaluation Strategy

2.6.4.1. Benchmark

We use the traditional supervised machine learning models (KNN, SVM and RF) as the end classifier in the benchmark framework (Figure 2.6(a)). Available data are all labeled with ground truths, which are manually extracted from video recordings. As shown in Figure 2.8, the validation dataset is the data from subject denoted as S_l where $l \in [1, A]$ and A is the total number of subjects in that dataset (Table 2.1). S is the symbol for all data from all subjects. $(S - S_l)$ contains data of the whole dataset minus data from subject indexed l. The training dataset and testing dataset containing data $(S - S_l)$ with a ratio of 8:2 as shown in Fig. 6(a).

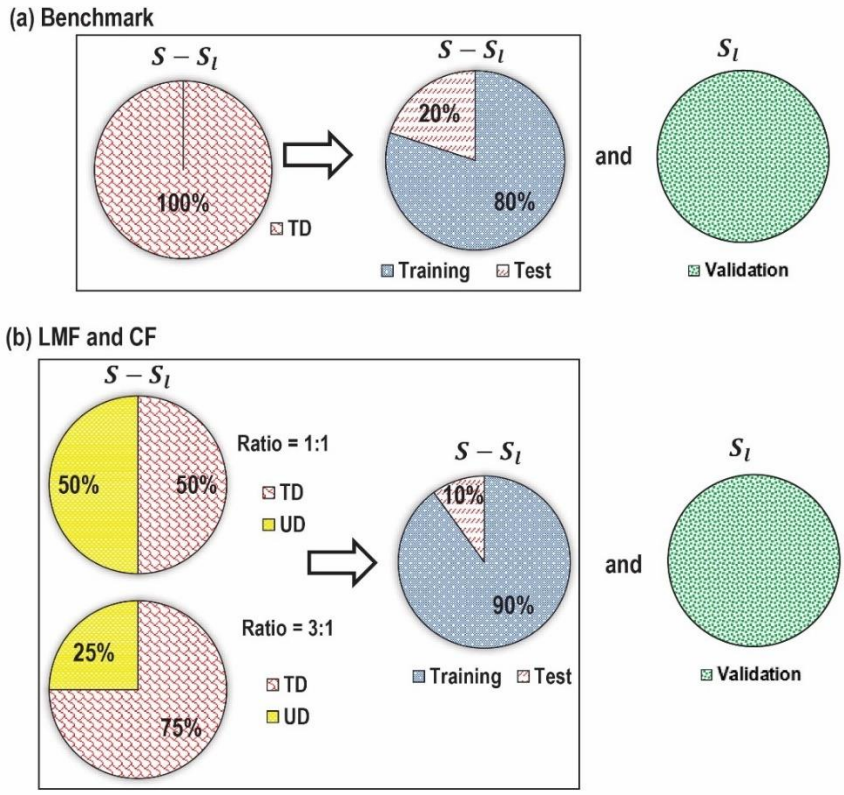

Figure 2.8 Evaluation strategy of (a) Benchmark: traditional machine learning framework; (b) LMF and CF. © 2021 IEEE. Reprinted with permission from [161].

2.6.4.2. LMF and CF

As shown in Figure 2.8(b), different from the dataset preparation for the benchmark, we split the available data *(S - S_l)* with two ratios (TD : UD = 1:1 or 3:1) following the defined data splitting strategies of subject characteristics and experiment process indexes, respectively. In total, we have four different data preparations to be used for comparison and analysis of the impact of different data splitting strategies and ratios for our proposed methods.

Note that we have an even number of subjects for all three datasets in Table 2.1, so that we can split the subjects with approximate ratios of 1:1 and 3:1. As each subject

repeats the experiment process five times, data from one experiment process is symbolled as S_{lq}, where S_l denotes the data from subject l and $q \in [1,5]$ is the index of experiment process. We only use four times' data $(S_{l1}, S_{l2}, S_{l3}, S_{l4})$ so that we can split the data by the ratio of 1:1 and 3:1 (TD : UD).

For LMF and CF, we split training and test dataset from both TD and UD with the ratio of 9:1 instead of 8:2 used for the benchmark, and the 10% of TD and UD together make the test dataset. Note that, all available data are labeled with ground truths from video recordings for the use of validation. To clarify, 90% of UD with labels from our label models are in the training dataset and 10% of UD with their true labels are in the test dataset for the LMF and CF framework.

2.6.5. Motion Recognition Results

Table 2.4 to Table 2.6 summarize the cross-validation accuracy of all subjects from benchmarks, LMF and CF frameworks for MODULE1 and MODULE2, respectively. For MODULE2, we present results from the probability check threshold value $P_{th} = 0.75$ for *Sequential Motion Dataset*, $P_{th} = 0.97$ for *Repetitive Motion Dataset* and $P_{th} = 0.95$ for *Route Map Dataset*. These P_{th} values provide an average overlap of about 60% to 70% between label functions and averaged conflicts less than 1%. Besides these P_{th} values for probability check, we also explore other values as shown in Figure 2.11.

In Table 2.4 to Table 2.6, the color in blue and red indicate the improved and degraded accuracy compared to that in the black (benchmark) with the same end classifier. As there is no available benchmark for LMF, we use the benchmark of

traditional RF, which has better results than SVM or KNN to quantify the accuracy improvement.

Table 2.4 Sequential motion dataset – cross-validation accuracy. © 2021 IEEE. Reprinted with permission from [161].

Framework-Classifier	**Benchmark**	**MODULE1**			
		User Characteristics		**Experiment Process Index**	
		1:1	3:1	1:1	3:1
LMF-Majority Vote	N/A	82.44%	92.32%	88.61%	93.87%
LMF-Snorkel Label Model	N/A	81.15%	89.63%	82.37%	89.67%
CF-KNN	73.41%	70.45%	72.47%	71.55%	72.78%
CF-SVM	80.04%	76.37%	78.99%	76.06%	78.24%
CF-RF	87.75%	85.01%	88.72%	85.07%	86.73%
Framework-Classifier	**Benchmark**	**MODULE2 (P_{th} = 0.75)**			
		User Characteristics		**Experiment Process Index**	
		1:1	3:1	1:1	3:1
LMF-Majority Vote	N/A	87.62%	91.94%	90.72%	92.50%
LMF-Snorkel Label Model	N/A	86.64%	92.12%	90.94%	92.97%
CF-KNN	73.41%	71.73%	72.03%	72.78%	72.27%
CF-SVM	80.04%	79.54%	79.10%	78.67%	78.91%
CF-RF	87.75%	83.17%	86.34%	85.90%	85.92%

Table 2.5 Repetitive motion dataset – cross-validation accuracy

Framework-Classifier	**Benchmark**	**MODULE1**			
		User Characteristics		**Experiment Process Index**	
		1:1	3:1	1:1	3:1
LMF-Majority Vote	N/A	98.09%	98.78%	98.77%	99.39%
LMF-Snorkel Label Model	N/A	97.34%	98.61%	98.77%	99.32%
CF-KNN	74.91%	75.46%	75.36%	74.65%	74.68%
CF-SVM	91.60%	91.78%	91.89%	91.63%	92.04%
CF-RF	96.68%	96.33%	96.80%	96.77%	96.79%
Framework-Classifier	**Benchmark**	**MODULE2 (P_{th} = 0.97)**			
		User Characteristics		**Experiment Process Index**	
		1:1	3:1	1:1	3:1
LMF-Majority Vote	N/A	97.89%	98.84%	98.87%	99.38%
LMF-Snorkel Label Model	N/A	97.78%	98.76%	98.88%	99.37%
CF-KNN	74.91%	75.27%	75.23%	74.61%	74.59%
CF-SVM	91.60%	91.75%	91.55%	91.82%	92.02%
CF-RF	96.68%	96.80%	96.54%	96.72%	97.08%

Table 2.6 Route map dataset – cross-validation accuracy. © 2021 IEEE. Reprinted with permission from [161].

Framework-Classifier	Benchmark	MODULE1			
		User Characteristics		Experiment Process Index	
		1:1	3:1	1:1	3:1
LMF-Majority Vote	N/A	95.85%	97.51%	97.29%	97.98%
LMF-Snorkel Label Model	N/A	94.71%	96.61%	96.83%	97.70%
CF-KNN	74.31%	75.53%	74.96%	74.39%	74.82%
CF-SVM	89.59%	88.60%	89.40%	89.39%	89.06%
CF-RF	93.08%	92.87%	93.80%	93.75%	93.80%
Framework-Classifier	**Benchmark**	**MODULE2 (P_{th} = 0.95)**			
		User Characteristics		**Experiment Process Index**	
		1:1	3:1	1:1	3:1
LMF-Majority Vote	N/A	95.56%	97.36%	97.39%	97.91%
LMF-Snorkel Label Model	N/A	95.52%	97.24%	97.34%	97.89%
CF-KNN	74.31%	75.36%	75.04%	74.32%	74.71%
CF-SVM	89.59%	88.67%	89.91%	89.54%	89.27%
CF-RF	93.08%	91.93%	93.93%	93.91%	93.95%

2.6.5.1. Sequential Motion Recognition

In Table 2.4, the CF does not work well where the results from most of the data splitting strategies and splitting ratios degrade up to 5%. However, the LMF works well and make improvements up to 6.12% and 5.12%, with both the majority vote model and the Snorkel label model, respectively.

2.6.5.2. Repetitive Motion Recognition

Our proposed methods improve an average up to 2.71% on the cross-validation accuracy from Table 2.5. Compared to CF, both MODULE1 and MODULE2 with LMF make improvements for any strategy or ratio of splitting data.

2.6.5.3. Route Map

In Table 2.6, when the SVM is used as the end classifier, our proposed methods do not work well on making improvements. Except this case, other strategies of building our proposed frameworks make improvements up to 4.90% with the data splitting strategy of experiment process index, ratio=3:1 and MODULE1.

2.6.5.4. Robustness

We use the cross-validation accuracy of all subjects to evaluate the robustness. In general, LMF provides better results than CF (Table 2.4 to Table 2.6). The LMF using MODULE1 with majority vote with TD : UD = 3:1 (based on experiment process index), produces the highest validation accuracy of all subjects for all three datasets. The results are detailed below:

- Compared to the best benchmark framework, it improves the accuracy up to 2.71% for *Repetitive Motion Dataset*, up to 4.90% for *Route Map Dataset*, and up to 6.12% for *Sequential Motion Dataset* with appropriate data splitting strategies and ratios. The CF also makes improvements. But for most data preparation scenarios, the improvements are not as good as that of the LMF for all three datasets.
- Table 2.7 presents the cross-validation results of sensitivity, specificity, precision, and F1-score. These metrics are close to each other, indicating that the LMF

framework has a balanced performance in identifying true positives, false positives, true negatives, and false negatives.

- Figure 2.9 shows its validation accuracy for each subject, compared with the best benchmark result (from RF). We can see improved and/or maintained (if it is already 100% with RF) for all subjects. Thus, the robustness is highly improved not only for cross-validation accuracy, but also for validation accuracy of individual subjects.

Figure 2.10 shows the confusion matrices (not normalized) from subject S_{20} as an example to present cross-classes performance. The LMF is trained with other subjects' data but is validated with subject S_{20}. The validation accuracy for subject S_{20} is 98.04%, 99.59% and 99.20% for the sequential motions, repetitive motions, and route map, respectively.

Table 2.7 Cross-validation metrics summary with LMF using MODULE1 with majority vote as the end classifier that provides the maximum improvements. © 2021 IEEE. Reprinted with permission from [161].

Cross-validation Metrics	Sequential Motion Dataset	Repetitive Motion Dataset	Route Map Dataset
Accuracy	93.87%	99.39%	97.98%
Sensitivity	93.17%	99.77%	96.16%
Specificity	95.94%	99.85%	99.67%
Precision	93.87%	98.09%	95.41%
F1-score	94.14%	99.76%	96.80%

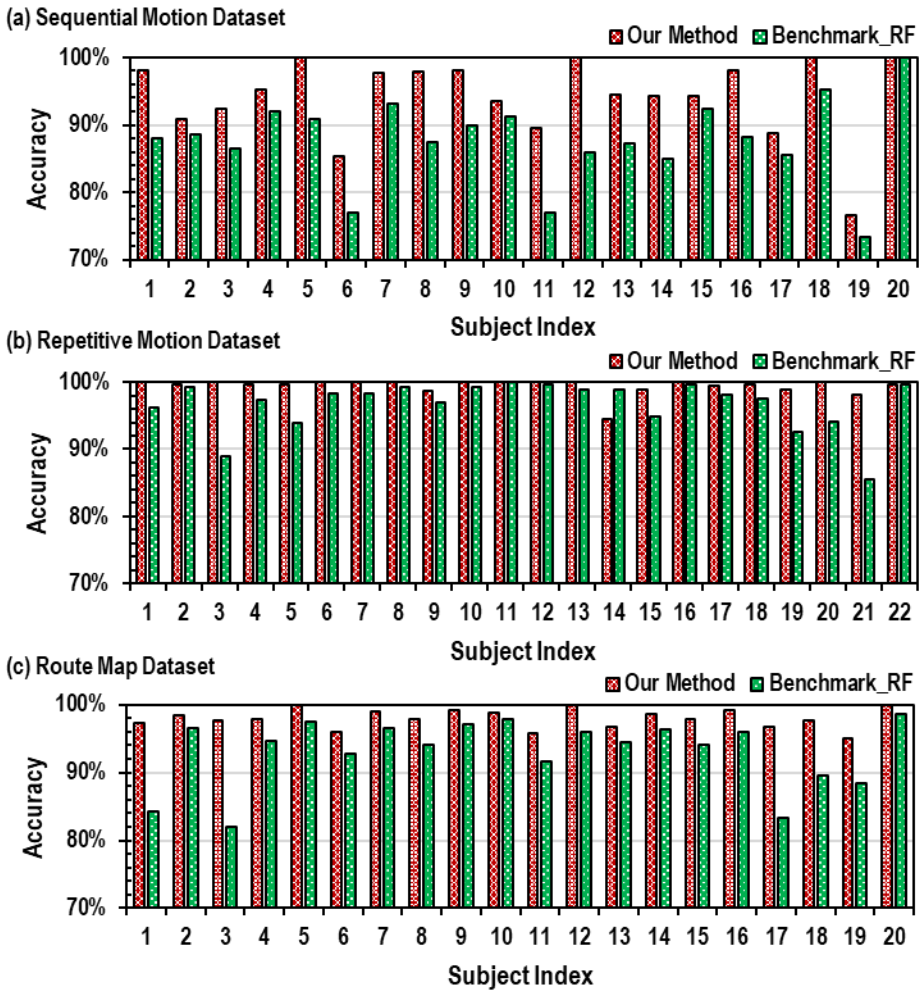

Figure 2.9 Validation accuracy of our method: LMF using MODULE1with majority vote with data preparation of TD : UD = 3:1 (based on experiment process index) , comparison to the best benchmark results for each subject. © 2021 IEEE. Reprinted with permission from [161].

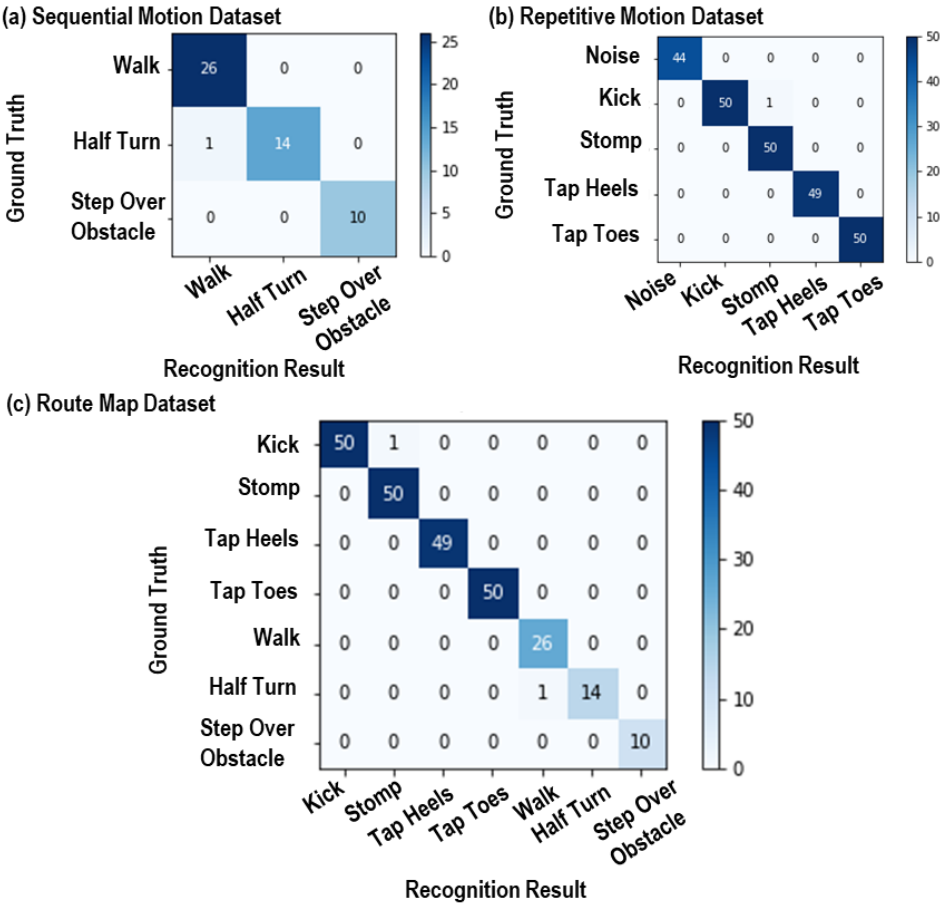

Figure 2.10 Confusion matrices from subject S_{20} as an example to show cross-classes performance a) *Sequential Motion Dataset*, b) *Repetitive Motion Dataset*, c) *Route Map Dataset*. © 2021 IEEE. Reprinted with permission from [161].

2.6.5.5. More Discussion on Fast Labeling Framework

2.6.5.5.1. Data Preparation

We explore two strategies of data splitting: TD and UD with two splitting ratios. In total, we have four different data preparations. The purpose of exploring data preparations is to understand how similarities of subject characteristics and their individual differences influence the results. The purpose of exploring different ratios is to evaluate how much time that we can save in labeling.

Regardless of the splitting strategies, from the red colored (degraded) and blue colored (improved) accuracies of columns of 1:1 and 3:1 ratio in Table 2.4 to Table 2.6, we can see that the 3:1 ratio makes more improvement than 1:1 ratio for the most cases, but not too much when both have improvements. Regardless of the splitting ratio, from columns of subject characteristics and experiment process index in Table 2.4 to Table 2.6, we can tell data splitting by experiment index is a better strategy as the improvements are more consistent and higher than the subject characteristic based splitting strategy for most cases. This explains that taking the subjects' similarities into consideration when preparing TD and UD can largely improve the evaluation performance. In addition, our proposed methods also make improvements by using subject characteristic based splitting strategy when it comes to individual differences.

2.6.5.5.2. Label Function

It is obvious that label functions are key components, as they implement noises of weak supervision into our frameworks by labeling UD. Here, we use weak classifiers as the label functions (chosen from a combination of KNN, SVM or RF). All these weak classifiers do not work well for the foot motion tasks and only trained by TD.

From the results, we find that MODULE2 is more robust compared to MODULE1 as it improves accuracies from most data preparations. The P_{th} value needs to be decided for the use of probability check for MODULE2 based on the label function properties. Figure 2.11 shows the relationship between the P_{th} value and the averaged conflicts and overlaps, the first four functions in MODULE2. If the P_{th} value is set too small, it is the same as MODULE1 since all label functions would provide a valid label

(not *ABSTAIN*). If the P_{th} value is set too large, the first four functions may provide *ABSTAIN* all the time and the final label would be decided by the 5^{th} label function only. Thus, when selecting the P_{th} value, we use the value that provides about 60% to 70% overlaps between label functions and small conflicts between each other. Table 2.8 gives an example of the MODULE2 we use for the route map dataset with $P_{th} = 0.95$ to show the label function properties. In our future work, we will explore how overlaps and conflicts affect the results and how to quantitively find the best values of P_{th}.

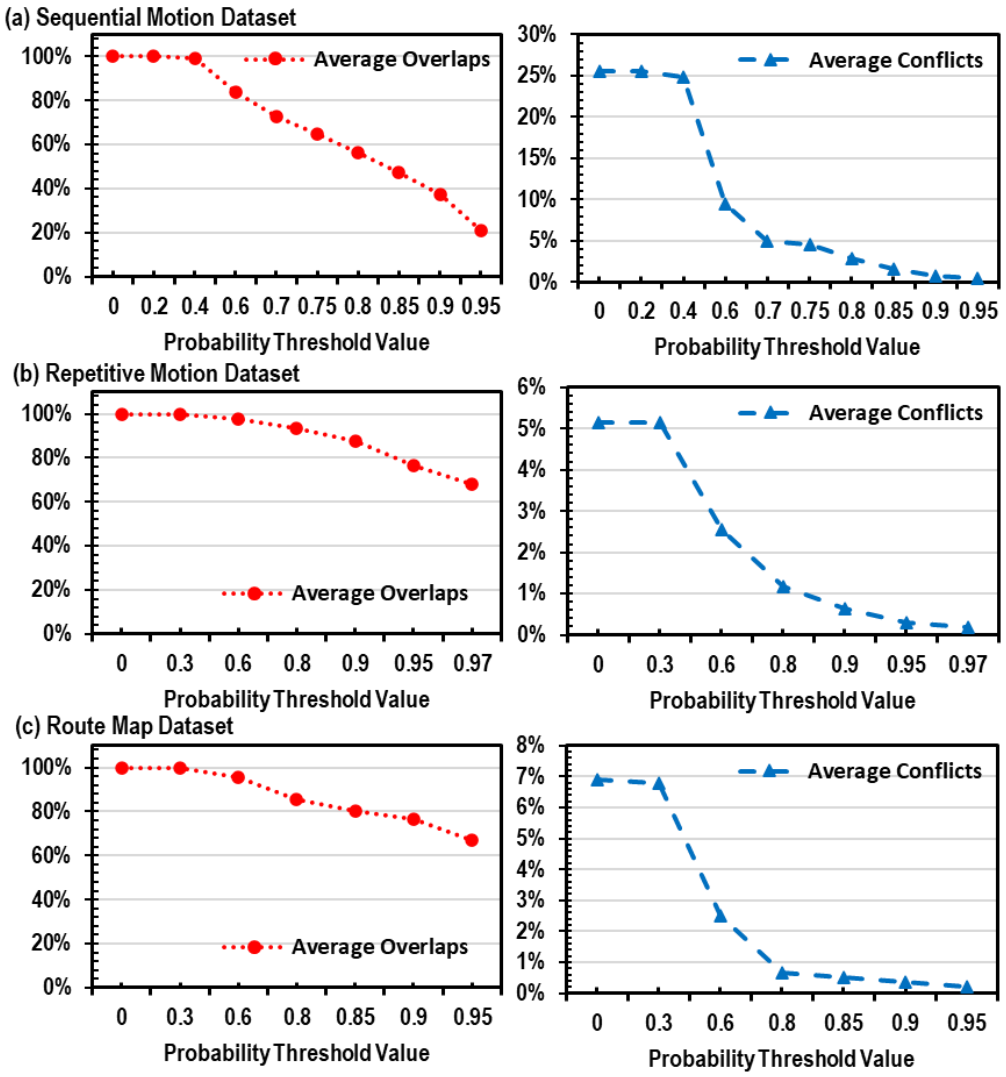

Figure 2.11 MODULE2: Properties vs. Probability threshold P_{th}. © 2021 IEEE. Reprinted with permission from [161].

Table 2.8 MODULE2: Label Function property summary. © 2021 IEEE. Reprinted with permission from [161].

Label Function	Polarity	Coverage	Overlaps	Conflicts
LF_1	Walk, half-turn, step over obstacle, tap heel, tap toes, kick foot, stomp (7 classes)	58.42%	58.42%	0.04%
LF_2	Walk, half-turn, step over obstacle, tap heel, tap toes, kick foot (6 classes)	52.87%	52.86%	0.00%
LF_3	Walk, half-turn, step over obstacle, tap heel (4 classes)	37.10%	37.10%	0.64%
LF_4	Walk, half-turn, step over obstacle, tap heel, kick foot (5 classes)	36.97%	36.97%	0.69%
LF_5	Walk, half-turn, step over obstacle, tap heel, tap toes, kick foot, stomp (7 classes)	1	68.98%	0.73%

2.7. Validation of Fast Labeling Framework on Mobility Analysis

To validate and apply our fast labeling framework to mobility analysis, we first prove that sequential motions (Gait -> U-turn -> Gait) can be reproduced with an average accuracy of 96.13% through testing with 6 elderlies and 16 young adults. Next, we extract 21 temporal motion features from reproduction results, rank these features through univariate feature ranking, and identify their importance to age-dependent mobility analysis. In the end, we analyze errors caused by reproduction and prove the applicability of the proposed method. We believe that this easy-to-use mobility monitoring approach with the simple setup can facilitate at-home mobility monitoring and evaluation for elderlies with high accuracies.

2.7.1. Method

The mobility analysis is performed in the following steps (Figure 2.12): acceleration data collection using the early version of MONI (Figure 2.13(a)), data

preprocessing with low pass filtering and segmentation into strides, sequential motion reproduction using the LMF and temporal motion extraction for mobility analysis. The LMF, recently developed by our team [161] can accurately reproduce continuous movements and provide ground truth labels for data collected from uncontrolled environments. In this letter, the LMF is fine-tuned with an optimized dataset split ratio and a label function module of 5 label functions. Each analysis step is detailed the following section.

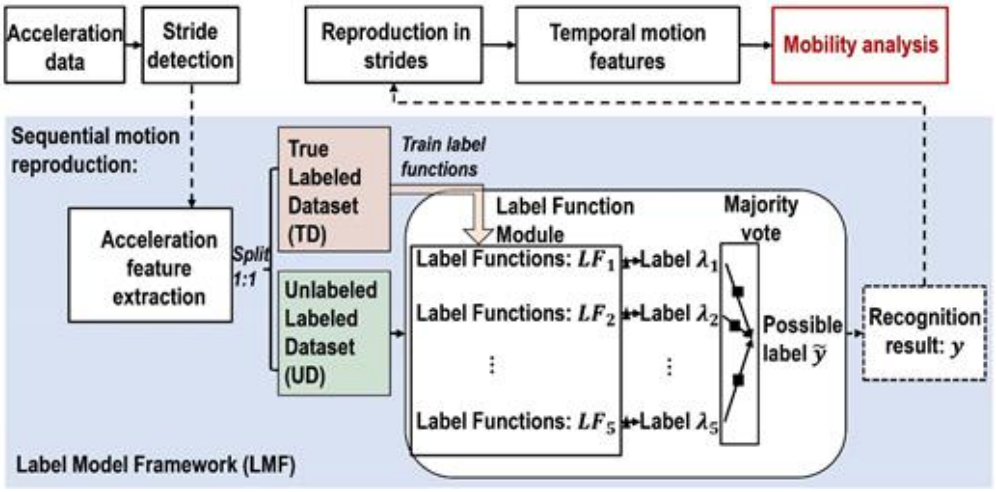

Figure 2.12 Flowchart of mobility analysis steps. © 2021 IEEE. Reprinted with permission from [184].

2.7.1.1. Experimental Setup

Each motion data set is collected following schematic in Figure 2.13(b). Each subject, wearing MONI on their right side, starts at a standing posture, walks 10 ft. (Gait-I), makes a U-turn at the U-turn point (U-turn), and then walks back to where the subject starts (Gait-II). The sequential motions include three periods of motions: Gait-I, U-turn, and Gait-II. We test our early version of MONI on 6 elderlies at a senior facility

(Figure 2.13(c)) and 16 healthy young adults in our lab (Figure 2.13(d)). Each subject performs the sequential motions 5 times and follows the "start" instruction each time on the same vinyl sheet. The ground truth is manually extracted from camera recordings.

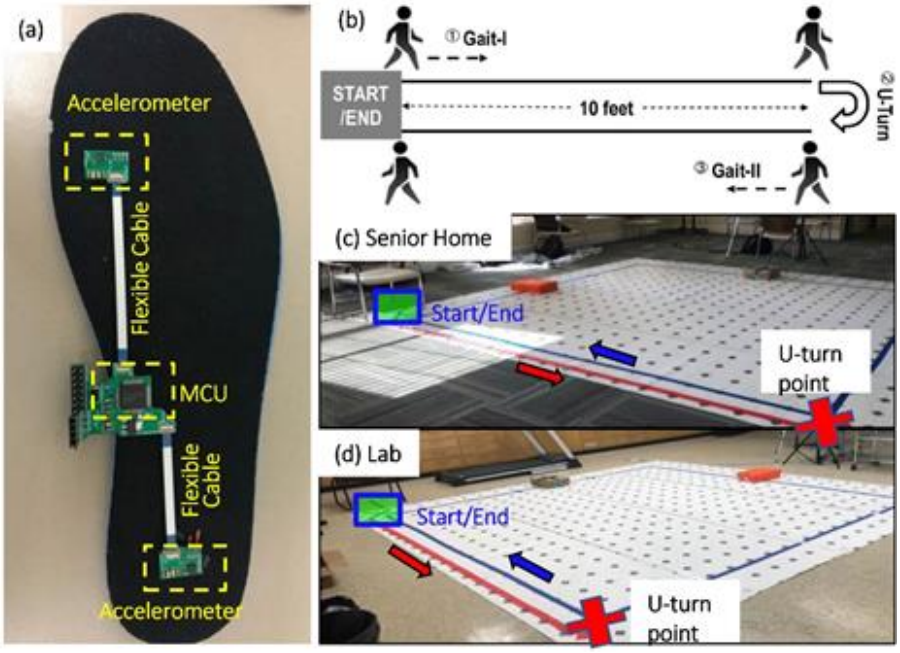

Figure 2.13 (a) Photographic representation of MONI (right-side); (b) Simple setup: a round-trip of 10-ft walking (Gait-I and Gait-II) and a U-turn; Experimental setup using a square vinyl sheet of 10-ft long at (c) the senior facility and (d) our research lab at Texas A&M University for sequential foot motion data collection: the blue and red tapes on one side of the mat indicating the start/end and U-turn point. © 2021 IEEE. Reprinted with permission from [184].

We group all subjects into two categories based on their age and summarize their characteristics in Table 2.9. This includes the average age, height, weight, shoe-size, gender, self-reported mobility limitation, and body mass index (BMI), where BMI> 25 is overweight.

Table 2.9 Statistics of subject characteristics. © 2021 IEEE. Reprinted with permission from [184].

Average	A. Elderly Group	B. Health Young Group
Age	82.83	23.60
Gender	*M (2), *F (4)	*M (14), *F (2)
Height	166.67 cm	174.47 cm
Weight	77.64 kg	70.91 kg
BMI	>25 (6), <=25 (0)	>25 (4), <= (12)
Shoe-size	8.67 (US)	9.27 (US)
Foot Motor Functionality Limitations	*N (4), *L (2)	*N (16)

[a] Male; [b] Female; [c] Normal; [d] Limited mobility due to motor dysfunctions

2.7.1.2. Sequential Motion Reproduction with Fast Labeling Framework

The acceleration data is first filtered by a 4th order Butterworth low-pass filter with a cut-off frequency of 10 Hz since the peak frequency of the motion is around 3-5 Hz for all the motion data. A stride detection method [161] is applied and segments the sequential motions into strides. Next, 150 statistical features [161] are extracted from each stride (acceleration data) to build a dataset *D*. We implement the LMF with weak supervision recently developed by our team [161] to reproduce sequential motions of gait and U-turn, as shown in the blue shaded area in Figure 2.12. The dataset *D* is first split into an optimized ratio of 1:1 to be true-labeled dataset (TD) and unlabeled dataset (UD), where true-labeled dataset is labeled with the ground truth manually extracted from camera recordings. The label function module consists of five weak classifiers, roughly trained by TD, including three Random Forest (RF) and two Support Vector Machine (SVM) with different hyperparameters. The first four label functions include two RF and two SVM. Each provides a recognition result (label) and run through a

possibility check on the confidence of the result. If the confidence of the result is higher than 90%, the label is recorded. Otherwise, the label is set as *ABSTAIN* (can't decide). The possibility check does not apply to the 5^{th} label function, which ensures the label function module provides at least one motion label. After the label function module provides a set of five labels including *ABSTAIN* if there is, the unweighted majority vote is applied to provide a final label, which is the label appears maximum number of times within the set of labels, except *ABSTAIN*. If there are tied options, the majority vote will select a final label randomly from the tied options.

2.7.1.3. Temporal Motion Features

In total, we extract 21 temporal motion features from the reproduced sequential motions. These are gait features and motion-related features referencing to TUG-derived parameters [172], including durations, stride parameters and phase-correlated features, as shown in Table 2. Univariate statistical tests are used to rank these features to differentiate elderly and healthy young groups. The Analysis of Variance (ANOVA) F-value [173] is calculated for each feature by Scikit-learn [174]. The features are ranked by the F-value. The highest represents the most relevance with age. The same features are also extracted from the true motion phases from camera recordings as the ground truth. The same method of feature ranking is applied to the ground truth, and the results of feature extraction and ranking from reproduction and ground truth are compared.

Table 2.10 Candidate temporal motion features for evaluation. © 2021 IEEE. Reprinted with permission from [184].

Motion	Temporal Motion Features	Total
Gait-I, Gait-II	motion duration, average stride duration, number of strides, cadence (strides/min), *stride-to-stride variability (standard deviation, mean, coefficient of variability)*	14
U-turn	motion duration, average stride duration, number of strides	3
Motion-correlated	total sequential motion duration, ratio of Gait-I and II durations, ratio of Gait-I and U-turn durations, ratio of Gait-II and U-turn durations	4

2.7.2. Results and Discussion

2.7.2.1. Results of Sequential Motion Reproduction

The reproduction accuracy is used to validate the LMF. All 22 subjects complete the sequential motions five times. The first four are used to build the dataset D, while last time is used to validate the reproduction. Within D, two times are treated as TD and the other two are UD. A traditional machine learning framework (RF as the classifier) is used as the benchmark, where the whole dataset D is labeled with ground truth manually extracted from the camera recording. Temporal motion features are extracted from the reproduction results from the last time of sequential motions and the ground truth. Errors of temporal motion feature extraction caused by the results of reproduction are analyzed for each age group. Figure 2.14(a) shows that the average reproduction accuracy for all subjects is improved from 91.55% (benchmark) to 96.13%. Figure 2.14(b) shows the reproduction examples for subject 1 (elderly) and subject 16 (adult) with an accuracy of 100%. For subject 10 and 13, the U-turn is not detected and thus they are removed for feature ranking within each group. The reason why LMF has better results in sequential motion reproduction than the benchmark is because the label function module introduces

weak supervision by providing labels from model-based label functions to the framework.

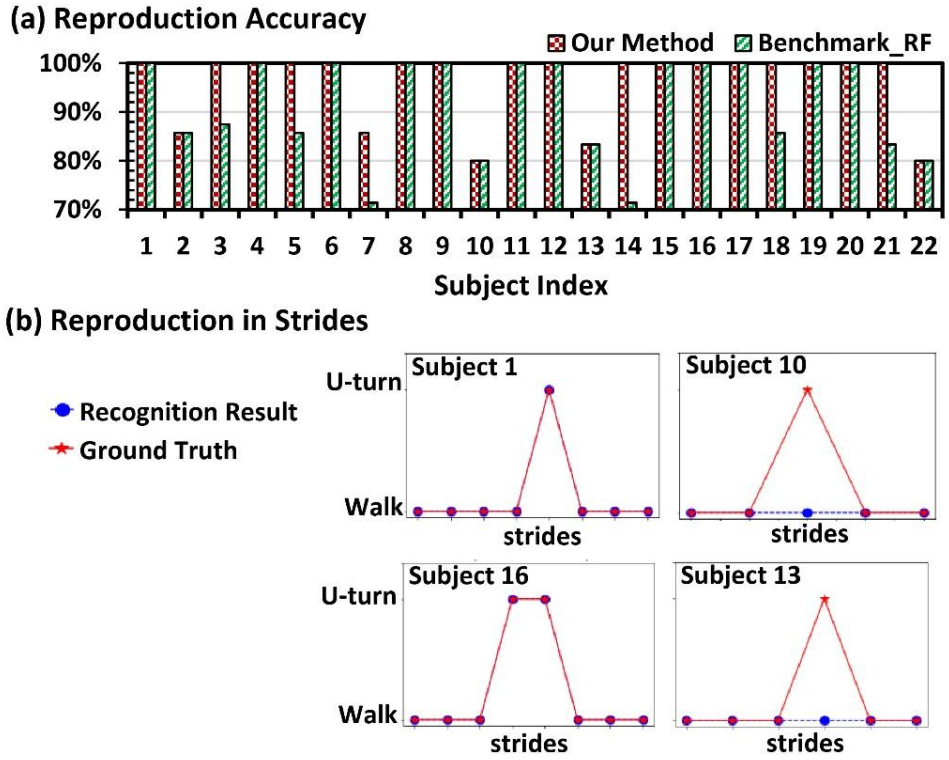

Figure 2.14 (a) Reproduction results for every subject comparison to benchmark; (b) Reproduction results for four subjects as examples. © 2021 IEEE. Reprinted with permission from [184].

2.7.2.2. Results of Temporal Motion Feature Ranking

Figure 2.15(a) shows the feature ranking from the reproduction results and the ground truth. From top to bottom, it is ranked as the most age-related to the least age-related. The top two features are stride-to-stride standard deviation (SD) and coefficient of variability (CV) from motion of Gait-II. The top two features from the reproduction results and the ground truth are the same. The feature space plot with the top two

mobility representing features in Figure 2.15(b), shows that the two groups are clearly separated, suggesting that these two features are correlated with age.

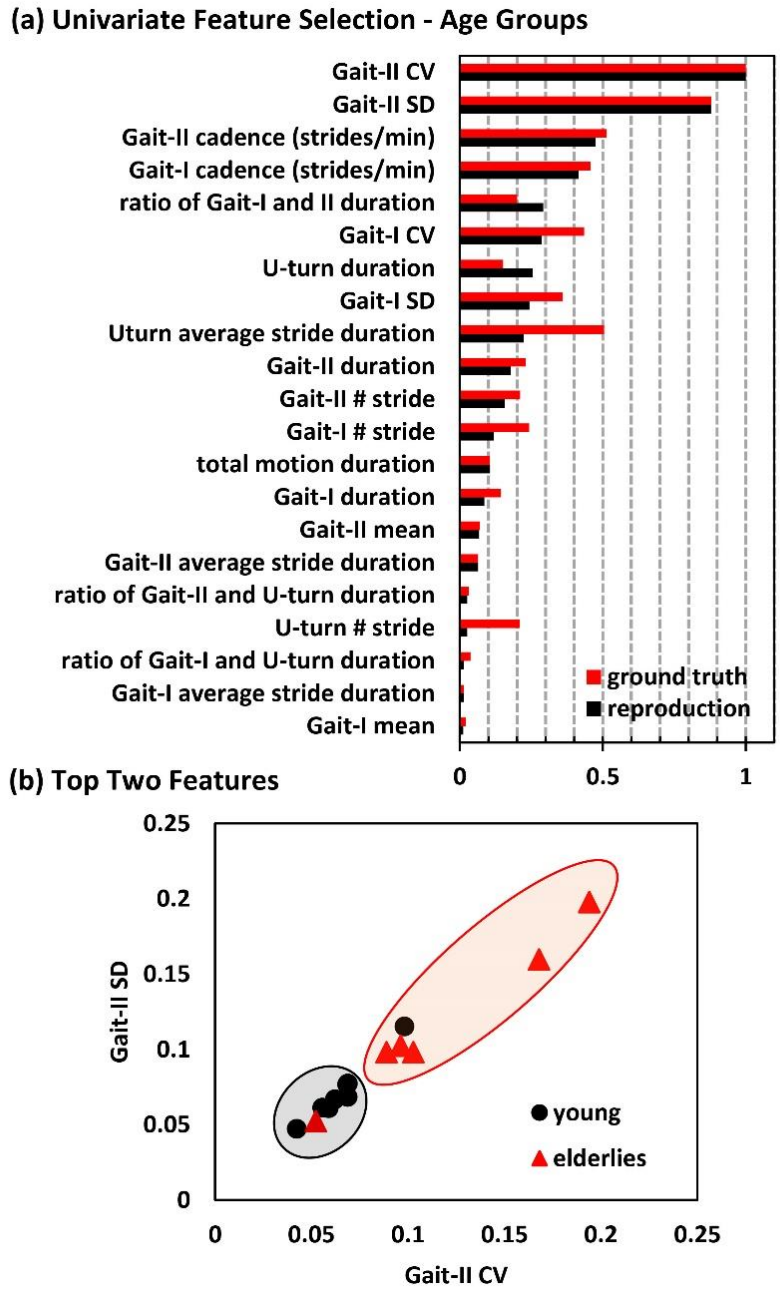

Figure 2.15 (a) Feature ranking; (b) Feature space plot with the top two features correlated with the two age groups. © 2021 IEEE. Reprinted with permission from [184].

2.7.2.3. Mobility Analysis

We observe that for both groups, the average stride duration, cadence, number of strides, ratio of Gait-I and II duration and ratio of Gait-II and U-turn duration have exhibited a linear increase with age. Group A uses a greater number of strides and longer durations to finish each motion, and shows a larger stride-to-stride variation and standard deviation compared to Group B. That is, the age-related mobility decline can be represented by typical features including a larger stride-to-stride variation, a larger cadence, a greater number of strides, and a longer duration of finishing the same motion task. The last feature is equivalent to smaller stride length since their walking distance for Gait I and II is 10 ft. These results agree with the literature finding [175] which reports step regularity and motion duration are top features to distinguish performance difference across ages after using multivariate analyses to identify aging effects on TUG.

2.7.2.4. Error Analysis

Table 2.11 shows feature errors caused by reproduction within Group A and B. The Error and Error % are both calculated against the ground truth and averaged by all subjects. The error for counting the number of strides is much larger than others (12.500%) as all finish walking with 2-5 strides, and a miscounting could cause significant error. The reproduction accuracy for all other temporal motion features is decent with an average error below 10%. From the feature ranking in results of Figure 2.15(a), the features of the number of strides for each motion are not top-ranked features by ground truths. Summarized from Table 2.11, the error caused by reproduction is acceptable and our proposed method as shown in Figure 2.12 is applicable.

Table 2.11 Average errors of temporal motion feature extraction from reproduction and the error percentage of each group. © 2021 IEEE. Reprinted with permission from [184].

Motion	Feature	A		B	
		Error	Error %	Error	Error %
Gait-I	*# stride*	-0.167	-5.556%	-0.071	-2.632%
	duration	-0.151	-4.530%	-0.080	-2.636%
	average stride duration	0.001	0.067%	-0.001	-0.085%
	cadence (strides/min)	-0.053	-0.094%	0.048	0.089%
	SD	-0.006	-7.509%	0.000	0.686%
	mean	0.007	0.684%	-0.002	-0.140%
	CV	-0.006	-8.649%	0.000	0.809%
Gait-II	*# stride*	0.000	0.000%	0.071	2.941%
	duration	0.000	0.000%	0.090	3.195%
	average stride duration	0.000	0.000%	0.001	0.061%
	cadence (strides/min)	0.000	0.000%	-0.027	-0.052%
	SD	0.000	0.000%	0.000	0.629%
	mean	0.000	0.000%	0.000	0.011%
	CV	0.000	0.000%	0.000	0.616%
U-turn	*# stride*	0.167	12.500%	0.000	0.000%
	duration	0.151	3.378%	-0.010	-0.260%
	average stride duration	-0.182	-5.201%	-0.034	-1.164%
Motion correlated	*total motion duration*	0.000	0.000%	0.000	0.000%
	ratio of Gait-I and II duration	-0.051	-5.457%	-0.083	-7.189%
	ratio of Gait-I and U-turn duration	-0.071	-9.011%	-0.015	-1.752%
	ratio of Gait-II and U-turn duration	-0.036	-4.342%	0.020	2.559%

2.7.2.5. Sequential Effects

Figure 2.15 suggests the sequential effects: though the motion of Gait-I and Gait-II are the same in nature, their feature importance ranking is different. As shown in Table 2.12, Gait-II is more important than Gait I while U-turn is the least important one for Group A and B, where number of * represents the importance of the phase (more *

means more important). Interestingly, we observed that if we group subjects based on their BMI: overweight group (10) and normal weight (12) in Table 1, the top two features are the same as these for age-related groups. However, for these groups, the most important motion is Gait-II while U-turn and Gait-I are close. To conclude, we believe that features from Gait-II can best assess both age and BMI-related mobility decline. Future work will include recruiting more elderly subjects and Middle Ages subjects to increase the data diversity and balance.

Table 2.12 Importance for Age and BMI-related mobility analysis. © 2021 IEEE. Reprinted with permission from [184].

	Age	BMI
Gait-I	**	*
U-turn	*	*
Gait-II	***	***

2.7.2.6. Conclusion

This letter proposes the use of MONI and setup for age-dependent mobility decline analysis. The proposed LMF achieves an accuracy of 96.13% to reproduce sequential foot motions of gaits and U-turns. On top of the reproduction results, 21 temporal motion features are extracted and analyzed with ANOVA to present the age-dependent mobility decline and sequential effects are proven to be important for mobility analysis. Errors associated with motion reproduction results are analyzed and the proposed method is proven to be applicable. This study provides a promising solution for elderlies to evaluate their mobility at home with simple setup using MONI through sequential motion reproduction.

2.8. Summary

We evaluate different data splitting strategies and splitting ratios to give an insight of how subjects' similarities and differences influence the performance of the proposed framework. Knowledge learned from these results are summarized below: (i) the LMF works better than the CF for all three datasets; (ii) for LMF, the majority vote model (slightly better) and the Snorkel label model have similar results for all three datasets; and (iii) the results from MODULE2 are more consistent and robust than those from MODULE1 for different data preparation cases.

Our proposed methods have the following uniqueness and advantages of: (i) the use of stride (the start to end of the stride) as the adaptive sliding window to segment continuous movements into data segments with a robust stride detection method, (ii) improvement of the cross-validation accuracy on different types of foot motion datasets with efficient computation based on traditional machine learning models of KNN, SVM and RF, (iii) thorough evaluation of strategies to group data into TD and UD, (iv) 25% to 50% of time savings in manually labeling training data, and (v) the use of weak supervision by using weak classifiers and LMF labeled training data to achieve high robustness needed by uncontrolled environments and new subjects.

It is worth to note that the size of *Sequential Motion Dataset* is much smaller than the other two datasets, and the walking data is two times more than the half-turn and step over obstacle data (unbalanced), so that its cross-validation accuracy is much lower than that of the other datasets. This can be addressed by using a larger and more balanced dataset in the future. We will explore auto feature selection, importance

ranking, advanced neuron network models to process larger datasets. We expect our proposed method would produce significant improvement of accuracy and robustness.

This chapter explores weak supervision-based fast labeling on continuous movements with a robust stride detection method for foot motion recognition. The results show improvements in validation accuracy for all the subjects. The chapter well addresses the challenge of recognizing foot motions from continuous movements in uncontrolled environments and provides a solution to robust and fast data labeling. Compared to existing studies as shown in Table 2.13, our method has a significantly better accuracy in motion recognition when applied to multiple motions.

Table 2.13 Comparison to existing studies.

Recognition method	**Segmentation**	**(No. of motions) Motion**	**Accuracy**	**No. of subjects**
Xgboost	Greedy Gaussian	(6) Lay down, Stand, Sit, Walk, Downstairs, Upstairs	79.4%	30
Adaboost	Sliding windows	(7) Walk, Sit, Stand, Run, Bicycle, Lay down, Upstairs	95.35%	10
Hierarchical hidden Markov	N/A	(4) Walk, Downstairs, Upstairs, Run	88.88%	N/A
Threshold judgements	Sliding windows	(4) Stand from a chair, Walk, Turn, Sit on the chair	92.33%	10
Recurrent Neural Networks	Sliding windows	(5) Walk, Sit, Stand up, Bend to pick object, Drink water, Fall	96%	16
More efficient Recurrent Neural Networks	Sliding windows	(>10) Activities from different public datasets	91%	25
Fast labeling framework (Our method)	**Stride and Sliding Window**	**(7) Lower limb motions (Route Map)**	**97.98%**	**20**

With MONI and setup for age-dependent mobility decline analysis, foot motion recognition using fast labeling framework is proven to be applicable before motion feature extraction and analysis. The proposed LMF achieves an accuracy of 96.13% to reproduce sequential foot motions of gaits and U-turns. On top of the reproduction results, 21 temporal motion features are extracted and analyzed with ANOVA to present the age-dependent mobility decline and sequential effects are proven to be important for mobility analysis. Errors associated with motion reproduction results are analyzed and the proposed method is proven to be applicable. This work provides a promising solution for elderlies to evaluate their mobility at home with simple setup using MONI through sequential motion reproduction.

2.9. Selected Motions for PD Falling Risk Evaluation

As shown in Table 2.14, within all the foot motions, we summarize from commonly used effective clinical exams and tests and select the most effective and simplest sequential motions: walking, and repetitive motion: toe tapping for PD falling risk evaluation.

Table 2.14 Foot motions used in clinical examinations and tests.

Application	Clinical tests	a	b	c	d	e	f	g
PD rating/diagnosis	UPDRS	x			x			
Balancing	BESTest	x	x	x	x	x		
Mobility and falling	Timed-up and Go	x	x					
Lower body (Leg)	Leg strength/dominance test						x	x
For elderlies, difficult to perform				x			x	x

a: Walk; b: Turn; c: Step over obstacle; d: Toe tapping; e: heel tapping; f: Kick; g: Stomp

3. WALKING-BASED FALLING RISK EVALUATION

Motor functionality decline caused by Parkinson's disease (PD) can be represented by gait disorders, leading to high risks of falling and serious injuries. Most existing studies on falling risk evaluation mainly rely on gait analysis using wearable sensors but do not usually provide quantitative results to patients. In real-life scenarios, walking is always associated with other activities, thus gait changes due to distracted attention. This study aims to investigate how PD patients perform during walking while holding a full cup of water in hand compared to age-matched healthy controls (HC) with Monitoring Insoles (MONI) developed in our lab. Experiments, including two tasks: walking and walking with water in hand, are done with 10 PD patients and 8 HCs. Results are compared between groups and between tasks through statistical analysis of 63 gait and 864 acceleration-axis features. The results suggest acceleration-axis features can better differentiate PD from HC during walking with water in hand with an accuracy of 82.37% compared to walking (72.63%). To evaluate falling risks with the task of walking with water in hand, a Bayesian Ridge model developed by gait and acceleration-axis features provides falling risk scores compatible with the Fall Risk Questionnaire (FRQ) developed by the U.S. Centers for Disease Control and Prevention (CDC) with an (error ± standard deviation) = (0.03±0.38). This study assesses and evaluates features of PD and HC in walking motion and walking while holding a cup of water to provide a more quantitative and understandable falling risk score to PD patients using MONI. Figure 3.1 is the abstract of Chapter 3.

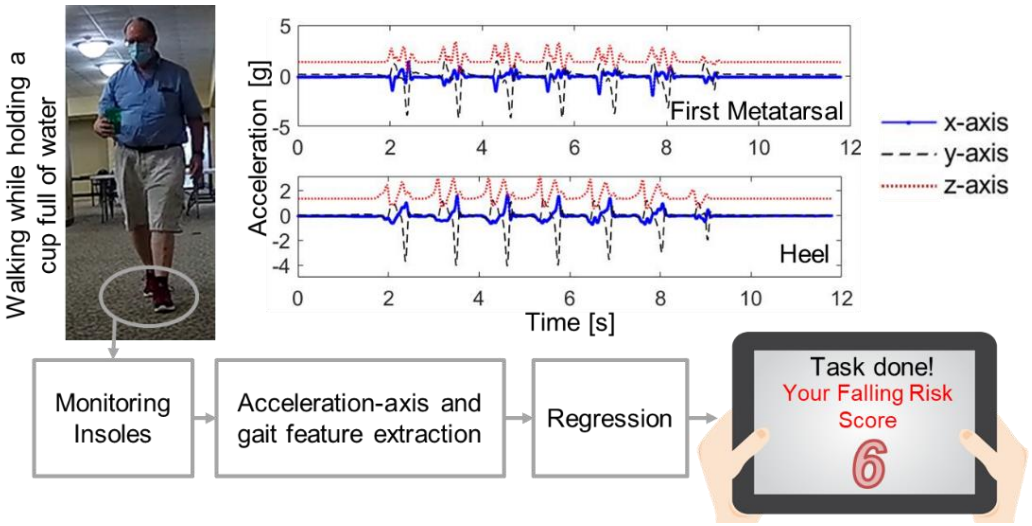

Figure 3.1 Graphical abstract of Chapter 3.

3.1. Walking Tasks

Aiming to reduce the burden of trips to clinics and provide an objective evaluation of falling risks in real time, research studies [44, 90, 176] focus on developing smart insoles to automatically evaluate walking in daily life to support falling risk estimation for elderlies. Other studies [177, 178] focus on gait analysis to detect motor functionality disorder in PD, such as freezing of gait and bradykinesia [179]. To predict the falling of PD, most recent studies focus on detecting pre-freezing of gait [11] with acceleration or force data and different machine learning methods, reporting 80-95% of accuracy [180]. However, such prediction only applies to PD in the mid-severe stages. Walking evaluated by these studies is a single task and most of the experiments done by the studies are controlled without considering environmental or physical factors. In daily routine, walking is always associated with other activities [181], such as carrying a cup of coffee. Such dual tasks distract attention from walking and may increase risks of

falling [182]. Thus, results from these studies, which only consider walking, are not accurate or do not reflect how PD patients perform in real-life scenarios. It is more valuable to evaluate dual tasks with smart insoles for PD and explain how they link to falling risks to assist with real-life applications.

Referencing to dual-task Timed-Up and Go test [183] and different one from existing studies [31] using smart insoles for gait analysis, our study aims to investigate the gait and acceleration-axis features of PD and age-matched healthy controls (HC) through two tasks: simple walking and walking with attention distracted by holding a full cup of water in hand, using upgraded Monitoring Insoles (MONI) [184]. Figure 3.2 shows the acceleration data plot of the two tasks.

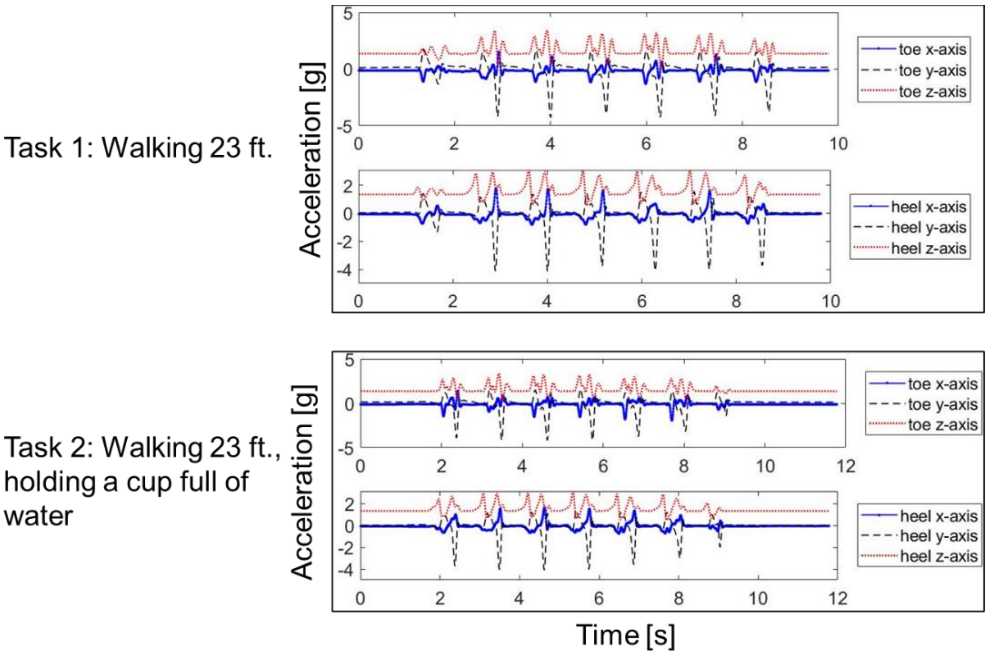

Figure 3.2 Acceleration data plots of the two tasks.

3.1.1. Experiment

The subject walks 23 ft. at his/her comfortable pace in a straight line in Task 1; and then repeats Task 1 with a full cup of water in a single hand as Task 2, as shown in Figure 3.3. Compared to Task 1, Task 2 requires the subject's attention to avoid spilling water at his/her best during walking. Thus, the experiment is more relevant to real-life scenarios where attention is distracted while walking. The motion data is recorded by a pair of MONI, including two accelerometers positioned at the heel and the first metatarsal area, respectively. The ground truth is recorded by a camera.

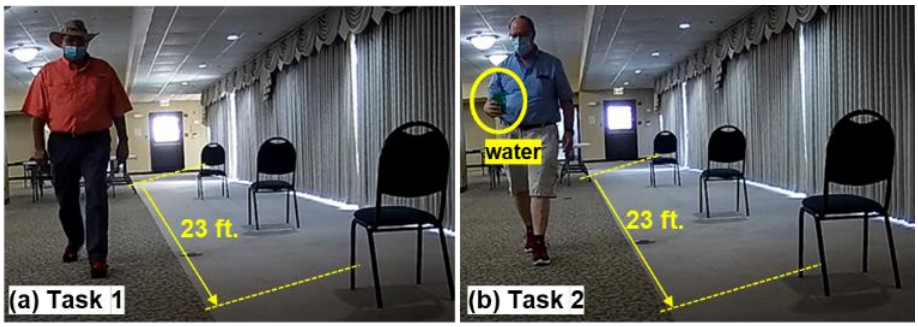

Figure 3.3 Subjects in experiment.

3.1.2. Subjects

In total, 10 PD patients and 8 HC subjects participated in the experiment. Subjects are grouped as PD and HC Group as recorded in Table 3.1 with the summarized information of each group. To determine if a subject is a faller or non-faller, FRQ with 12 YES/NO questions is used, which is validated to have a high correlation to clinical falling examination [15]. Every subject filled the questionnaire before the experiment. FRQ is transformed into a score, scaling in between [0, 14] when a YES counts as 1 point. The scaling is up to 14 points since the first two questions count for 2 points each.

Table 3.1 Group summary: subjects' characteristics.

Group	PD	HC
Gender	Female (2) [b], Male (8)	Female (6), Male (2)
Age	(51-60) (1), (61-70) (5) (71-80) (3), (Over 80) (1)	(61-70) (5), (71-80) (3)
PD Stage	1 (5), 2 (2), 3 (1), 4 (2)	N/A
Falling	Faller (7), Non-faller (3)	Faller (1), Non-faller (7)
Falling Score (mean ± std [a])	5.70 ± 3.40	1.50 ± 1.60

3.2. Gait Features

Human walking is a periodical movement, represented by strides. A stride (two steps) is divided into gait phases of stance (heel strike to toe-off) and swing (toe-off to heel strike) [15]. It has been proven that gait events can be extracted from accelerometry signals [33]. Gait events of heel strike and toe-off of the left and right foot can be directly extracted from MONI. From heel strike and toe-off events, the following gait features (Figure 3.4) can be extracted for both right and left sides.

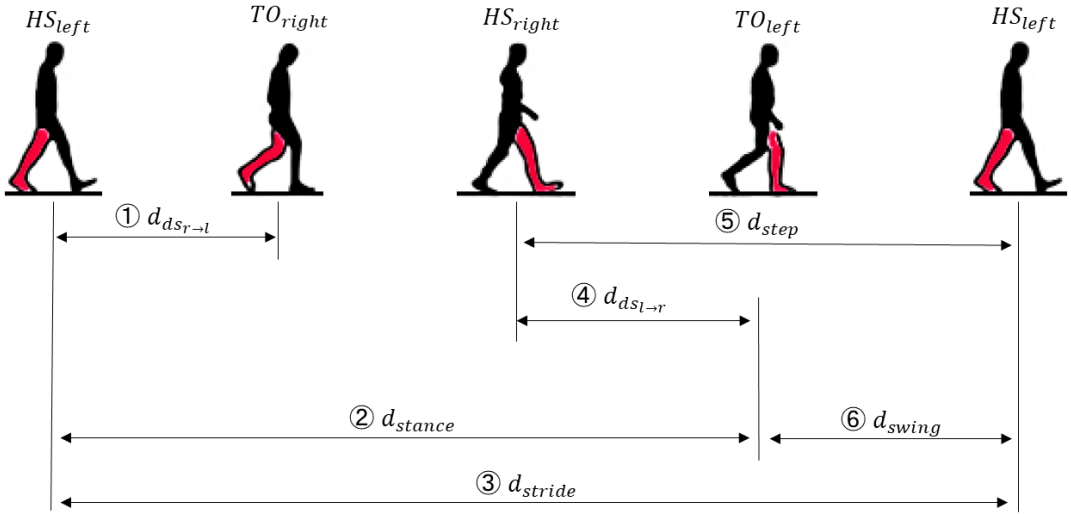

①Double support duration (weight shift right -> left)
②Stance duration
③Stride duration
④Double support duration (weight shift left -> right)
⑤Step duration
⑥Step duration Swing duration

Figure 3.4 Gait events and gait phases definition.

In the following subsections, we state the method of identifying gait events and the results, following by gait feature extraction.

3.2.1. Gait Event and Phase Identification

To remove high-frequency noises within acceleration data, a 4th order Butterworth low-pass filter with 2.5Hz cut-off frequency is used. Walking including four events in a stride: left heel strike (HS_{left}), left toe-off (TO_{left}), right heel strike (HS_{right}) and right toe-off (TO_{right}) are identified with differential transformation. As Figure 3.5 shows, HS_{left} and HS_{right} are detected from the z-axis of the heel acceleration while TO_{left} and TO_{right} are detected from the y-axis of the first metatarsal

acceleration. First, differential calculations are applied to the y-axis data of the heel and first metatarsal. Next, the heel strike event is detected as the mean of the peak and the zero-crossing prior to the peak from the differentiation from the heel y-axis acceleration. With the detected heel strike event, its prior toe-off event is found as the zero-crossing before the peak of y-axis data from the first metatarsal. To extract gait parameters, the detected events are put in arrays and defined as A_{HSleft}, A_{TOleft}, $A_{HSright}$ and $A_{TOright}$.

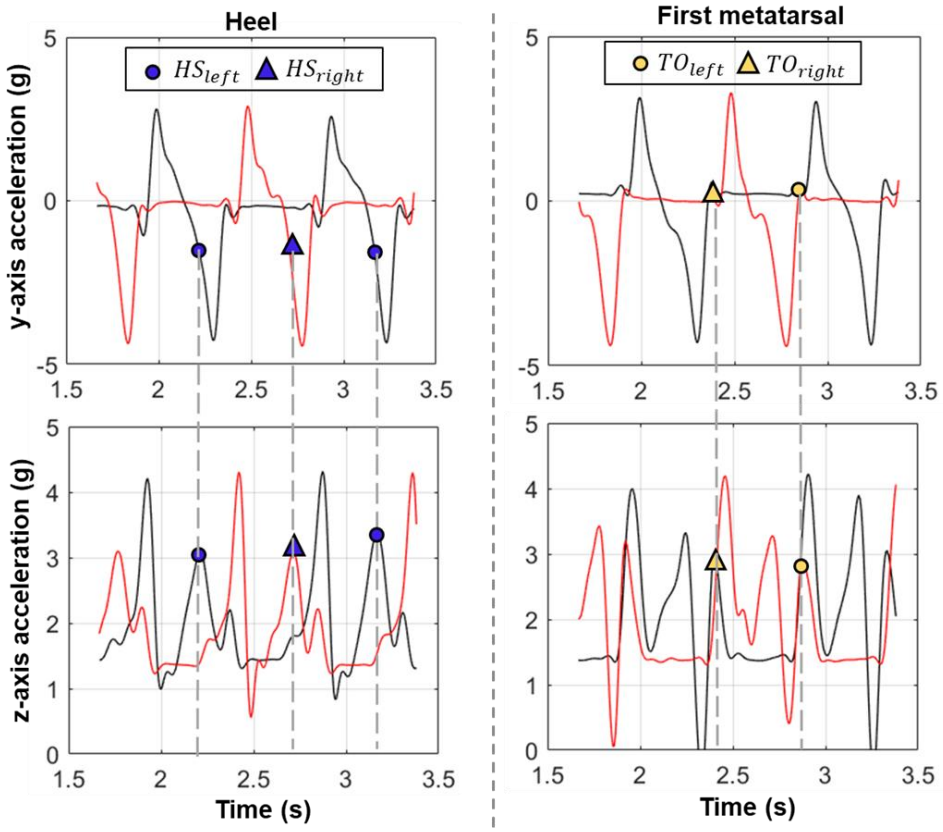

Figure 3.5 Gait events pinpointed on heel and first metatarsal acceleration traces (data from left side in black; data from right side in red).

Table 3.2 shows results of the correct number of gait events detected by our method compared to video recordings in percentage for the two tasks and two groups, respectively.

Table 3.2 Gait event detection accuracy.

	PD	HC
Task 1	97.86%	97.37%
Task 2	98.34%	97.28%

Compared to the other studies listed in Table 3.3, our work shows a compatible accuracy and works well for walking and walking with water.

Table 3.3 Comparison to existing studies using different methods.

Method	**Task**	**Sensor**	**No. of PD**	**No. of HC**	**Accuracy**
Zero-crossing detection (specific features)[28]	Walk	IMU	6	0	100%
SVM[29]		IMU	49	0	93.9%
4-state Finite State Machine + SVM[30]		IMU	1	1	93%
Heuristics & thresholds on features[31]		Accelerometer	12	11	>94%
Frequency-domain Transform[32]		Accelerometer	128	0	97%
Our method	Walk	Accelerometer	10	8	98%
	Walk with water	Accelerometer	10	8	98%

3.2.2. Gait Feature Extraction

Since the subject starts walking with either right or left side, the first left toe-off is defined to be the first event during walking for all subjects, and thus any event from $A_{HSright}$ and $A_{TOright}$ ahead of 1st element in A_{TOleft} is removed from the arrays when extracting stride duration and gait phases of swing, step, stance, and double support

duration. Due to the unstable speed at the start and the end of the tasks, the first and the last stride is also removed. 4 types of functions are applied to stride and 4 gait phases (5 in total): mean, standard deviation (std), variability (var) and coefficient of variance (CoV), which makes 20 features in total. Ratios between gait phases to stride duration are calculated (4 features) and the total number of strides from a single side before any removal is another feature. In total, 25 gait features are extracted from a single side. In addition, 13 features are extracted with both sides. Before any removal on event arrays, the total task duration can be extracted as the duration between the first and the last event, as one feature. Gait symmetry is calculated with 3 methods (ratio index, symmetry index, and Robinson index) [185] for left and right swing, stance, step, and double support duration (12 features). Thus, in total, 63 gait features are extracted.

3.3. Acceleration-axis Features

Since PD symptoms are within the 2-12 Hz range, the acceleration data is filtered with a low-pass filter with a 12 Hz cut-off frequency. Based on A_{HSleft}, A_{TOleft}, $A_{HSright}$ and $A_{TOright}$ after removals, the start and the end of each stride are identified and thus acceleration data can be segmented into stride, swing, and step. In total, 432 acceleration-axis features are extracted from a single side. That is, 18 statistical features are extracted from 4 axes of the 2 accelerometers within each stride, swing, and step, respectively. The 18 statistical features include: mean, minimum, maximum, median, std, CoV, peak-to-peak amplitude (PPA), Percentile=10, 25, 50, 75, 90, interquartile range, skewness, kurtosis, signal power, root mean square (RMS) and the number of

positive peaks. Axes include x, y, z, and the std of x, y, and z. In total, 864 acceleration-axis features (2 sides) are extracted for each task.

3.4. Feature Analysis

As shown in Figure 3.6, to identify features with statistically significant differences between the means of PD and HC groups for the same task and the means between tasks for the same group, a two-way Analysis of Variance (ANOVA) with replication is used for 864 acceleration-axis features. The result of two-way ANOVA provides p-values of group factor, task factor, and interaction. If the p-value for interaction is not significant, a pairwise comparison is performed to check if the significance exists in groups (PD: Task1 vs. Task2, HC: Task1 vs. Task2) or in tasks (Task1: PD vs. HC; Task2: PD vs. HC) with Turkey's Test [186]. For gait features, Mann-Whitney U Test [187] is used to identify the features with significant differences between the means of groups, and Wilcoxon Signed Rank Test [188] is used to identify the features with significant differences between the means of tasks. The reason for using different statistical analyses is because data of gait features is not normally distributed, but data of acceleration-axis features follows a normal distribution, checked with Shapiro-Wilk Test [189].

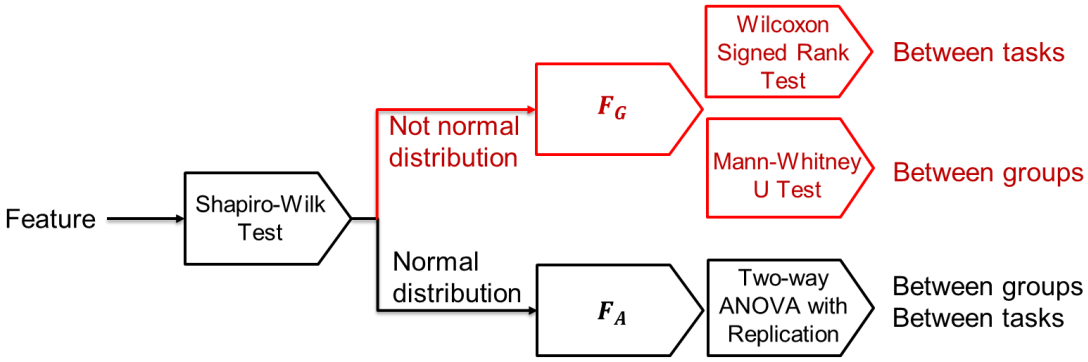

Figure 3.6 Methods of Identifying Statistically Significant Differences between two means.

3.4.1. Results of Gait Feature Analysis

3.4.1.1. Between Groups

In our experiment, HC uses an average of 7.28s to finish Task 1 while PD uses 7.70s; and HC uses 7.77s to finish Task 2 while PD uses 7.93s. Thus, Task 2 takes longer to finish for both groups. It is noticed that both groups use larger stride duration and a greater number of strides in Task 2. The ratio of stance in a stride shows a significant difference in Task 2 (63.08%) than Task 1 (59.34%) for PD compared to HC (Task 2: 63.90% and Task 1: 61.87%), which means PD uses a longer stance duration to stabilize the walking performance in Task 2, These features have the changes with the same trending for two groups between Task 1 and Task 2 as shown in Table 3.4 Summary of duration and number of strides for each group and task.

Table 3.4 Summary of duration and number of strides for each group and task.

Group	**PD-Task1**	**HC-Task1**	**PD-Task2**	**HC-Task2**
Task Duration (s)	7.70	7.28	7.93	7.77
Stride Duration (s)	1.05	1.07	1.13	1.12
Number of Stride	6.75	7.5	7	7.25

The results indicate no statistically significant difference between the mean of PD and HC for all gait features of the two tasks. The feature with the most significance is the symmetry angle of the left and right stride duration (p-value = 0.191) in Task 2 as shown in Figure 3.7, where PD is a bit unbalanced in gait symmetry in Task 2. Notice that PD and HC have the same symmetry angle in Task 1, but Task 2 changes the gait symmetry of PD walking performance (Figure 3.7).

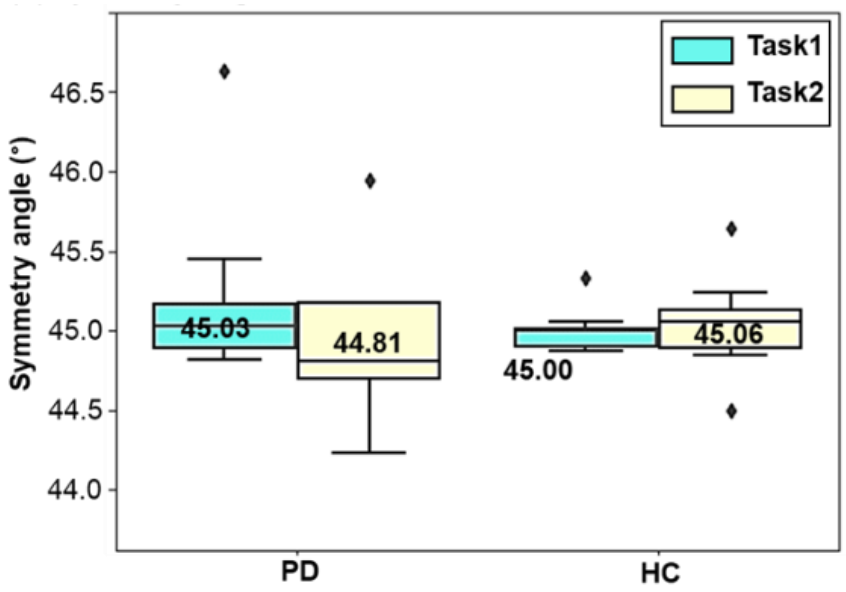

Figure 3.7 Symmetry angle (Inverse Tangent $(\frac{left\ stride\ duration}{right\ stride\ duration}) \times 180/pi$) where 45 degree is 100% symmetry.

3.4.1.2. Between Tasks for PD

The results indicate significant differences between tasks in ratio of stance duration in a stride, ratio of swing duration in a stride, number of strides to finish tasks, and average stance duration for PD. The p-values are summarized in Table 3.5. These

features specify that PD group user longer duration when foot is on the ground in Task 2 than Task 1, as the ratio of stance in a stride is 63.08% for Task 2 vs. 59.34% for Task 1.

Table 3.5 Gait features with significant differences between tasks for PD.

Feature name	p-value
Ratio of left stance in a stride	0.004
Ratio of left swing in a stride	0.006
Right number of strides	0.026
Left average stance duration	0.049

3.4.2. Results of Acceleration-axis Feature Analysis

3.4.2.1. Between Groups

The feature with the most significant difference between groups is the acceleration value at percentile=10 from the y-axis of left side first metatarsal acceleration in a stride from Task 2 (p-value = 0.006), where PD has a very small acceleration value (mean: 0.016 g) compared to HC (mean: 0.049 g) as shown in Figure 3.8. Other features show significant differences are the median acceleration value of the z-axis from the left first metatarsal acceleration during swing (p-value = 0.015, Figure 3.9), the interquartile range of std-axis from the left heel acceleration during swing (p-value = 0.018), and the skewness of x-axis from the first metatarsal acceleration in a stride (p-value = 0.027) from Task 1.

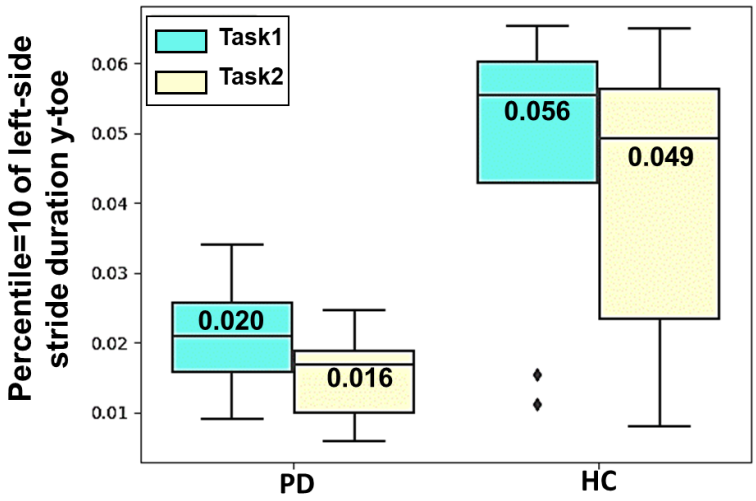

Figure 3.8 Feature with the most significant difference between groups from Task 2.

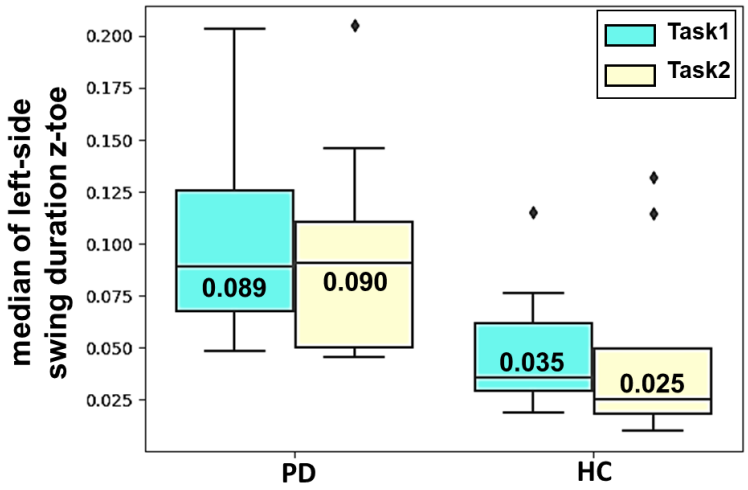

Figure 3.9 Feature with the most significant difference between groups from Task 1.

3.4.2.2. Between Tasks for PD

Two-way ANOVA results show there are statistically significant interactions between the factors of groups and tasks for acceleration-axis features. With the pairwise

comparison, there is no significant difference in acceleration-axis features found for HC between Task 1 and Task 2. However, only one feature (Kurtosis of z-axis from right-side heel acceleration in a step) with p-value = 0.037 shows a significant difference between Task 1 and Task 2 for PD (Figure 3.10).

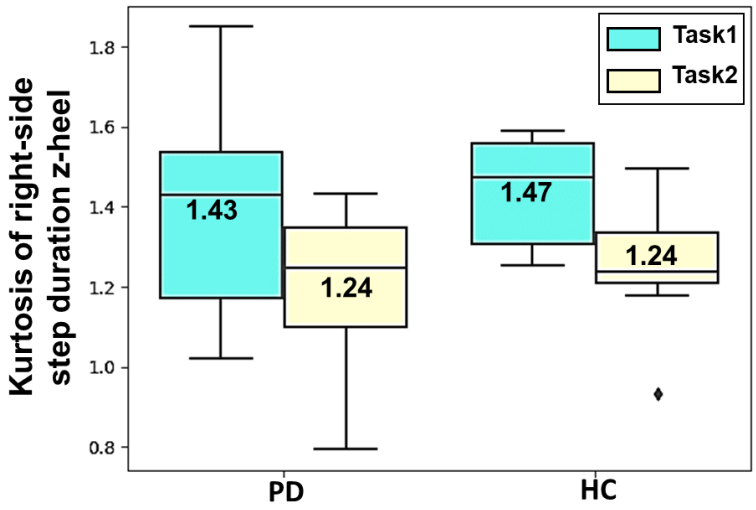

Figure 3.10 Feature with significant differences between tasks for PD.

3.5. PD vs. HC Classification

Through identifying the features with significant differences, conclusions can be made to assess feature differences between PD and HC for the two tasks. Classification of PD and HC is performed to further consolidate the conclusion about the importance of gait and acceleration-axis features, respectively. Classification models of Random Forest (RF), Support Vector Machine (SVM), and K-Nearest-Neighbors (KNN) are used and only the model that provides the best results is reported in results.

Concluding from feature analysis, gait features do not have statistically significant differences between the means of groups while acceleration-axis features are

in the opposite. Classification of PD and HC is performed based on gait feature set F_{Gs} and acceleration-axis feature set F_{As} for Task 1 and Task 2, where F_{Gs} includes the same type of gait features and F_{As} includes the same type of acceleration-axis features extracted from a single stride and its gait phases. To fairly evaluate, a non-randomly 5-fold Cross-Validation (CV) and a random shuffling 8-fold CV are used. As Table 3.6 shows, the F_{As} shows more accuracy in PD and HC classification compared to F_{Gs}; and Task 2 provides higher accuracy compared to Task 1, which means Task 2 can better differentiate PD from HC. The classification results verify the statistical feature analysis.

Table 3.6 Classification results.

	Task 1		Task 2	
Dataset Type	F_{Gs}	F_{As}	F_{Gs}	F_{As}
Model	RF	RF	SVM	RF
5-fold CV	61.79%	64.00%	70.57%	80.57%
8-fold Random Shuffle CV	75.00%	81.25%	92.19%	84.17%
Average Accuracy	68.40%	72.63%	81.38%	82.37%

3.6. Falling Risk Evaluation

With gait and acceleration-axis features, falling risks are estimated by the scores compatible to the FRQ that provides PD quantitative analysis of their falling risk under Task 1 and Task 2, respectively. A baseline method without feature selection and an optimized method with Pearson's correlation feature selection are then compared. In the optimized method, the features with a p-value of Pearson's correlation to the falling score less than 0.005 are selected. In Task 1, 2 gait features (Table 3.7) and 63 acceleration-axis features are selected; in Task 2, 3 gait features (Table 3.8) and 72 acceleration-axis features are selected. Regression models of Linear Regression (LR),

Kernel Ridge (KR), Bayesian Ridge (BR), and Gradient Boosting Regressor (GBR) are used and only the best model is reported in results below.

Table 3.7 Gait features with significant linear correlation to falling risk score: Task 1.

Feature name		**Pearson p-value**
Number of strides	left	0.012
Total time to finish task	Start->end	0.035

Table 3.8 Gait features with significant linear correlation to falling risk score: Task 2.

Feature name		**Pearson p-value**
Number of strides	left	0.001
Total time to finish task	Start->end	0.014
Number of strides	right	0.025

After analyzing the walking performance between PD and HC, and between Task 1 and Task 2, falling risks are estimated through three different feature sets: F_{Gs}, F_{As} and the combination $(F_{Gs} + F_{As})$. With regression methods previously introduced, a score is provided to be compatible with FRQ which is used for falling risk estimation in clinical prescreening. The average accuracy and std of the two evaluation methods are used, as shown in Figure 3.11, to determine the improvement of the optimized method and the best results. The best outcome (error±std) from the baseline method is (0.25±0.41) from BR developed with F_{As} from Task 2. With feature selection in the optimized method, all results are improved. The best result (0.03±0.38) is from BR developed with $(F_{Gs} + F_{As})$

from Task 2. Hence, it concludes that compared to walking (Task 1), walking with water in hand (Task 2) can better assess falling risks for PD and HC.

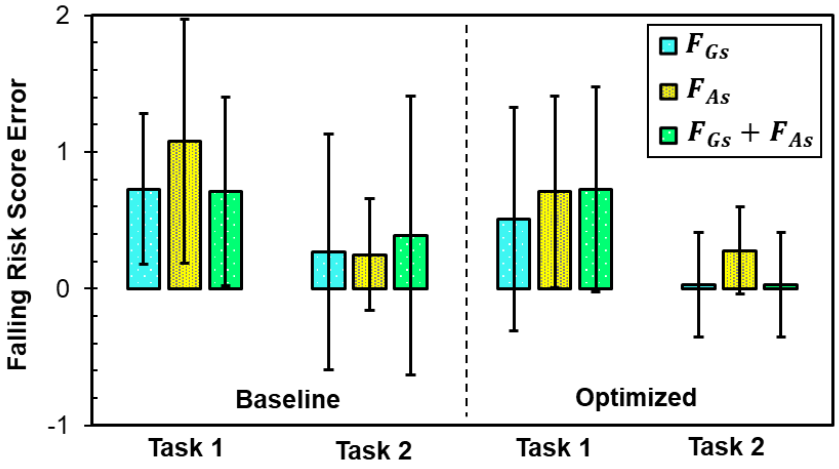

Figure 3.11 Average error ± std of falling risk estimation scores between non-randomly 5-fold CV and random shuffling 8-fold CV.

3.7. Summary

In this Chapter, we study and identify the feature differences between PD and HCs in walking and walking while holding a full cup of water in hand (closer to real-life scenarios). It concludes that acceleration-axis features from Task 2 – walking with water in hand can differentiate PD from HC the best with 82.37% accuracy. Meanwhile, falling risks are evaluated with BR regression through walking with water in hand and provide quantitative results to PD patients, compatible with FRQ with (error±std) = (0.03±0.38) in scoring. With the use of MONI, the proposed method can be transformed into a mobile game and provide a real-time evaluation to PD patients in daily practice and support physical therapy with the recorded evaluation results.

4. TOE TAPPING-BASED FALLING RISK EVALUATION

Typical symptoms of Parkinson's disease (PD) include freezing of gait, shuffling steps, and stooped posture, which introduce high risks of falling. Existing studies characterize and analyze PD symptoms through walking using wearable sensors. In addition, toe tapping is often used in clinical motor examination representing rotational agility in lower extremities, which is a critical factor in PD motor functionality and relates to falling. In this letter, we investigate the time and acceleration feature differences between PD patients and their age-matched healthy control (HC) subjects through alternating and synchronized toe tapping. Monitoring Insoles (MONI) are used to collect acceleration data with 10 PD patients and 9 HC subjects. In total, 87 time-axis and 1152 acceleration-axis features are extracted and analyzed between the two groups. The results suggest acceleration-axis features are with more significance in differing PD and HC than time-axis features. The results show toe tapping motion can better distinguish PD and HC with an accuracy of 87.65% using the acceleration-axis feature set compared to 57.07% with time-axis feature set. To help PD patient understand their falling, falling risks are estimated in scores using Linear Regression, with (error ± standard deviation) = (0.97±0.85) to be compatible to Fall Risk Questionnaire (FRQ) developed by the U.S. Centers for Disease Control and Prevention (CDC). Our method and the experiment can be easily transformed into a mobile game for daily life use and provides falling risk scores to PD patients without occupying spaces.

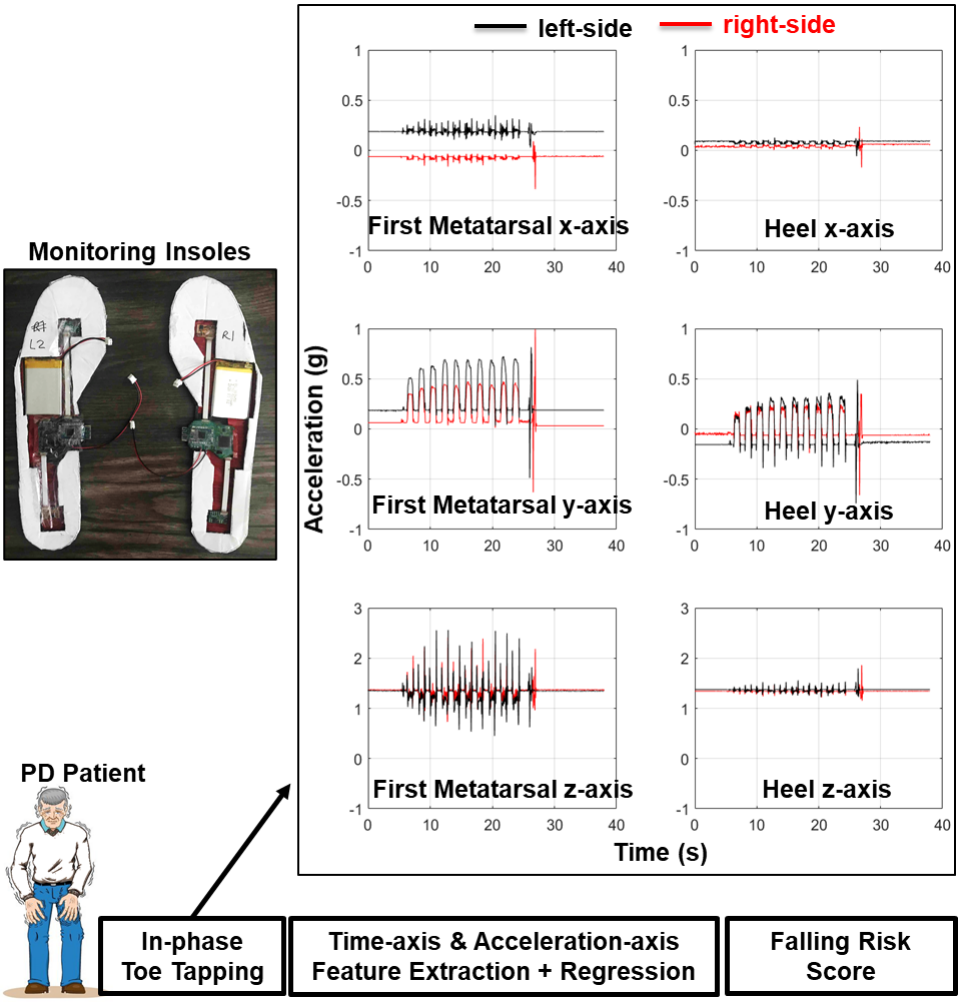

Figure 4.1 Graphical abstract of Chapter 4.

4.1. Toe Tapping Tasks

Gait analysis and characterization are vital in falling risk estimation for PD [190]. Existing methods focus on evaluating walking performance with wearable sensors to produce objective falling analysis or prediction in daily life automatically. Numerous studies [178, 179, 191] extract gait parameters from straight/treadmill walking using inertial measurement units (IMU), and then compare PD's gait to age-matched healthy

control (HC) subjects to make conclusions of falling risks [192]. However, the controlled experiment does not represent real-life scenarios, and the complicated setup of sensors is not suitable for daily life use. Some other studies develop smart wearable devices, such as insoles [44], to segment sequential motions (including sequence of walking, turning, and stepping over obstacles) and then extract gait parameters to study sequential effects [184] to falling, but do not provide any quantitative or understandable results to patients. Our recent study [193] estimates scores of falling risks referencing to Falling Risk Questionnaire (FRQ) [5] through walking with a cup of water in hand and can be applied to different stages of PD, but it requires a 23 ft. walking due to the reason that walking typically requires 10 to 33 ft. so that gait can be analyzed.

Compared to walking, toe tapping is another motion included in clinical motor examination tests [24] but does not require large space. Up to date, it is not well investigated how the performance represents falling risks by smart wearable devices. Very few studies [194] report PD's rhythmic toe tapping performance compared to HC subjects to assess leg muscles. Thus, there is an immediate need to explore how toe tapping relates to falling risks and develop new methods and tools for falling risk evaluation for PD patients for daily life use.

This work focuses on analyzing time-axis and acceleration-axis feature differences of toe tapping motion of PD and HC through alternative (anti-phase) and synchronized (in-phase) toe tapping tasks [195] in a game setting where subjects were wearing a pair of Monitoring Insoles (MONI) to perform tasks following indicators.

4.1.1. Experiment

Using coordination dynamics [195], two tasks were designed for bipedal control with toe tapping motion. A pair of MONI, containing two accelerometers at the heel and first metatarsal area, respectively, was used to collect foot motion data. Task 1 was the anti-phase movement, which required alternative toe tapping between the left and the right foot. Task 2 was the in-phase movement which was synchronized toe tapping. For both tasks, the motion frequency between the left and the right foot was 1:1.

A user interface was designed with left and right foot indicators, as shown in Figure 4.2, with initialization/configuration of task selection, period duration and number of cycles included in the task. The indicators changed colors to blue or yellow during the task at 1s interval as shown in Figure 4.3. When the color changed to blue, it meant dropping toes to the ground; when changing to yellow, it meant lifting toes. During the task, the heel worked like a pivot which only rotated. One period was defined as the duration between two yellow colors (2s), as shown in Figure 4.3(c). Within the 20s task duration, there were 10 periods in total. When the task stopped, the indicators were in red color. Each subject practiced each task twice and data was recorded for the third trial.

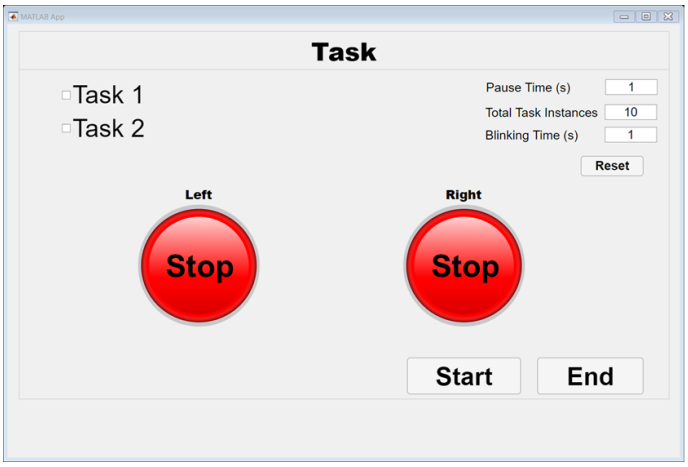

Figure 4.2 Desktop APP user interface (Initialization).

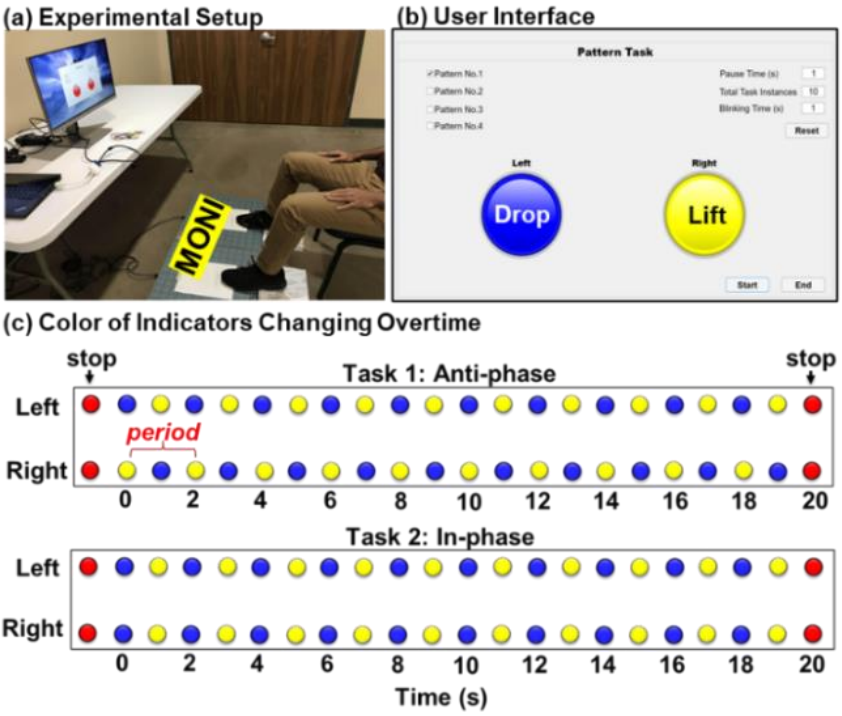

Figure 4.3 (a) Experimental setup; (b) User interface (during task); (c) Colors of indicators changing during Task 1 and Task 2.

Figure 4.4 and Figure 4.5 show the acceleration data plot of Task 1 and Task 2, respectively. It shows clear differences between PD and HC, as well as between PD

stages. To show the differences clearly, Figure 4.6 is a zoomed view of 2 cycles of right side and 1 cycle of left side in Task 1. We can clearly see the shaking of the acceleration during the task between PD stage 4, PD stage 2 and HC.

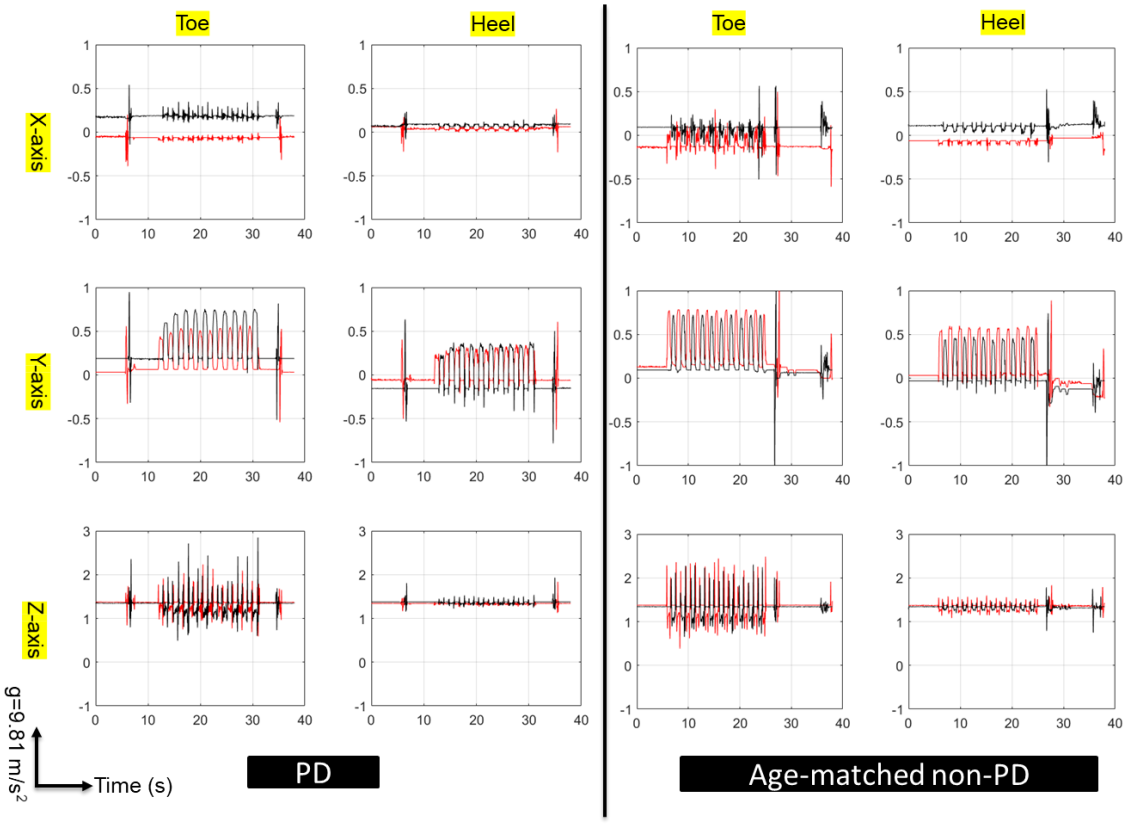

Figure 4.4 Task 1: acceleration data plot of PD and HC.

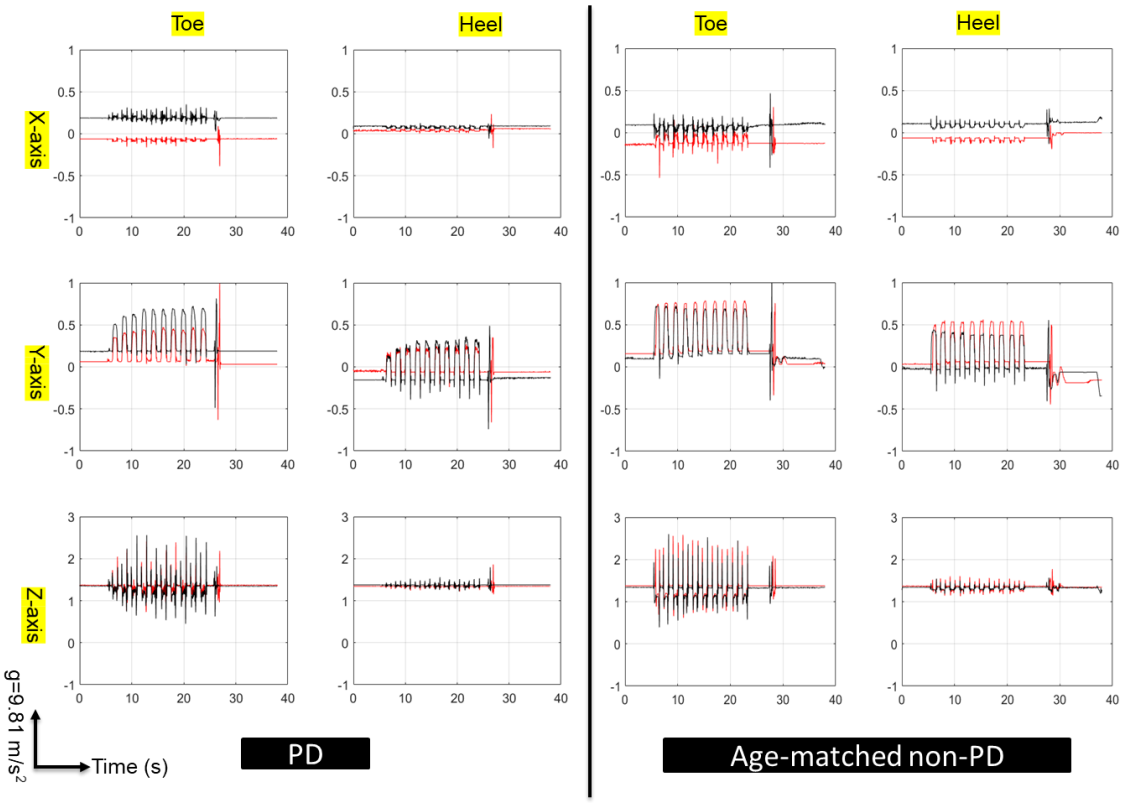

Figure 4.5 Task 2: acceleration data plot of PD and HC.

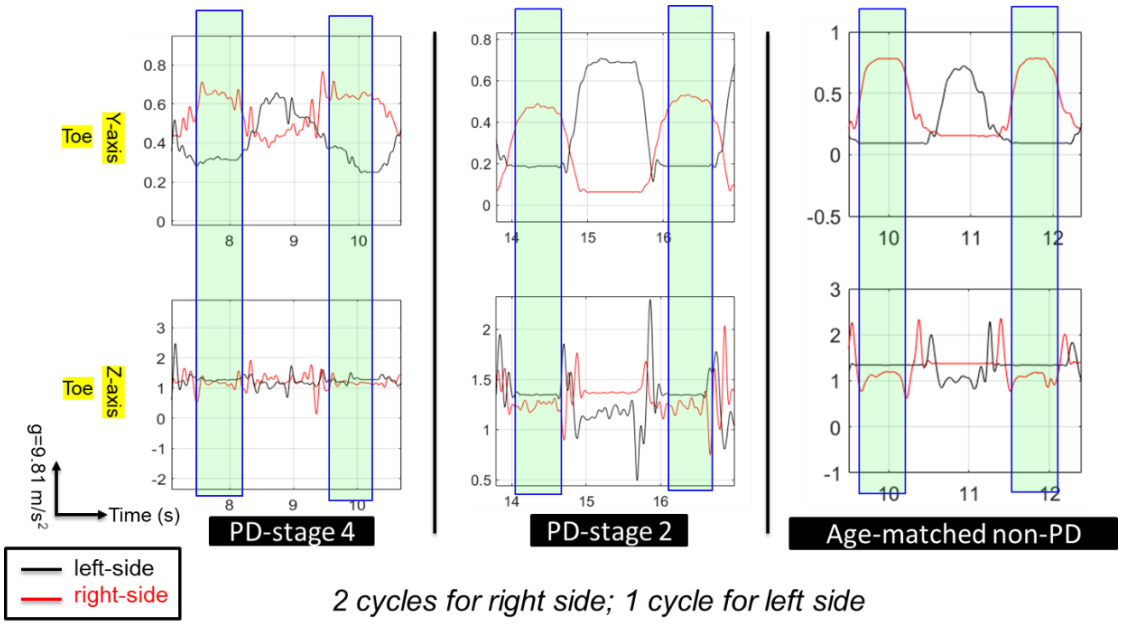

Figure 4.6 Zoomed view of Task 1 acceleration data (y and z-axis) between PD stage 4, PD stage 2 and HC.

4.1.2. Subjects

In total, 10 PD patients and 8 HC subjects participated in the experiment. Task 1 was more difficult for PD than Task 2. Thus, 2 PD patients (PD Stage 4) cannot follow or perform Task 1, but they finished Task 2. Subjects were grouped as PD-Task1, PD-Task2 and HC, as shown in Table 4.1 with the summarized information of each group. Validated to have a high correlation to clinical falling examination [6, 7], a self-rated Fall Risk Questionnaire (FRQ) including 12 YES/NO questions, developed by the U.S. Centers for Disease Control and Prevention (CDC) was filled out by subjects to determine a subject's characteristics of fall. The FRQ answers were transformed into a score to quantify falling risks in scores, scaling in between [0, 14] when a YES counts as

1 point. The scaling was up to 14 points because the first two questions count for 2 points each.

Table 4.1 Group summary: subjects' characteristics.

Group	PD-Task1	PD-Task2	HC
Gender	F [a] (2) [b], M [c] (6)	F (2), M (8)	F (8), M (1)
Age	(51-60) (1) (61-70) (4) (71-80) (2) (Over 80) (1)	(51-60) (1) (61-70) (5) (71-80) (3) (Over 80) (1)	(61-70) (5) (71-80) (4)
PD Stage	1 (4) 2 (2) 3 (1) 4 (1)	1 (4) 2 (2) 3 (1) 4 (3)	N/A
Falling	Faller (6), Non-faller (2)	Faller (8), Non-faller (2)	Non-faller (9)
Falling Score (mean ± std [f])	6.13 ± 3.48	6.20 ± 3.08	1.00 ± 1.31

4.2. Toe Tapping Event and Phase Identification

Toe tapping motion (Figure 4.7) includes 4 events: lift/drop start/end. With the 4 events identified, one motion period can be segmented into 4 phases: lift, in-the-air, drop and on-the-ground. Firstly, a low-pass filter filtered raw acceleration data with a cut-off frequency of 2.5 Hz. From the filtered acceleration data, y-axis data from the first metatarsal acceleration clearly showed the phases (Figure 4.8(a)). Thus, events and phases were identified with y-axis data and applied to all axes. Next, discrete differential transformation was applied to the y-axis of the first metatarsal acceleration (Figure 4.8(b)). To extract the events within a cycle (defined as C: lift start to drop end), the positive peak and negative peak were identified and then zero-crossings before and after the peaks are found to be the events.

Figure 4.7 Toe tapping motion.

A total task duration included 10 periods for both Task 1 and Task 2. Besides period, phase and cycle, cycle difference was defined as the duration difference between the two continuous cycles; lift interval (L) was defined as the duration between two lift start events and drop interval (D) was defined as the duration between two drop end events.

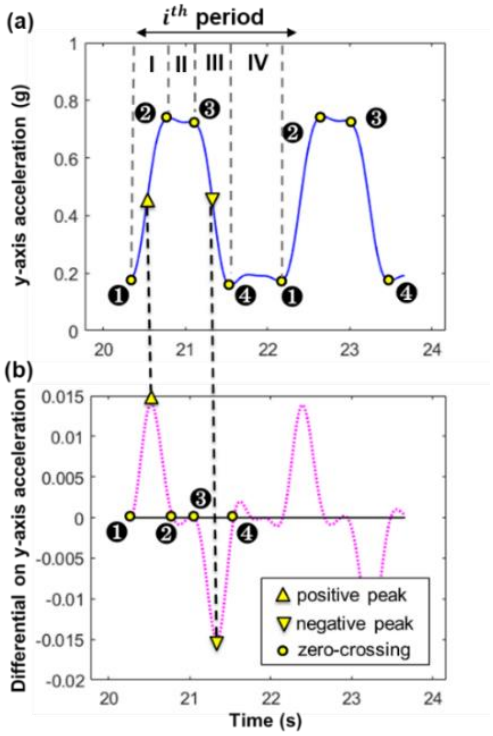

Figure 4.8 (a) Toe tapping motion events: ❶Lift Toe Start, ❷Lift Toe End, ❸Drop Toe Start, ❹Drop Toe End; Phases: Lift Phase (I), In-the-air Phase (II), Drop Phase (III), On-the-ground Phase (IV), Period (Phase I->IV), Cycle (Phase I->III); (b) Method of segmentation.

4.3. Feature Extraction

4.3.1. Time-axis Features

In total, 87 time-axis features were extracted. From a single side, 40 time-axis features were extracted from 5 functions of (minimal, maximal, mean, standard deviation and variability) applied to 8 different durations (Phase I-IV, C, cycle difference, L and D) from the 8 continuous periods in the middle of the task. Two more extra features were extracted: the number of periods when Phase II = 0 and the number of periods when Phase IV = 0. From both sides, 3 constant error of ratios (CER) [195] were calculated as $CER_x = \frac{mean(x_{left})}{mean(x_{right})} - 1$; where x is L, D or cycle difference.

4.3.2. Acceleration-axis Features

The acceleration-axis features were extracted from Phase I-III and C, respectively. From a single side, 18 statistical features were extracted from 4 axes (x, y, z and the standard deviation (std) of (x, y, z)) of the two accelerometers. A mean function was applied to the acceleration in the 8 continuous periods in the middle, respectively, for segmentations of Phases I-III and C. Thus, in total, there were 1152 acceleration-axis features extracted from two sides (1152 = 2 sides * 4 axes * 2 accelerometers * 18 features * 4 segmentations * 1 function).

4.4. Feature Analysis

The time-axis and acceleration-axis features were checked with Shapiro-Wilk Test to be a normal distribution. Since the group is an independent factor while the task is a dependent factor, features were analyzed with a two-way Analysis of Variance

(ANOVA) with replication to determine if there is any feature with a statistically significant difference in mean between groups for the same task. Through identifying the features with significant differences, conclusions can be made if time-axis or acceleration-axis features are more critical when differing PD and HC.

4.4.1. Results of Time-axis Features

4.4.1.1. Between Groups

The results indicated only one feature with statistical significance between means of PD and HC: right-side minimal drop interval from Task 1 with a p-value of 0.031, as shown in Figure 4.9. It showed PD uses smaller drop intervals (mean: 1.46) during the periods compared to HC (mean: 1.61) in Task 1, while the two groups had the same drop intervals for Task 2. As expected, the results indicated PD patients performed like HC subjects in the simpler synchronized tapping.

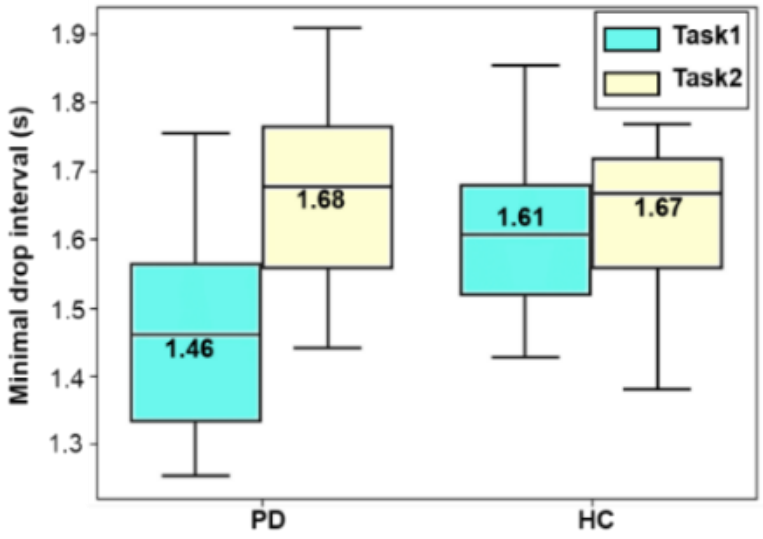

Figure 4.9 Time-axis feature with significance.

CER is the metric to evaluate their bipedal control performance (CER=0 means perfect control during the task). To evaluate for groups, the absolute error of CER is calculated as the average of absolute CER value. Absolute errors of CER_L and CER_D for HC Task 1 is 0.054 and 0.039 vs. 0.034 and 0.009 for PD Task 1. Absolute errors of CER_L and CER_D for HC Task 2 is 0.007 and 0.006 vs. 0.017 and 0.019 for PD Task 2. We found PD performed better than HC in Task 1 while worse than HC in Task 2. In HC group, two subjects performed very poorly in Task 1 with 0.1590 and 0.1818. The ANOVA results of CERs did not show a significant difference between the two groups' mean.

4.4.2. Results of Acceleration-axis Features

4.4.2.1. Between Groups

The results indicated 15 features with significant differences between groups for Task 1 (Table 4.2) and 11 features for Task 2 (Table 4.3). Two features were the same as shown in Figure 4.10. The minimal right-side heel z-axis acceleration in phase III had a p-value of 0.013 for Task 1 and 0.003 for Task 2. The signal power of the left-side first metatarsal z-axis acceleration from Phase I was 0.022 for both tasks. Within all these features, 9 of them were extracted from phase I, 12 were from Phase II; 0 is from Phase III and 5 were from the cycle. The results indicated dropping was more important than lifting and in-the-air phases. From these acceleration-axis features (acceleration values), we concluded that PD used minor control during dropping toes while applying more control during lifting than HC.

Table 4.2 Acceleration-axis features with significant differences between groups: Task 1.

Feature name	p-value: (PD, task1) vs. (HC, task1)
interquartile range of left-side lift duration std-heel	0.006
minimal of right-side cycle duration y-toe	0.007
percentile = 25 of left-side drop duration y-heel	0.010
minimal of right-side drop duration z-heel	0.013
skewness of left-side lift duration x-toe	0.017
number of positive peaks of left-side lift duration std-toe	0.019
signal power of left-side lift duration z-toe	0.022
mean of right-side lift duration x-toe	0.023
percentile = 75 of right-side drop duration std-heel	0.030
minimal of right-side drop duration y-heel	0.033
median of right-side lift duration x-heel	0.037
percentile = 90 of right-side drop duration z-toe	0.038
coefficient of variance of left-side drop duration z-toe	0.040
percentile = 75 of left-side drop duration y-toe	0.049
mean of right-side cycle duration x-toe	0.049

Table 4.3 Acceleration-axis features with significant differences between groups: Task 2.

Feature name	(PD, task2) vs. (HC, task2)
minimal of right-side drop duration z-heel	0.003
mean of right-side lift duration std-toe	0.010
skewness of right-side drop duration z-toe	0.016
signal power of left-side lift duration z-toe	0.022
coefficient of variance of left-side cycle duration z-toe	0.030
minimal of right-side lift duration y-toe	0.030
mean of right-side drop duration std-toe	0.030
minimal of right-side drop duration y-toe	0.030
signal power of left-side lift duration y-toe	0.034
peak-to-peak amplitude of left-side cycle duration z-toe	0.038
percentile = 50 of left-side drop duration std-toe	0.038

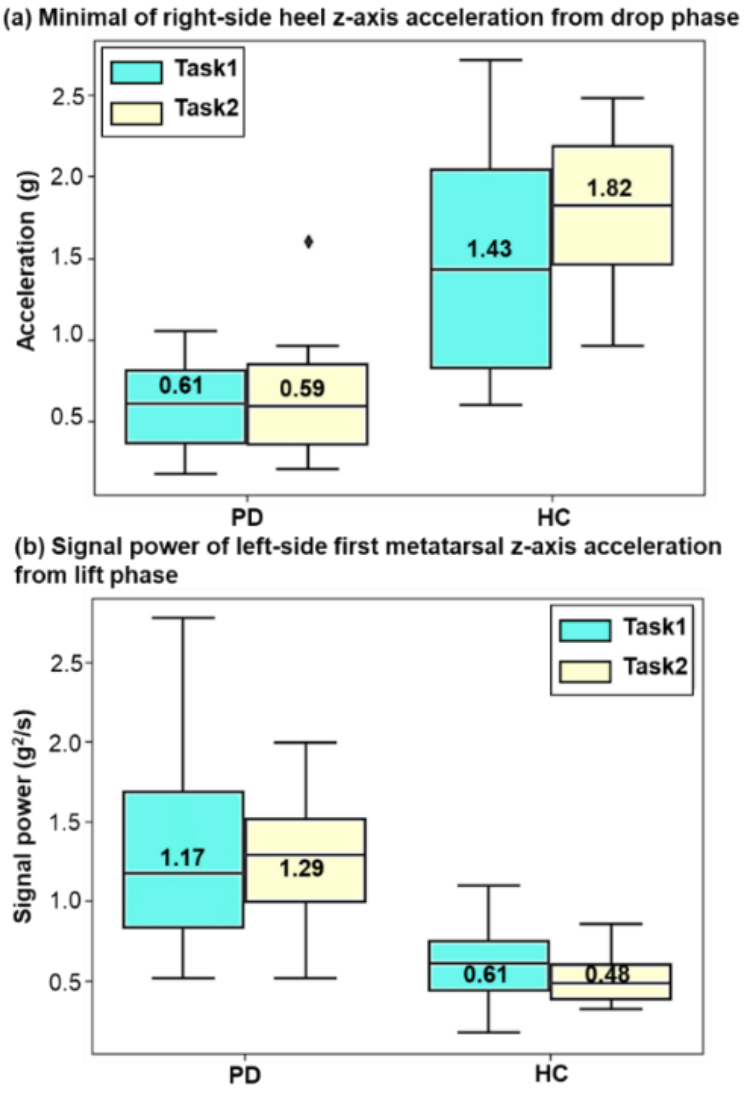

Figure 4.10 Acceleration-axis features showing significance in both tasks.

4.5. PD vs. HC Classification

The classification of PD and HC was performed to further prove the conclusion with the two types of features from the tasks. Classification models of Random Forest (RF), Support Vector Machine (SVM), and K-Nearest-Neighbors (KNN) were used in this work.

We found acceleration-axis features had more significance since there was only one time-axis feature statistically significant differences between the means of groups while there were 26 acceleration-axis features in total for both tasks. Classification of PD and HC was performed based on time-axis feature set F_{ts}, which included the same type of time-axis features. The acceleration-axis feature set F_{as} included the same type of acceleration-axis features extracted from a single period in Task 1 and Task 2, respectively. Same as our previous work of walking analysis, a non-randomly 5-fold Cross-Validation (CV) and a random shuffling 8-fold CV were used for evaluation. As shown in Table 4.4, the F_{as} indicated more accuracy in PD and HC classification compared to F_{ts} for both tasks. Task 1 and Task 2 were very similar in results of classifying PD and HC. The classification results verified the statistical feature analysis.

Table 4.4 Classification results.

	Task 1		Task 2	
Dataset Type	F_{ts}	F_{as}	F_{ts}	F_{as}
Model	KNN	KNN	SVM	RF
5-fold CV Mean	51.03%	74.53%	50.51%	78.71%
8-fold Random Shuffling Mean	62.50%	95.62%	63.64%	96.59%
Average Accuracy	56.76%	85.08%	57.07%	87.65%

4.6. Falling Risk Evaluation

Falling risks were estimated in scores compatible with the FRQ that provides PD quantitative feedback of their falling risks under Task 1 and Task 2, respectively. A baseline method without feature selection and an optimized method with Pearson's correlation feature selection were compared with time-axis and acceleration-axis features. In the optimized method, the features with a p-value of Pearson's correlation to

the falling score of less than 0.005 were selected. In Task 1, 6 time-axis features and 37 acceleration-axis features were selected; In Task 2, 6 time-axis features and 77 acceleration-axis features were selected. Regression models of Linear Regression (LR), Kernel Ridge (KR), Bayesian Ridge (BR), and Gradient Boosting Regressor (GBR) were used to predict the score.

Falling risks were estimated through three different feature sets: F_{ts}, F_{as}, and the combination ($F_{ts} + F_{as}$). With the regression method introduced, a score was provided to be compatible with FRQ. The average accuracy and std of the two evaluation methods were shown in Figure 4.11 Average error ± std of falling risk estimation scores between non-randomly 5-fold CV and random shuffling 8-fold CV.to determine the improvement of the optimized method and the best results. The best result (error ± std) from the baseline method was (1.36±0.92) from GBR developed with ($F_{ts} + F_{as}$) from Task 1. With feature selection in the optimized method, overall results from Task 2 were improved. The best result (0.97±0.85) was from LR developed with F_{as} from Task 2. Thus, it concluded Task 2 can better assess falling risks for PD and HC when using feature selection.

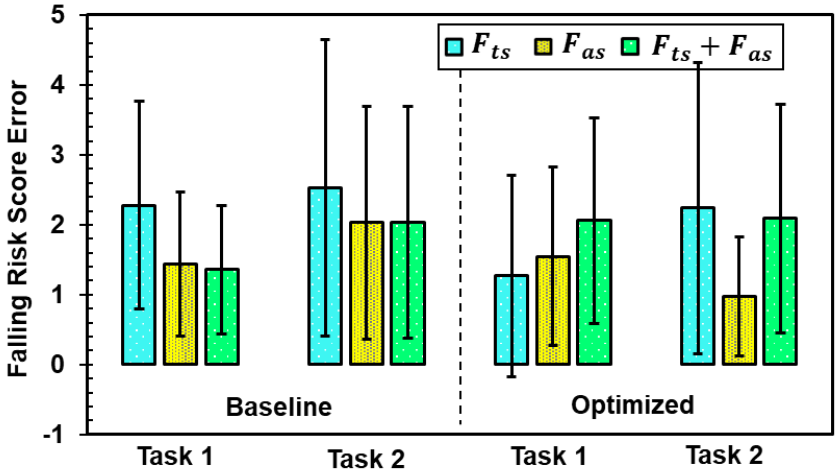

Figure 4.11 Average error ± std of falling risk estimation scores between non-randomly 5-fold CV and random shuffling 8-fold CV.

4.7. Summary

The feature analysis results suggest Task 1 had more significant features than Task 2. However, Task 2 had slightly better accuracy in classification and falling risk estimation. This result may attribute to the poor performance in Task 1 from the two HC subjects. More subjects will be participating in the future, and a long-term experiment with PD can be conducted to determine if these toe-tapping tasks can be used as cognitive training for PD to lower falling risks.

This study investigated toe tapping motion feature difference between PD patients and HC subjects. It concluded acceleration-axis features were with more importance than time-axis features when differentiating PD and HC through the two-way ANOVA with replication method. Compared to walking, the in-phase toe tapping motion showed better accuracy in distinguishing PD and HC (87.65%) and provided (error±std) = (0.97±0.85) falling risk scores compared to FRQ. This work provided a

different perspective of estimating falling risks through toe tapping, which can be simply transformed into mobile games for daily life use compared to traditional method of gait analysis.

5. SUMMARY

5.1. Comparison to Existing Studies

5.1.1. PD vs. HC Classification

Compared to the existing studies [12, 13, 21, 196, 197] that use different methods, sensors and motion tasks for PD and HC classification and detection, the results of our method in Chapter 3 and Chapter 4 are compatible, but the results are not the most accurate, as shown in Table 5.1. The reason is that the number of PD patients and HC subjects are smaller than the other studies. To further discuss, we compute the patient similarity using normalized Euclidean Distance as shown in Figure Appendix A.1. It shows a large difference between our PD patients.

Table 5.1 Comparison to existing studies using different types of motors and motions.

Method	Sensor	Motion	PD	HC	Accuracy
KNN	Microphone	Pronounce	23	8	90%
Hidden Markov	Force	Walk	15	16	90%
RF	Force	Walk	93	73	74%
CNN	Force & Acceleration	Write	14	21	87%
Wavelet analysis + SVM	Acceleration	Walk	15	16	90%
Our work	Acceleration	Walk with water	10	8	82%
	Acceleration	In-phase Toe Tapping	10	8	88%

5.1.2. Falling Risk Score

Table 5.2 presents the comparison between our method of falling risk evaluation to the most similar study [14]. Firstly, our method uses MONI which is specifically

designed and developed for falling risk evaluation for PD where only accelerometers are included. The tasks and number of PD patients and HC subjects are similar as both studies involve sequential and repetitive foot motion but with variations. The only difference is we are using FRQ as ground truth, which is validated by clinical studies to have a high correlation to clinical tests; while the other study is using comparison between PD and HC so their falling scores are difficult to validate.

Table 5.2 Comparison to the most similar existing study.

Method	**Study [14]: score method**	**Our method**
Device	Commercial Insole	MONI
Sensors	Force Bending sensor	Accelerometer
Tasks	• Lean with single leg (with a belt) • Walk	• Walk with water • Toe tapping
PD	7 (stage 2, 3)	8-10 (stage1-4)
HC	10 HC, 12 students	8-9 HC
Ground Truth	Comparison between groups	FRQ
Model	Balancing Model (math)	Regression
Scale	[0,100]	[0,14]
Error	N/A	0.03 (walk with water) 0.95 (in-phase toe tapping)

5.2. Contributions

To summarize, this dissertation aims to provide quantitative analysis of falling risks for PD patients in daily life to help prevent falling through analyzing foot motions in easy setups and simple processes using MONI. MONI is designed and developed for daily life use. The proposed data processing method includes robust foot motion recognition to identify the foot motions from uncontrolled daily life environments and feature extraction and selection for quantitative falling risk evaluation. The fast-labeling

framework very well addresses the two challenges of robust foot motion recognition and is validated to produce small errors in the next step: feature extraction. Walking and toe tapping motions are analyzed and proven to be useful for falling risk evaluation for PD.

5.3. Future Work

To further validate the results in Chapter 3 and Chapter 4, more experiments should be carried out by more PD patients with vs. without similar symptoms and disease progression status. Medication states and PD stages may be incorporated with current data processing technique to better address the heterogenicity of PD patients.

MONI can be better designed to provide better comfort for daily uses. An APP can be designed to transform experimental tasks into mobile games while motion recognition, feature extraction and falling risk scoring can be integrated into one APP for real-time processing. And thus, a falling risk score can be generated after each game play (task performance and evaluation) and a long-term data profiling can be generated to provide doctors with medical assistance.

REFERENCES

[1] P. H. Pelicioni *et al.*, "Falls in Parkinson's disease subtypes: risk factors, locations and circumstances," *International journal of environmental research public health,* vol. 16, no. 12, p. 2216, 2019.

[2] J. Pressley *et al.*, "The impact of comorbid disease and injuries on resource use and expenditures in parkinsonism," *Neurology,* vol. 60, no. 1, pp. 87-93, 2003.

[3] P.-H. Chen *et al.*, "Gait disorders in Parkinson's disease: assessment and management," *International Journal of Gerontology,* vol. 7, no. 4, pp. 189-193, 2013.

[4] C. A. Beck *et al.*, "National randomized controlled trial of virtual house calls for Parkinson disease," *Neurology,* vol. 89, no. 11, pp. 1152-1161, 2017.

[5] R. L. Vivrette *et al.*, "Development of a fall-risk self-assessment for community-dwelling seniors," *Journal of aging and physical activity,* vol. 19, no. 1, pp. 16-29, 2011.

[6] L. Z. Rubenstein *et al.*, "Validating an evidence-based, self-rated fall risk questionnaire (FRQ) for older adults," *Journal of Safety Research,* vol. 42, no. 6, pp. 493-499, 2011.

[7] N. Kitcharanant *et al.*, "Validity and reliability of the self-rated fall risk questionnaire in older adults with osteoporosis," *BMC musculoskeletal disorders,* vol. 21, no. 1, pp. 1-9, 2020.

[8] A. G. S. Panel on Prevention of Falls in Older Persons and B. G. Society, "Summary of the updated American Geriatrics Society/British Geriatrics Society clinical practice guideline for prevention of falls in older persons," *Journal of the American Geriatrics Society,* vol. 59, no. 1, pp. 148-157, 2011.

[9] S. Papapetropoulos, "Patient diaries as a clinical endpoint in Parkinson's disease clinical trials," *CNS neuroscience & therapeutics,* vol. 18, no. 5, pp. 380-387, 2012.

[10] N. Kamata *et al.*, "Overestimation of stability limits leads to a high frequency of falls in patients with Parkinson's disease," *Clinical Rehabilitation,* vol. 21, no. 4, pp. 357-361, 2007.

[11] A. L. S. De Lima *et al.*, "Freezing of gait and fall detection in Parkinson's disease using wearable sensors: a systematic review," *Journal of neurology,* vol. 264, no. 8, pp. 1642-1654, 2017.

[12] A. Khorasani and M. R. Daliri, "HMM for classification of Parkinson's disease based on the raw gait data," *Journal of medical systems,* vol. 38, no. 12, pp. 1-6, 2014.

[13] N. El-Bendary *et al.*, "FALL DETECTION AND PREVENTION FOR THE ELDERLY: A REVIEW OF TRENDS AND CHALLENGES," *International Journal on Smart Sensing & Intelligent Systems,* vol. 6, no. 3, 2013.

[14] J. C. Ayena *et al.*, "Home-based risk of falling assessment test using a closed-loop balance model," *IEEE transactions on neural systems and rehabilitation engineering,* vol. 24, no. 12, pp. 1351-1362, 2015.

[15] D. Jarchi *et al.*, "A review on accelerometry-based gait analysis and emerging clinical applications," *IEEE reviews in biomedical engineering,* vol. 11, pp. 177-194, 2018.

[16] B. Yang and F. Chenglong, "Inertial Measurement Unit and Fall Risk Assessment in the Elderly," *Chinese Journal of Rehabilitation Theory and Practice,* no. 7, pp. 780-784, 2015.

[17] S. Usmani *et al.*, "Latest research trends in fall detection and prevention using machine learning: A systematic review," *Sensors,* vol. 21, no. 15, p. 5134, 2021.

[18] X. Chai *et al.*, "Smart wearables with sensor fusion for fall detection in firefighting," *Sensors,* vol. 21, no. 20, p. 6770, 2021.

[19] A. Hakim *et al.*, "Smartphone based data mining for fall detection: Analysis and design," *Procedia computer science,* vol. 105, pp. 46-51, 2017.

[20] N. D. Pah *et al.*, "Detecting Effect of Levodopa in Parkinson's Disease Patients Using Sustained Phonemes," *IEEE Journal of Translational Engineering in Health and Medicine,* vol. 9, pp. 1-9, 2021.

[21] C. R. Pereira *et al.*, "Deep learning-aided Parkinson's disease diagnosis from handwritten dynamics," in *2016 29th SIBGRAPI Conference on Graphics, Patterns and Images (SIBGRAPI)*, 2016, pp. 340-346: Ieee.

[22] A. Talitckii *et al.*, "Avoiding misdiagnosis of Parkinson's disease with the use of wearable sensors and artificial intelligence," *IEEE Sensors Journal,* vol. 21, no. 3, pp. 3738-3747, 2020.

[23] F. B. Horak *et al.*, "The balance evaluation systems test (BESTest) to differentiate balance deficits," *Physical therapy,* vol. 89, no. 5, pp. 484-498, 2009.

[24] C. G. Goetz *et al.*, "Movement Disorder Society‐sponsored revision of the Unified Parkinson's Disease Rating Scale (MDS‐UPDRS): scale presentation and clinimetric testing results," *Movement disorders: official journal of the Movement Disorder Society,* vol. 23, no. 15, pp. 2129-2170, 2008.

[25] G. M. Weiss *et al.*, "Smartwatch-based activity recognition: A machine learning approach," in *2016 IEEE-EMBS International Conference on Biomedical and Health Informatics (BHI)*, 2016, pp. 426-429: IEEE.

[26] M. Shoaib *et al.*, "Complex human activity recognition using smartphone and wrist-worn motion sensors," *Sensors,* vol. 16, no. 4, p. 426, 2016.

[27] R. Saini *et al.*, "A novel framework of continuous human-activity recognition using Kinect," *Neurocomputing,* vol. 311, pp. 99-111, 2018.

[28] Y. Kim and T. Moon, "Human detection and activity classification based on micro-Doppler signatures using deep convolutional neural networks," *IEEE geoscience and remote sensing letters,* vol. 13, no. 1, pp. 8-12, 2015.

[29] X. Li *et al.*, "A survey of deep learning-based human activity recognition in radar," *Remote Sensing,* vol. 11, no. 9, p. 1068, 2019.

[30] Y. Wang *et al.*, "A data fusion-based hybrid sensory system for older people's daily activity and daily routine recognition," *IEEE Sensors Journal,* vol. 18, no. 16, pp. 6874-6888, 2018.

[31] E. S. Sazonov *et al.*, "Monitoring of posture allocations and activities by a shoe-based wearable sensor," *IEEE Transactions on Biomedical Engineering,* vol. 58, no. 4, pp. 983-990, 2010.

[32] F. Lin *et al.*, "Toward unobtrusive patient handling activity recognition for injury reduction among at-risk caregivers," *IEEE Journal of biomedical and health informatics,* vol. 21, no. 3, pp. 682-695, 2016.

[33] F. Attal *et al.*, "Physical human activity recognition using wearable sensors," *Sensors,* vol. 15, no. 12, pp. 31314-31338, 2015.

[34] H. Zhu *et al.*, "A sequence-to-sequence model-based deep learning approach for recognizing activity of daily living for senior care," *Journal of biomedical informatics,* vol. 84, pp. 148-158, 2018.

[35] C. Zhu and W. Sheng, "Wearable sensor-based hand gesture and daily activity recognition for robot-assisted living," *IEEE Transactions on Systems, Man, and Cybernetics-Part A: Systems and Humans,* vol. 41, no. 3, pp. 569-573, 2011.

[36] M. Zeng *et al.*, "Understanding and improving recurrent networks for human activity recognition by continuous attention," in *Proceedings of the 2018 ACM International Symposium on Wearable Computers*, 2018, pp. 56-63.

[37] H. Li *et al.*, "Bi-LSTM Network for Multimodal Continuous Human Activity Recognition and Fall Detection," *IEEE Sensors Journal,* vol. 20, no. 3, pp. 1191-1201, 2019.

[38] S. Ashry *et al.*, "CHARM-Deep: Continuous Human Activity Recognition Model Based on Deep Neural Network using IMU Sensors of Smartwatch," *IEEE Sensors Journal*, 2020.

[39] B. Fida *et al.*, "Varying behavior of different window sizes on the classification of static and dynamic physical activities from a single accelerometer," *Medical engineering & physics,* vol. 37, no. 7, pp. 705-711, 2015.

[40] A. Ignatov, "Real-time human activity recognition from accelerometer data using Convolutional Neural Networks," *Applied Soft Computing,* vol. 62, pp. 915-922, 2018.

[41] J. Liono *et al.*, "Optimal time window for temporal segmentation of sensor streams in multi-activity recognition," in *Proceedings of the 13th International Conference on Mobile and Ubiquitous Systems: Computing, Networking and Services*, 2016, pp. 10-19.

[42] C. S. Hemalatha and V. Vaidehi, "Frequent bit pattern mining over tri-axial accelerometer data streams for recognizing human activities and detecting fall," *Procedia Computer Science,* vol. 19, pp. 56-63, 2013.

[43] M. T. Uddin *et al.*, "Random forests based recognition of human activities and postural transitions on smartphone," in *2016 5th International Conference on Informatics, Electronics and Vision (Iciev)*, 2016, pp. 250-255: IEEE.

[44] Z. Yang *et al.*, "A smart environment-adapting timed-up-and-go system powered by sensor-embedded insoles," *IEEE Internet of Things Journal,* vol. 6, no. 2, pp. 1298-1305, 2018.

[45] N. Yala *et al.*, "Towards improving feature extraction and classification for activity recognition on streaming data," *Journal of Ambient Intelligence and Humanized Computing,* vol. 8, no. 2, pp. 177-189, 2017.

[46] K. Li *et al.*, "Applying multivariate segmentation methods to human activity recognition from wearable sensors' data," *JMIR mHealth and uHealth,* vol. 7, no. 2, p. e11201, 2019.

[47] J.-H. Li *et al.*, "Segmentation and Recognition of Basic and Transitional Activities for Continuous Physical Human Activity," *IEEE Access,* vol. 7, pp. 42565-42576, 2019.

[48] A. Zhang *et al.*, "Weakly-supervised learning for Parkinson's disease tremor detection," in *2017 39th Annual International Conference of the IEEE Engineering in Medicine and Biology Society (EMBC)*, 2017, pp. 143-147: IEEE.

[49] A. Papadopoulos *et al.*, "Detecting Parkinsonian Tremor from IMU Data Collected In-The-Wild using Deep Multiple-Instance Learning," *IEEE Journal of Biomedical and Health Informatics,* 2019.

[50] T. Toda *et al.*, "Mobile activity recognition through training labels with inaccurate activity segments," in *Proceedings of the 13th International Conference on Mobile and Ubiquitous Systems: Computing, Networking and Services*, 2016, pp. 57-64.

[51] A. Ratner *et al.*, "Snorkel: Rapid training data creation with weak supervision," in *Proceedings of the VLDB Endowment. International Conference on Very Large Data Bases,* 2017, vol. 11, no. 3, p. 269: NIH Public Access.

[52] B. M. Eskofier *et al.*, "An overview of smart shoes in the internet of health things: gait and mobility assessment in health promotion and disease monitoring," *Applied Sciences*, vol. 7, no. 10, p. 986, 2017.

[53] N. Hegde *et al.*, "A comparative review of footwear-based wearable systems," *Electronics*, vol. 5, no. 3, p. 48, 2016.

[54] H. Nagano and R. K. Begg, "Shoe-insole technology for injury prevention in walking," *Sensors*, vol. 18, no. 5, p. 1468, 2018.

[55] P. Lopez-Meyer *et al.*, "Automatic detection of temporal gait parameters in poststroke individuals," *IEEE Transactions on Information Technology in Biomedicine*, vol. 15, no. 4, pp. 594-601, 2011.

[56] L. S. Lincoln *et al.*, "An elastomeric insole for 3-axis ground reaction force measurement," in *2012 4th IEEE RAS & EMBS International Conference on Biomedical Robotics and Biomechatronics (BioRob)*, 2012, pp. 1512-1517: IEEE.

[57] A. M. Howell *et al.*, "Kinetic gait analysis using a low-cost insole," *IEEE Transactions on Biomedical Engineering*, vol. 60, no. 12, pp. 3284-3290, 2013.

[58] S. Crea *et al.*, "A wireless flexible sensorized insole for gait analysis," *Sensors*, vol. 14, no. 1, pp. 1073-1093, 2014.

[59] T. Tamm *et al.*, "Smart insole sensors for sports and rehabilitation," in *Nanosensors, Biosensors, and Info-Tech Sensors and Systems 2014*, 2014, vol. 9060, p. 90600L: International Society for Optics and Photonics.

[60] D. A. Jacobs and D. P. Ferris, "Estimation of ground reaction forces and ankle moment with multiple, low-cost sensors," *Journal of neuroengineering and rehabilitation,* vol. 12, no. 1, p. 90, 2015.

[61] J. H. Low *et al.*, "A pressure-redistributing insole using soft sensors and actuators," in *2015 IEEE International Conference on Robotics and Automation (ICRA)*, 2015, pp. 2926-2930: IEEE.

[62] L. Motha *et al.*, "Instrumented rubber insole for plantar pressure sensing," *Organic Electronics,* vol. 23, pp. 82-86, 2015.

[63] A. M. Tan *et al.*, "Design of low cost smart insole for real time measurement of plantar pressure," *Procedia Technology,* vol. 20, pp. 117-122, 2015.

[64] D. Vilarinho *et al.*, "POFBG-embedded cork insole for plantar pressure monitoring," *Sensors,* vol. 17, no. 12, p. 2924, 2017.

[65] C. Deng *et al.*, "Self‐Powered Insole Plantar Pressure Mapping System," *Advanced Functional Materials,* vol. 28, no. 29, p. 1801606, 2018.

[66] A. G. Leal-Junior *et al.*, "Polymer optical fiber for in-shoe monitoring of ground reaction forces during the gait," *IEEE Sensors Journal,* vol. 18, no. 6, pp. 2362-2368, 2018.

[67] M. Abdelhady *et al.*, "A High-Fidelity Wearable System for Measuring Lower-Limb Kinetics and Kinematics," *IEEE Sensors Journal,* vol. 19, no. 24, pp. 12482-12493, 2019.

[68] I. Acharya *et al.*, "A Force-Sensing Insole to Quantify Impact Loading to the Foot," *Journal of biomechanical engineering,* vol. 141, no. 2, 2019.

[69] R. Eguchi and M. Takahashi, "Insole-Based Estimation of Vertical Ground Reaction Force Using One-Step Learning With Probabilistic Regression and Data Augmentation," *IEEE Transactions on Neural Systems and Rehabilitation Engineering,* vol. 27, no. 6, pp. 1217-1225, 2019.

[70] R. Eguchi *et al.*, "Estimation of Vertical Ground Reaction Force Using Low-cost Insole with Force Plate-free Learning from Single Leg Stance and Walking," *IEEE journal of biomedical and health informatics,* 2019.

[71] Z. Hao *et al.*, "3D Printed Smart Orthotic Insoles: Monitoring a Person's Gait Step by Step," *IEEE Sensors Letters,* 2019.

[72] A. G. Leal-Junior *et al.*, "3D-printed POF insole: Development and applications of a low-cost, highly customizable device for plantar pressure and ground reaction forces monitoring," *Optics & Laser Technology,* vol. 116, pp. 256-264, 2019.

[73] W. Lee *et al.*, "Characterization of elastic polymer-based smart insole and a simple foot plantar pressure visualization method using 16 electrodes," *Sensors,* vol. 19, no. 1, p. 44, 2019.

[74] J. Park *et al.*, "Foot Plantar Pressure Measurement System Using Highly Sensitive Crack-Based Sensor," *Sensors,* vol. 19, no. 24, p. 5504, 2019.

[75] I. Sorrentino *et al.*, "A Novel Sensorized Skin Insole for Sensing Feet Pressure Distributions," *arXiv preprint arXiv:1910.06370,* 2019.

[76] W. Wang *et al.*, "Self-Powered Smart Insole for Monitoring Human Gait Signals," *Sensors,* vol. 19, no. 24, p. 5336, 2019.

[77] Q. Zhang *et al.*, "A low-cost and highly integrated sensing insole for plantar pressure measurement," *Sensing and Bio-Sensing Research,* vol. 26, p. 100298, 2019.

[78] S. J. M. Bamberg *et al.*, "Gait analysis using a shoe-integrated wireless sensor system," *IEEE transactions on information technology in biomedicine,* vol. 12, no. 4, pp. 413-423, 2008.

[79] H. Noshadi *et al.*, "HERMES: mobile system for instability analysis and balance assessment," *ACM Transactions on Embedded Computing Systems (TECS),* vol. 12, no. 1s, p. 57, 2013.

[80] A. M. Cristiani *et al.*, "An instrumented insole for long term monitoring movement, comfort, and ergonomics," *IEEE Sensors Journal,* vol. 14, no. 5, pp. 1564-1572, 2014.

[81] T. Liu *et al.*, "Triaxial joint moment estimation using a wearable three-dimensional gait analysis system," *Measurement,* vol. 47, pp. 125-129, 2014.

[82] F. Martínez-Martí *et al.*, "Embedded sensor insole for wireless measurement of gait parameters," *Australasian physical & engineering sciences in medicine,* vol. 37, no. 1, pp. 25-35, 2014.

[83] R. Das and N. Kumar, "Investigations on postural stability and spatiotemporal parameters of human gait using developed wearable smart insole," *Journal of medical engineering & technology,* vol. 39, no. 1, pp. 75-78, 2015.

[84] I. González *et al.*, "An ambulatory system for gait monitoring based on wireless sensorized insoles," *Sensors,* vol. 15, no. 7, pp. 16589-16613, 2015.

[85] A. Piau *et al.*, "A smart insole to promote healthy aging for frail elderly individuals: Specifications, design, and preliminary results," *JMIR rehabilitation and assistive technologies*, vol. 2, no. 1, p. e5, 2015.

[86] F. Lin *et al.*, "Smart insole: A wearable sensor device for unobtrusive gait monitoring in daily life," *IEEE Transactions on Industrial Informatics*, vol. 12, no. 6, pp. 2281-2291, 2016.

[87] R. Delgado-Gonzalo *et al.*, "Real-time gait analysis with accelerometer-based smart shoes," in *2017 39th Annual International Conference of the IEEE Engineering in Medicine and Biology Society (EMBC)*, 2017, pp. 148-148c: IEEE.

[88] N. Hegde *et al.*, "The pediatric SmartShoe: wearable sensor system for ambulatory monitoring of physical activity and gait," *IEEE transactions on neural systems and rehabilitation engineering*, vol. 26, no. 2, pp. 477-486, 2017.

[89] J. Ma *et al.*, "Optimizing Gait Parameters and Insole Sensor Positioning for Parkinson's Disease Assessment," in *Proceedings of the 2017 4th International Conference on Biomedical and Bioinformatics Engineering*, 2017, pp. 43-47.

[90] N. Roth *et al.*, "Synchronized sensor insoles for clinical gait analysis in home-monitoring applications," *Current Directions in Biomedical Engineering*, vol. 4, no. 1, pp. 433-437, 2018.

[91] C. Wang *et al.*, "Soft-Material-Based Smart Insoles for a Gait Monitoring System," *Materials*, vol. 11, no. 12, p. 2435, 2018.

[92] Y. Charlon *et al.*, "Design and Evaluation of a Connected Insole to Support Healthy Aging of Frail Patients at Home," *Wireless Sensor Network,* vol. 11, no. 05, p. 67, 2019.

[93] D. Chen *et al.*, "Bring Gait Lab to Everyday Life: Gait Analysis in Terms of Activities of Daily Living," *IEEE Internet of Things Journal,* 2019.

[94] D. Chen *et al.*, "Smart Insole Based Indoor Localization System for Internet of Things Applications," *IEEE Internet of Things Journal,* 2019.

[95] R. Hua and Y. Wang, "Monitoring Insole (MONI): A Low Power Solution towards Daily Gait Monitoring and Analysis," *IEEE Sensors Journal,* 2019.

[96] A. M. Ngueleu *et al.*, "Design and Accuracy of an Instrumented Insole Using Pressure Sensors for Step Count," *Sensors,* vol. 19, no. 5, p. 984, 2019.

[97] X. Qian *et al.*, "The Smart Insole: A Pilot Study of Fall Detection," in *EAI International Conference on Body Area Networks*, 2019, pp. 37-49: Springer.

[98] M. Chen *et al.*, "Intelligent shoes for abnormal gait detection," in *2008 IEEE International Conference on Robotics and Automation*, 2008, pp. 2019-2024: IEEE.

[99] D. Drobny *et al.*, "Saltate!: a sensor-based system to support dance beginners," in *CHI'09 Extended Abstracts on Human Factors in Computing Systems*, 2009, pp. 3943-3948: ACM.

[100] K. Kong and M. Tomizuka, "A gait monitoring system based on air pressure sensors embedded in a shoe," *IEEE/ASME Transactions on mechatronics,* vol. 14, no. 3, pp. 358-370, 2009.

[101] P. Paulick *et al.*, "StabilitySole: Embedded sensor insole for balance and gait monitoring," in *International Conference on Digital Human Modeling*, 2011, pp. 171-177: Springer.

[102] J. Berengueres *et al.*, "A smart pressure-sensitive insole that reminds you to walk correctly: An orthotic-less treatment for over pronation," in *2014 36th Annual International Conference of the IEEE Engineering in Medicine and Biology Society*, 2014, pp. 2488-2491: IEEE.

[103] S. I. Lee *et al.*, "Objectively quantifying walking ability in degenerative spinal disorder patients using sensor equipped smart shoes," *Medical engineering & physics*, vol. 38, no. 5, pp. 442-449, 2016.

[104] M. Munoz-Organero *et al.*, "Assessing walking strategies using insole pressure sensors for stroke survivors," *Sensors*, vol. 16, no. 10, p. 1631, 2016.

[105] M. J. Domínguez-Morales *et al.*, "Smart Footwear Insole for Recognition of Foot Pronation and Supination Using Neural Networks," *Applied Sciences*, vol. 9, no. 19, p. 3970, 2019.

[106] Z. Lin *et al.*, "A Triboelectric Nanogenerator‐Based Smart Insole for Multifunctional Gait Monitoring," *Advanced Materials Technologies*, vol. 4, no. 2, p. 1800360, 2019.

[107] C. Wang *et al.*, "Preliminary Clinical Application of Textile Insole Sensor for Hemiparetic Gait Pattern Analysis," *Sensors*, vol. 19, no. 18, p. 3950, 2019.

[108] E. S. Sazonov *et al.*, "Development of SmartStep: An insole-based physical activity monitor," in *2013 35th Annual International Conference of the IEEE*

Engineering in Medicine and Biology Society (EMBC), 2013, pp. 7209-7212: IEEE.

[109] A. De Santis *et al.*, "A simple object for elderly vitality monitoring: The smart insole," in *2014 IEEE/ASME 10th International Conference on Mechatronic and Embedded Systems and Applications (MESA)*, 2014, pp. 1-6: IEEE.

[110] Z. Zhang and S. Poslad, "Improved use of foot force sensors and mobile phone GPS for mobility activity recognition," *IEEE Sensors Journal*, vol. 14, no. 12, pp. 4340-4347, 2014.

[111] M. Haescher *et al.*, "Capwalk: A capacitive recognition of walking-based activities as a wearable assistive technology," in *Proceedings of the 8th ACM International Conference on PErvasive Technologies Related to Assistive Environments*, 2015, p. 35: ACM.

[112] Y. Han *et al.*, "A self-powered insole for human motion recognition," *Sensors*, vol. 16, no. 9, p. 1502, 2016.

[113] N. Hegde *et al.*, "One size fits all electronics for insole-based activity monitoring," in *2017 39th Annual International Conference of the IEEE Engineering in Medicine and Biology Society (EMBC)*, 2017, pp. 3564-3567: IEEE.

[114] N. Hegde *et al.*, "Automatic recognition of activities of daily living utilizing insole-based and wrist-worn wearable sensors," *IEEE journal of biomedical and health informatics*, vol. 22, no. 4, pp. 979-988, 2017.

[115] R. Hua and Y. Wang, "Daily Locomotor Movement Recognition with a Smart Insole and a Pre-defined Route Map: Towards Early Motor Dysfunction Detection," in *2019 IEEE Healthcare Innovations and Point of Care Technologies,(HI-POCT)*, 2019, pp. 87-90: IEEE.

[116] Y. Yu *et al.*, "Automatic Biomechanical Workload Estimation for Construction Workers by Computer Vision and Smart Insoles," *Journal of Computing in Civil Engineering*, vol. 33, no. 3, p. 04019010, 2019.

[117] D. J. Matthies *et al.*, "ShoeSoleSense: proof of concept for a wearable foot interface for virtual and real environments," in *Proceedings of the 19th ACM Symposium on Virtual Reality Software and Technology*, 2013, pp. 93-96.

[118] A. G. Bianchessi *et al.*, "A novel electric vehicle for smart indoor mobility," *IEEE Transactions on Intelligent Transportation Systems*, vol. 15, no. 4, pp. 1429-1440, 2014.

[119] T. Kim *et al.*, "Pressure or Movement? Usability of Multi-Functional Foot-Based Interfaces," in *Proceedings of the 2018 Designing Interactive Systems Conference*, 2018, pp. 1219-1227: ACM.

[120] H. Oagaz *et al.*, "VRInsole: An unobtrusive and immersive mobility training system for stroke rehabilitation," in *2018 IEEE 15th International Conference on Wearable and Implantable Body Sensor Networks (BSN)*, 2018, pp. 5-8: IEEE.

[121] X. Shi *et al.*, "Accurate and Fast Classification of Foot Gestures for Virtual Locomotion," in *2019 IEEE International Symposium on Mixed and Augmented Reality (ISMAR)*, 2019, pp. 178-189: IEEE.

[122] D. J. Matthies *et al.*, "CapSoles: who is walking on what kind of floor?," in *Proceedings of the 19th International Conference on Human-Computer Interaction with Mobile Devices and Services*, 2017, pp. 1-14.

[123] S.-I. Choi *et al.*, "User Identification from Gait Analysis Using Multi-Modal Sensors in Smart Insole," *Sensors,* vol. 19, no. 17, p. 3785, 2019.

[124] D. S. Elvitigala *et al.*, "GymSoles: Improving Squats and Dead-Lifts by Visualizing the User's Center of Pressure," in *Proceedings of the 2019 CHI Conference on Human Factors in Computing Systems,* 2019, p. 174: ACM.

[125] S. C. Regueme *et al.*, "A therapeutic insole device for postural stability in older people with type 2 diabetes. A feasibility study (SENSOLE Part I)," *Frontiers in medicine,* vol. 6, 2019.

[126] M. Sasagawa *et al.*, "Lower Limb Muscle Activity Control by using Jamming Footwear," in *2019 41st Annual International Conference of the IEEE Engineering in Medicine and Biology Society (EMBC)*, 2019, pp. 3302-3305: IEEE.

[127] L. Tang *et al.*, "Functional gradient structural design of customized diabetic insoles," *Journal of the mechanical behavior of biomedical materials,* vol. 94, pp. 279-287, 2019.

[128] A. Muro-De-La-Herran *et al.*, "Gait analysis methods: An overview of wearable and non-wearable systems, highlighting clinical applications," *Sensors,* vol. 14, no. 2, pp. 3362-3394, 2014.

[129] G. Bhat *et al.*, "Online human activity recognition using low-power wearable devices," in *2018 IEEE/ACM International Conference on Computer-Aided Design (ICCAD)*, 2018, pp. 1-8: IEEE.

[130] T. Sztyler and H. Stuckenschmidt, "Online personalization of cross-subjects based activity recognition models on wearable devices," in *2017 IEEE International Conference on Pervasive Computing and Communications (PerCom)*, 2017, pp. 180-189: IEEE.

[131] Y. Sun and B. Lo, "An artificial neural network framework for gait-based biometrics," *IEEE journal of biomedical and health informatics*, vol. 23, no. 3, pp. 987-998, 2018.

[132] B. Wang *et al.*, "FreeWalker: A smart insole for longitudinal gait analysis," in *2015 37th Annual International Conference of the IEEE Engineering in Medicine and Biology Society (EMBC)*, 2015, pp. 3723-3726: IEEE.

[133] K. Aoike and K. Nagamune, "Gait analysis with six axes inertial sensor and force sensor for daily motion," in *2016 11th International Conference on Computer Science & Education (ICCSE)*, 2016, pp. 27-28: IEEE.

[134] J. Rueterbories *et al.*, "Methods for gait event detection and analysis in ambulatory systems," *Medical engineering & physics*, vol. 32, no. 6, pp. 545-552, 2010.

[135] O. D. Lara and M. A. Labrador, "A survey on human activity recognition using wearable sensors," *IEEE communications surveys & tutorials*, vol. 15, no. 3, pp. 1192-1209, 2012.

[136] S. Chen *et al.,* "Toward pervasive gait analysis with wearable sensors: A systematic review," *IEEE journal of biomedical and health informatics,* vol. 20, no. 6, pp. 1521-1537, 2016.

[137] R. C. King *et al.,* "Application of data fusion techniques and technologies for wearable health monitoring," *Medical engineering & physics,* vol. 42, pp. 1-12, 2017.

[138] J. Figueiredo *et al.,* "Automatic recognition of gait patterns in human motor disorders using machine learning: A review," *Medical engineering & physics,* vol. 53, pp. 1-12, 2018.

[139] J. Woodburn and P. Helliwell, "Observations on the F-Scan in-shoe pressure measuring system," *Clinical Biomechanics,* vol. 11, no. 5, pp. 301-304, 1996.

[140] A. Putti *et al.,* "The Pedar® in-shoe system: Repeatability and normal pressure values," *Gait & posture,* vol. 25, no. 3, pp. 401-405, 2007.

[141] B. J. Braun *et al.,* "Validation and reliability testing of a new, fully integrated gait analysis insole," *Journal of foot and ankle research,* vol. 8, no. 1, p. 54, 2015.

[142] A. Lajevardi-Khosh *et al.,* "Center of pressure in a walking boot shifts posteriorly in patients following lower leg fracture," *Gait & posture,* vol. 70, pp. 218-221, 2019.

[143] P. Truong *et al.,* "Stride counting in human walking and walking distance estimation using insole sensors," *Sensors,* vol. 16, no. 6, p. 823, 2016.

[144] A. R. Alfonso *et al.*, "Novel pressure-sensing smart insole system used for the prevention of pressure ulceration in the insensate foot," *Plastic and Reconstructive Surgery Global Open*, vol. 5, no. 12, 2017.

[145] J. DeBerardinis *et al.*, "Assessing the validity of pressure-measuring insoles in quantifying gait variables," *Journal of rehabilitation and assistive technologies engineering*, vol. 5, p. 2055668317752088, 2018.

[146] A. Kalinauckas, "Wearable technology," *Engineering & Technology*, vol. 10, no. 4, pp. 36-43, 2015.

[147] O. Dehzangi *et al.*, "Activity Detection using Fusion of Multi-Pressure Sensors in Insoles," in *2018 24th International Conference on Pattern Recognition (ICPR)*, 2018, pp. 3315-3321: IEEE.

[148] W. Seiberl *et al.*, "Accuracy and precision of loadsol® insole force-sensors for the quantification of ground reaction force-based biomechanical running parameters," *European journal of sport science*, vol. 18, no. 8, pp. 1100-1109, 2018.

[149] M. Zequera *et al.*, "The" PAROTEC" Foot Pressure Measurement System and its Calibration Procedures (2005)," in *2006 International Conference of the IEEE Engineering in Medicine and Biology Society*, 2006, pp. 4135-4139: IEEE.

[150] M. Bravo-Aguilar *et al.*, "The influence of running on foot posture and in-shoe plantar pressures," *Journal of the American Podiatric Medical Association*, vol. 106, no. 2, pp. 109-115, 2016.

[151] S. Mohammed *et al.*, "Recognition of gait cycle phases using wearable sensors," *Robotics and Autonomous Systems,* vol. 75, pp. 50-59, 2016.

[152] M. F. Antwi-Afari *et al.*, "Wearable insole pressure system for automated detection and classification of awkward working postures in construction workers," *Automation in Construction,* vol. 96, pp. 433-441, 2018.

[153] B. J. Braun *et al.*, "Long-term pathological gait pattern changes after talus fractures—dynamic measurements with a new insole," *International orthopaedics,* vol. 42, no. 5, pp. 1075-1082, 2018.

[154] R. Nagahara and J.-B. Morin, "Sensor insole for measuring temporal variables and vertical force during sprinting," *Proceedings of the Institution of Mechanical Engineers, Part P: Journal of Sports Engineering and Technology,* vol. 232, no. 4, pp. 369-374, 2018.

[155] J. He *et al.*, "Unsupervised gait retraining using a wireless pressure-detecting shoe insole," *Gait & posture,* vol. 70, pp. 408-413, 2019.

[156] S. Sivakumar *et al.*, "Artificial neural network based ankle joint angle estimation using instrumented foot insoles," *Biomedical Signal Processing and Control,* vol. 54, p. 101614, 2019.

[157] S.-S. Lee *et al.*, "Classification of Gait Type Based on Deep Learning Using Various Sensors with Smart Insole," *Sensors,* vol. 19, no. 8, p. 1757, 2019.

[158] C. A. Abbott *et al.*, "Innovative intelligent insole system reduces diabetic foot ulcer recurrence at plantar sites: a prospective, randomised, proof-of-concept study," *The Lancet Digital Health,* vol. 1, no. 6, pp. e308-e318, 2019.

[159] V. Agostini *et al.*, "Segmentation and classification of gait cycles," *IEEE Transactions on Neural Systems and Rehabilitation Engineering,* vol. 22, no. 5, pp. 946-952, 2013.

[160] J. Klucken *et al.*, "Unbiased and mobile gait analysis detects motor impairment in Parkinson's disease," *PloS one,* vol. 8, no. 2, p. e56956, 2013.

[161] R. Hua and Y. Wang, "Robust Foot Motion Recognition Using Stride Detection and Weak Supervision-based Fast Labelling," *IEEE Sensors Journal*, vol. 21, no. 14, pp. 16245 - 16255, 2021.

[162] M. Susi *et al.*, "Motion mode recognition and step detection algorithms for mobile phone users," *Sensors,* vol. 13, no. 2, pp. 1539-1562, 2013.

[163] H. Zhang *et al.*, "A handheld inertial pedestrian navigation system with accurate step modes and device poses recognition," *IEEE Sensors Journal,* vol. 15, no. 3, pp. 1421-1429, 2014.

[164] Q. Riaz *et al.*, "One small step for a man: Estimation of gender, age and height from recordings of one step by a single inertial sensor," *Sensors,* vol. 15, no. 12, pp. 31999-32019, 2015.

[165] T. T. Ngo *et al.*, "Similar gait action recognition using an inertial sensor," *Pattern Recognition,* vol. 48, no. 4, pp. 1289-1301, 2015.

[166] M. Lueken *et al.*, "Peak Detection Algorithm for Gait Segmentation in Long-Term Monitoring for Stride Time Estimation using Inertial Measurement Sensors," in *2019 IEEE EMBS International Conference on Biomedical & Health Informatics (BHI)*, 2019, pp. 1-4: IEEE.

[167] A. Rampp *et al.*, "Inertial sensor-based stride parameter calculation from gait sequences in geriatric patients," *IEEE transactions on biomedical engineering,* vol. 62, no. 4, pp. 1089-1097, 2014.

[168] T. Pfau *et al.*, "A hidden Markov model-based stride segmentation technique applied to equine inertial sensor trunk movement data," *Journal of biomechanics,* vol. 41, no. 1, pp. 216-220, 2008.

[169] M. T. Koroglu *et al.*, "A deep learning strategy for stride detection," in *2018 IEEE SENSORS*, 2018, pp. 1-4: IEEE.

[170] M. Janidarmian *et al.*, "A comprehensive analysis on wearable acceleration sensors in human activity recognition," *Sensors,* vol. 17, no. 3, p. 529, 2017.

[171] S. H. Bach *et al.*, "Learning the structure of generative models without labeled data," *Proceedings of machine learning research,* vol. 70, p. 273, 2017.

[172] B. R. Greene *et al.*, "Quantitative falls risk assessment using the timed up and go test," *IEEE Transactions on Biomedical Engineering,* vol. 57, no. 12, pp. 2918-2926, 2010.

[173] E. R. Girden, *ANOVA: Repeated measures* (no. 84). Sage, 1992.

[174] O. Kramer, "Scikit-learn," in *Machine learning for evolution strategies*: Springer, 2016, pp. 45-53.

[175] D. Vervoort *et al.*, "Multivariate analyses and classification of inertial sensor data to identify aging effects on the Timed-Up-and-Go Test," *PLoS One,* vol. 11, no. 6, p. e0155984, 2016.

[176] N. Hegde and E. Sazonov, "Smartstep: A fully integrated, low-power insole monitor," *Electronics,* vol. 3, no. 2, pp. 381-397, 2014.

[177] R. Alkhatib *et al.*, "Machine learning algorithm for gait analysis and classification on early detection of parkinson," *IEEE Sensors Letters,* vol. 4, no. 6, pp. 1-4, 2020.

[178] M. I. M. Refai *et al.*, "Gait and dynamic balance sensing using wearable foot sensors," *IEEE transactions on neural systems rehabilitation engineering,* vol. 27, no. 2, pp. 218-227, 2018.

[179] P. Pierleoni *et al.*, "A smart inertial system for 24h monitoring and classification of tremor and freezing of gait in Parkinson's disease," *IEEE Sensors Journal,* vol. 19, no. 23, pp. 11612-11623, 2019.

[180] F. Demrozi *et al.*, "Toward a Wearable System for Predicting Freezing of Gait in People Affected by Parkinson's Disease," *IEEE journal of biomedical health informatics,* vol. 24, no. 9, pp. 2444-2451, 2019.

[181] P. R. Brustio *et al.*, "Dual-task training in older adults: The effect of additional motor tasks on mobility performance," *Archives of gerontology geriatrics,* vol. 75, pp. 119-124, 2018.

[182] E. O'Connell and M. Guidon, "Fear of falling and dual-task performance in people with Parkinson's disease," *European Journal of Physiotherapy,* vol. 18, no. 3, pp. 167-172, 2016.

[183] P. S. Pohl *et al.*, "Dual Task Timed Up-and-Go for Older Adults with and Without Balance Deficits," *Physical Occupational Therapy In Geriatrics,* vol. 37, no. 4, pp. 247-259, 2019.

[184] R. Hua and Y. Wang, "Age-dependent Mobility Decline Analysis through Sequential Foot Motion Reproduction," *IEEE Sensors Letters,* 2021.

[185] S. Viteckova *et al.*, "Gait symmetry measures: A review of current and prospective methods," *Biomedical Signal Processing Control,* vol. 42, pp. 89-100, 2018.

[186] H. Abdi and L. J. Williams, "Tukey's honestly significant difference (HSD) test," *Encyclopedia of research design,* vol. 3, no. 1, pp. 1-5, 2010.

[187] P. E. McKnight and J. Najab, "Mann‐Whitney U Test," *The Corsini encyclopedia of psychology,* pp. 1-1, 2010.

[188] R. F. Woolson, "Wilcoxon signed‐rank test," *Wiley encyclopedia of clinical trials,* pp. 1-3, 2007.

[189] P. Royston, "Approximating the Shapiro-Wilk W-test for non-normality," *Statistics computing,* vol. 2, no. 3, pp. 117-119, 1992.

[190] A. Channa *et al.*, "Wearable solutions for patients with parkinson's disease and neurocognitive disorder: A systematic review," *Sensors,* vol. 20, no. 9, p. 2713, 2020.

[191] J. C. Schlachetzki *et al.*, "Wearable sensors objectively measure gait parameters in Parkinson's disease," *PloS one,* vol. 12, no. 10, p. e0183989, 2017.

[192] M. W. Creaby and M. H. Cole, "Gait characteristics and falls in Parkinson's disease: A systematic review and meta-analysis," *Parkinsonism related disorders,* vol. 57, pp. 1-8, 2018.

[193] R. Hua *et al.*, "Insole-based Falling Risk Evaluation for Patients with Parkinson's Disease through Walking while Holding a Cup of Water," *IEEE Sensors Letters,* under review 2022.

[194] S. Taniguchi *et al.*, "Assessment of leg muscle activity using toe tapping in patients with Parkinson's disease: comparison of two types of toe tapping," *Journal of physical therapy science,* vol. 30, no. 5, pp. 689-693, 2018.

[195] D. M. Kennedy *et al.*, "The role of auditory and visual models in the production of bimanual tapping patterns," *Experimental brain research,* vol. 224, no. 4, pp. 507-518, 2013.

[196] F. M. Pfister *et al.*, "High-resolution motor state detection in Parkinson's disease using convolutional neural networks," *Scientific reports,* vol. 10, no. 1, pp. 1-11, 2020.

[197] K. Açıcı *et al.*, "A random forest method to detect Parkinson's disease via gait analysis," in *International conference on engineering applications of neural networks*, 2017, pp. 609-619: Springer.

APPENDIX A

PD PATIENTS AND HEALTHY CONTROL SUBJECTS

The gender, age group, motor functionality, such as gait functions, PD stage for patients, are encoded into numbers to calculate Euclidean Distance. Figure Appendix A.1 shows the normalized Euclidean Distance [0, 1] between each pair of PD patients, where 1 (darkest color) means 100% similar and 0 (lightest color) means no similarity. The patients with index (#) 1, 3, 4, 5 and 11 participate the experiment more than 3 times within 2 months. There are 3 patients who are with 100% similarity to each other (patient # 6, #8 and #10). The lowest similarity is 0 between patient # 3 and #9.

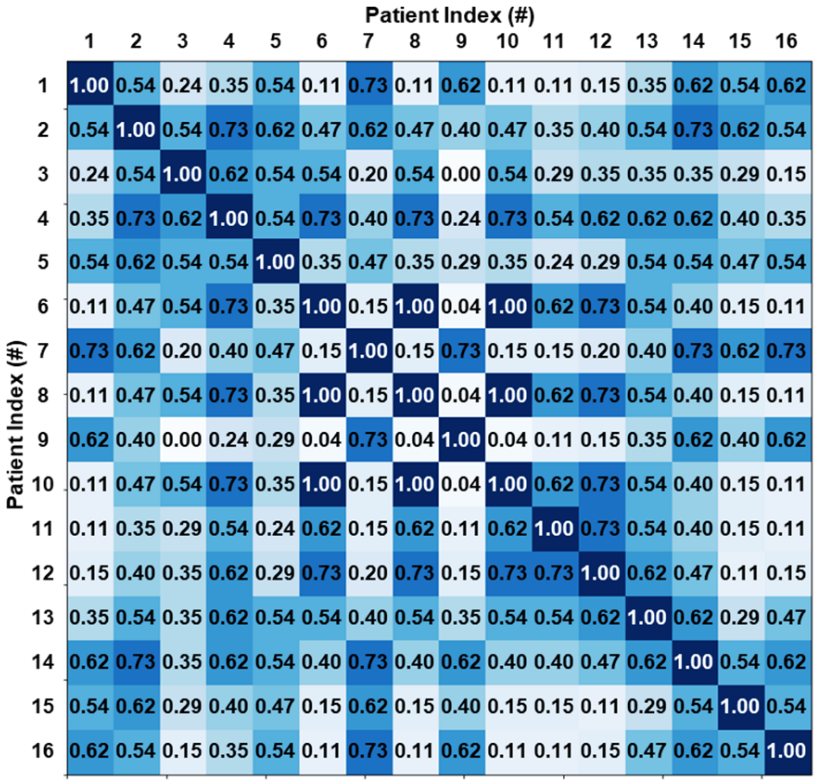

Figure Appendix A.1 PD patients' similarity.

Within the 16 PD patients, 10 of them participated the experiment in Chapter 3 and Chapter 4. Notice that few PD patients can't finish the toe tapping tasks. #2 PD patients' data were lost during experiment. Within 11 HC subjects, 8 of them participated the experiment in Chapter 3 and Chapter 4. Table Appendix A.1 shows the participance of PD patients, while Table Appendix A.2 shows the participance of HC subjects. The indexes in Table Appendix A.1 are the same as the indexes in Figure Appendix A.1.

Table Appendix A.1 Participance of PD patients in experiment in Chapter 3 and Chapter 4.

PD Index	Walk Task 1	Walk Task 2	Toe Tapping Task 1	Toe Tapping Task 2
1	walker	walker		
2				
3	x	x	x	x
4	x	x		
5	x	x	x	x
6	x	x	x	x
7	x	x	x	Can't do
8	x	x	x	x
9	x	x	x	x
10	x	x	x	x
11	x	x		
12	x	x	x	x
13			Can't do	Can't do
14			x	x
15			x	Can't do
16			Can't do	Can't do

Table Appendix A.2 Participance of HC in experiment in Chapter 3 and Chapter 4.

HC Index	Walk Task 1	Walk Task 2	Toe Tapping Task 1	Toe Tapping Task 2
1	x	x	x	x
2			x	x
3	x	x	x	x
4	x	x	x	x
5	x	x	x	x
6	x	x		
7	x	x	x	x
8	x	x		
9	x	x	x	x
10			x	x
11			x	x